IMPACT OF WIND GENERATOR INFED ON DYNAMIC PERFORMANCE OF A POWER SYSTEM

BY

MD. AHSANUL ALAM

A Dissertation Presented to the

DEANSHIP OF GRADUATE STUDIES

KING FAHD UNIVERSITY OF PETROLEUM & MINERALS

DHAHRAN, SAUDI ARABIA

In Partial Fulfillment of the

Requirements for the Degree of

DOCTOR OF PHILOSOPHY

In

ELECTRICAL ENGINEERING

APRIL 2010

KING FAHD UNIVERSITY OF PETROLEUM & MINERALS
DHAHRAN 31261, SAUDI ARABIA

DEANSHIP OF GRADUATE STUDIES

This dissertation, written by **MD. AHSANUL ALAM** under the direction of his dissertation advisor and approved by his dissertation committee, has been presented to and accepted by Dean of Graduate Studies, in partial fulfillment of the requirements for the degree of **DOCTOR OF PHILOSOPHY IN ELECTRICAL ENGINEERING.**

Dissertation Committee

Dr. Abu Hamed M. Abdur Rahim (Chairman)

Dr. Mohammad A. Abido (Co-Chairman)

Dr. Ibrahim M. El-Amin (Member)

Dr. Samir A. Al-Baiyat (Member)

Dr. Ibrahim O. Habiballah (Member)

Dr. Samir H. Abdul-Jauwad
Department Chairman

Dr. Salam A. Zummo
Dean of Graduate Studies

Date 29/5/10

عمادة الدراسات العليا
DEANSHIP OF GRADUATE STUDIES

Dedicated

to

my Parents

ACKNOWLEDGEMENTS

I have my sincerest appreciation for the help, assistance and advice that many people have given me on countless occasions during the course of my graduate work. I am very grateful to all of them. First, I would like to express my profound gratitude to Professor A. H. M. Abdur Rahim for his guidance, support and encouragement. I have always admired his knowledge, intuition and vision. He has been a wonderful advisor, who has continuously inspired and motivated me to complete many challenging research assignments. Most importantly, he has successfully instilled in me a passion for scientific research, which will continue to guide me for many more years to come.

I am deeply indebted to my co-advisor Professor M. A. Abido for his guidance and support. He has spared a lot of his valuable time during last summer vacation. I am grateful to Professor El-Amin for his valuable advice during my proposal presentation, and especially for being wonderful course instructor. The other members of my doctoral committee, Professor Samir Al Baiyat, and Associate Professor Ibrahim O. Habiballah, have spared their valuable times and given their thoughtful suggestions, and I would like to thank them all for that.

Acknowledgement is due to King Fahd University of Petroleum & Minerals for supporting my Ph D studies and this research work. I am thankful to Dr. Samir H. Abdul Jauwad, Chairman EE Dept, for providing an excellent environment of research in the department.

I am very thankful to my wife for her patience, understanding and support throughout my entire graduate life. She has always been there when I have needed her, helping me in all possible ways. She has constantly given me inspirations and encouragement. She has never hesitated to sacrifice her weekends and holidays for the cause of my study and research.

My parents, brothers and sister, who think I am the pride of the family, have done so much for me from my very childhood until this point, that they deserve the very best of my appreciation. Were it not for my father's guidance, my mother's hard work and the other members' endurance, it would not be possible for me to achieve the highest in education. My parent-in-law, brother-in-law and other in-laws have also contributed a great deal by constantly encouraging me and helping me in the pursuit of knowledge. I would like to extend my special thanks to them. I have had the good will of numerous other relatives all along my student life and I would like to acknowledge the as well. A special thank goes to Mohammad Abdul Malek for his help and cooperation in many occasions particularly for making Arabic Translation of my dissertation abstract.

Above all, I would like to glorify Almighty ALLAH Subhana wa ta'la for giving me knowledge and patience to carry out this work.

TABLE OF CONTENTS

LIST OF TABLES

LIST OF FIGURES

NOMENCLATURE

I. Symbols

A. Induction Generator, Transmission line, load and Control circuit

d-q	Direct and quadrature axes of generator
R_s, R_r	Stator, rotor resistance
x_s, x_r	Stator, rotor reactance
x_m	Mutual reactance
ψ_{ds}, ψ_{qs}	d, q axes stator flux linkage
ψ_{dr}, ψ_{qr}	d, q axes rotor flux linkage
i_{ds}, i_{qs}	d, q axes stator current
i_{dr}, i_{qr}	d, q axes rotor current
v_{ds}, v_{qs}	d, q axes stator voltage
ω_e	Generator rotor angular speed
ω_b	Base angular speed
V_s	Generator terminal voltage
V_{sr}	Generator terminal reference voltage
P_m, P_e	Input mechanical, output electrical power of generator
H_g, D	Inertia constant, damping coefficient of generator
K_{sE}, T_{sE}	Gain, time constant of exciter circuit
T_w	Wash-out block time constant
Y	Admittance
g, b	Conductance, susceptance
ΔB	Injected susceptance

u	Control input
x'	Transient reactance
e'_d, e'_q	d, q component of voltage behind x'
T'_o	Rotor time constant
R, X	Resistance, reactance of transmission line

B. Aerodynamic Subsystem and Drive Train

ρ	Air density
A	Swept area by the turbine blade
C_p	Turbine power coefficient
V_w	Wind speed
β	Blade pitch angle
λ	Blade-tip speed ratio
Ω	Mechanical angular velocity of turbine
R	Blade length of a turbine
K_s	Shaft stiffness constant
θ_s	Shaft twist angle
H_t	Turbine inertia constant
ω_t, ω_r	Angular speed of turbine rotor, generator rotor
D_s, D_t, D_g	Damping constant of shaft, turbine, generator
T_m	Mechanical torque of turbine
T_e	Electromagnetic torque

C. Energy Storage System and Controlled Devices

m	modulation index STATCOM VSC
ψ	Phase-angle of STATCOM voltage
D_r	Duty ratio of dc-dc converter
I_{st}	STATCOM injected current
V_{st}	STATCOM output voltage
V_{dc}	DC link voltage of STATCOM

C_{dc}	DC link capacitance of STATCOM
V_{sc}	Voltage across supercapacitor
C_{sc}	Supercapacitor capacitance
L_{sc}	Supercapacitor circuit inductance
I_{sc}	Supercapacitor current
E_{sc}	Supercapacitor internal voltage
L_{st}	Inductance of STATCOM circuit
R_{st}	Resistance of STATCOM circuit
R_b	Battery resistance
V_{batt}	Battery voltage
I_{batt}	Battery current
P_{st}	STATCOM injected real power
Q_{st}	STATCOM injected reactive power

D. Synchronous Generator

x_d, x_q	Reactance (d axis, q axis)
x'_d, x'_q	Transient reactance (d axis, q axis)
T'_{do}, T'_{qo}	Open-circuit field time constant (d axis, q axis)
H	Inertia constant
r_s	Stator resistance
K_A, T_A	Exciter gain, time constant
E_{fd}	Generator field voltage
V_t	Generator terminal voltage
D	Damping coefficient
δ	Machine rotor angle
T_m, T_e	Mechanical torque, Electromagnetic torque
T_D	Damping torque

II. Abbreviations

IG	Induction generator

IM	Induction machine
DFIG	Doubly fed induction generator
SCIG	Squirrel-cage induction generator
SG	Synchronous generator
WT	Wind turbine
PMSG	Permanent magnet synchronous generator
PCC	Point of common coupling
ESS	Energy storage system
BESS	Battery energy storage system
SCESS	Supercapacitor energy storage systems
ESR	Equivalent series resistance
SMES	Super magnetic energy storage
FC	Fixed capacitor
TSC	Thyristor switched capacitor
TCR	Thyristor controlled reactor
STATCOM	Static synchronous compensator
VSC	Voltage source converter
VSI	Voltage source inverter
SVC	Static var compensator
FACTS	Flexible AC transmission system
AC	Alternating current
DC	Direct current
HVDC	High voltage direct current
PI	Proportional plus integral
PID	Proportional-integral-derivative
SPWM	Sinusoidal pulse width modulation
FERC	Federal Energy Regulatory Commission
LVRT	Low voltage ride through
FRT	Fault ride through

DISSERTATION ABSTRACT

Name: MD. AHSANUL ALAM

Title: IMPACT OF WIND GENERATOR INFEED ON DYNAMIC PERFORMANCE OF A POWER SYSTEM

Degree: DOCTOR OF PHILOSOPHY

Major Field: ELECTRICAL ENGINEERING

Date of Degree: APRIL 2010

Wind energy is one of the most prominent sources of electrical energy in the years to come. A tendency to increase the amount of electricity generation from wind turbine can be observed in many countries. One of the major concerns related to the high penetration level of the wind energy into the existing power grid is its influence on power system dynamic performance.

In this thesis, the impact of wind generation system on power system dynamic performance is investigated through detailed dynamic modeling of the entire wind generator system considering all the relevant components. Nonlinear and linear models of a single machine as well as multimachine wind-AC system have been derived. For the dynamic model of integrated wind-AC system, a general transformation matrix is determined for the transformation of machine and network quantities to a common reference frame. Both time-domain and frequency domain analyses on single machine and multimachine systems have been carried out. The considered multimachine systems are – A 4 machine 12 bus system, and 10 machine 39 bus New England system. Through eigenvalue analysis, impact of asynchronous wind system on overall network damping has been quantified and modes responsible for the instability have been identified. Over with a number of simulation studies it is observed that for a induction generator based wind generation system, the fixed capacitor located at the generator terminal cannot

normally cater for the reactive power demand during the transient disturbances like wind gust and fault on the system. For weak network connection, system instability may be initiated because of induction generator terminal voltage collapse under certain disturbance conditions.

Incorporation of dynamic reactive power compensation scheme through either variable susceptance control or static compensator (STATCOM) is found to improve the dynamic performance significantly. Further improvement in transient profile has been brought in by supporting STATCOM with bulk energy storage devices. Two types of energy storage system (ESS) have been considered – battery energy storage system, and supercapacitor based energy storage system. A decoupled P – Q control strategy has been implemented on STATCOM/ESS.

It is observed that wind generators when supported by STATCOM/ESS can achieve significant withstand capability in the presence of grid fault of reasonable duration. It experiences almost negligible rotor speed variation, maintains constant terminal voltage, and resumes delivery of smoothed (almost transient free) power to the grid immediately after the fault is cleared.

Keywords: Wind energy, induction generator, dynamic performance of wind generators, energy storage system, decoupled P – Q control, multimachine system.

Doctor of Philosophy Degree
King Fahd University of Petroleum & Minerals, Dhahran
April 2010

ملخص البحث

الاسم : محمد أحسن العالم
عنوان الرسالة : تـأثير مولـد الكهربـاء باسـتخدام الريـاح فـي أداء نظـام الطاقـة الكهربائية
الدرجة : درجة الدكتوراة في الفلسفة
التخصص : الهندسة الكهربائية
تاريخ التخرج : أبريل 2010

ستكون طاقة الرياح من أبرز مصادر الطاقة الكهربائية في السنوات المقبلة ؛ إذ يظهر اتجاه عدد من الدول لزيادة كمية الكهرباء المولدة من الطواحين الهوائية ، لكن ارتفاع نسبة طاقة الرياح في شبكة الكهرباء الحالية قد يؤثر في أداء نظام الطاقة الكهربائية .

يستقصى في هذه الرسالة تأثير نظام توليد الكهرباء باستخدام الرياح في أداء نظام الطاقة الكهربائية ، وذلك من خلال نماذج تحاكي نظام توليد الكهرباء باستخدام الرياح ، وتأخذ جميع عناصره في الحسبان . وقد أوجدت النماذج الخطية وغير الخطية لكل من النظام أحادي الجهاز ، والنظام متعدد الأجهزة الذي تشكل الرياح أحد مصادر طاقته الكهربائية . واستخدمت مصفوفة تحويل عامة لنموذج النظام الأخير بغرض توحيد الإطار المرجعي لجميع مكونات الشبكة . ثم أجريت التحليلات في النطاق الزمني والنطاق الترددي للنظام أحادي الجهاز ، ولنظامين متعددي الأجهزة هما : النظام ذو الأربعة أجهزة والاثني عشر رابطا ، ونظام إنجلترا الجديد ذو العشرة أجهزة والتسعة والثلاثين رابطا . وحدد مدى تأثير نظام الرياح غير المتزامن في توهين التذبذبات في الشبكة باستخدام تحليل القيم الذاتية ، وكذلك حددت الأنساق المسؤولة عن انعدام الاستقرار .

وقد لوحظ بعد دراسة عدد من هذه الأنظمة المحاكاة أن المكثف الموجود على طرف المولد الحثي في نظام توليد الكهرباء باستخدام الرياح غير قادر عادة على تلبية طلب الطاقة الارتكاسية عند حدوث اضطرابات عابرة : كعاصفة ، أو خلل في النظام . وقد يفقد النظام استقراره في مناطق ضعيفة الاتصال بالشبكة بسبب انهيار الجهد في طرف المولد الحثي في ظل ظروف اضطراب معينة .

ولقد ظهر جليا أن تعويض الطاقة الارتكاسية باستخدام معوض متزامن (STATCOM) أو متغير المهاودة يحسن الأداء ، وازداد التحسن في الوضع العابر عند دعم المعوض المتزامن بأجهزة لتخزين الطاقة ، حيث استعين بنظامين لتخزين الطاقة : يستخدم أحدهما بطارية ، بينما يستخدم الآخر مكثفا ممتازا . ونفذت في هذه الحالة خطة تحكم مستقلة بكل من الطاقتين الحقيقية والارتكاسية ، ولوحظ في هذه الحالة كذلك أن مولدات الطاقة باستخدام الرياح قادرة على الصمود مع وجود خلل في الشبكة لمدة معقولة ؛ فسرعة دوار المولد لا تتغير إلا بشكل طفيف ، والجهد في طرف المولد ثابت ، وتوصيل الطاقة السوية – الخالية تقريبا من الوضع العابر – إلى الشبكة يستأنف بعد إصلاح الخلل مباشرة .

كلمات البحث : طاقة الرياح ، المولد الحثي ، أداء مولدات الطاقة باستخدام الرياح ، نظام تخزين الطاقة ، التحكم المستقل بكل من الطاقتين الحقيقية والارتكاسية ، النظام متعدد الأجهزة .

درجة الدكتوراة في الفلسفة

جامعة الملك فهد للبترول والمعادن ، الظهران

أبريل 2010

CHAPTER 1

INTRODUCTION

1.1 WIND POWER AND ELECTRIC GRID

Environmental concerns and escalating fuel price have led to the rapid development of wind power generation technologies during the past two decades. A single wind turbine can produce 200 times more power than its equivalent two decades ago [1, 2]. Modern commercially available wind turbines have ratings of 1.5 MW to 5 MW, and the first 10MW wind turbine is expected by the year 2010. A tendency to erect more and more wind turbines can be observed in power industry. Wind turbines in USA produce about 2% of total generation [3]. Presently wind power meets 3% of the total electricity demand in Europe [4]**,** and this development will continue to grow in coming years. It seems that in the near future wind turbines may start to influence the behavior of electrical power systems. Because of such developments, extensive research is being carried out on the subject of wind generation. Topics of focus are: feasibility studies and development of wind models, connection to the grid, hybrid systems, power quality studies, energy capture maximization, optimized power output.

Wind turbines are a variable and random source of mechanical energy. To convert this form of energy to electrical energy, all types of generators, *viz*. DC, synchronous and induction generators have been attempted [5]. Among these, induction generators (IGs) are widely used as wind generators since they are relatively inexpensive, rigid, and require low maintenance. Although variable-speed wind turbines (WTs) are getting popularity, a substantial percentage of the total installations are of fixed-speed types with cage-rotor IG [6].

The wind generators are connected to the medium voltage (MV) level of the power system by a step-up transformer. Both high and low voltage DC systems have been considered for integration of wind generation with the AC system [7-9]. Connecting a wind generator to a transmission line in a network without any control can potentially be troublesome and may result in suboptimal performance. Such simple connections may give rise to unacceptable voltage rise at the grid, without delivering the maximum available power at the desired efficiency [10]. If the interconnection of the wind farm is made to a weak grid system, fluctuating output power results in a highly variable voltage at the PCC and therefore, reactive power control is required to regulate the system voltage [11]. The response of the system following faults is also of great concern [12].

1.2 ANALYSIS OF POWER SYSTEM WITH WIND INFEED

The composition of wind power generation system is characterized by wind turbine which has high inertia and low shaft stiffness between the turbine and the generator rotor [13, 14]. Generally, it uses induction generator (IG) that lacks inherent

excitation system and relies on unsteady input source. When connected with the conventional power grid, these induction generators interact asynchronously with the synchronous generators. Consequently, the entire power generation system behavior is different from the conventional one.

The assessment of the effects of the wind power penetration to an existing power system necessitates the calculation of voltage and frequency profiles and examination of instability issues. As in the case of all AC systems, two types of instability issues may arise when a wind system is integrated in an AC system. These are: dynamic stability, and transient stability. In systems consisting solely of synchronous generation, loss of synchronism is the normal mode of transient failure. However, in networks having both wind and conventional synchronous generation, transient failure may be encountered for other reasons such as the collapse of system voltage. The transient and dynamic stability of a power system are usually assessed through time-domain as well as frequency-domain analysis using large-signal and small-signal models respectively [15-17]. Although time-domain simulation offers direct appreciation of the wind generation system dynamic behavior in terms of visual clarity, it is not able to identify and quantify the cause of problems. This complementary information can be obtained with eigen-value studies [14]. On the other hand, only determination of eigen-values is not sufficient for describing post fault behavior especially for the case of induction generator based wind systems [18].

1.3 ENHANCEMENT AND CONTROL SYSTEM

Operation of a wind farm under disturbances within the nearby power system poses great cause of concern. Faults in the network can lead to voltage instabilities and loss of

synchronism in conventional power systems. Since wind farms are typically composed of only induction machines, the loss of synchronism is no longer a concern. However, tripping of the generators due to undervoltage and overspeed of the wind generators can result in voltage stability problems and even small disturbances may lead to widespread tripping and associated instabilities. To enhance transient stability different methods have been suggested focusing on voltage recovery and speed control.

If only the voltage level is restored, the magnetic field of the generators can be re-established and then electromagnetic torque can be restored, and therefore a quick recovery of voltage and re-establishment of the electromagnetic torque are crucial. The overspeed of a generator may also be limited by controlling the input mechanical torque. Turbines equipped with a pitching system have the advantage of actively controlling the input mechanical torque by pitching, which will effectively limit the acceleration of the generator system. Various control approaches have been suggested including fuzzy-logic [19], minimum variance control [20], or PI control [21]. For fixed-speed rotor short-circuited induction generator with stall-regulated wind turbines, there is no active control methods available to control the input mechanical power, and therefore the effective approach would be the use of a reactive power compensator to help the voltage recovery. A fast reactive power control would improve the voltage and help to re-establish the machine magnetic field and torque. Different shunt FACTS devices are preferred for this purpose. SVC with State feedback control, output feedback control [22], PI control [23], fuzzy-logic control [24] are reported to have improved steady-state as well as dynamic performance of wind generation system. STATCOM is recognized as fastest FACTS device with capability to provide reactive power support at low voltage. Output feedback

linear quadratic control [25], decoupled current control [26], fuzzy-logic control [27, 28], PI control [29, 30] of STATCOM have been reported for its application either in wind system or all AC system. Recent studies show that transient performance of wind generation system can be enhanced using STATCOM with bulk energy storage devices [31, 32] or braking resistor [33]. However, proper control strategies are necessary in order to achieve full benefits of STATCOM.

1.4 RESEARCH PROBLEM DEFINITION

Early wind generators supplied only isolated loads. With the growth in wind generation, the excess generation was fed to grid where facilities existed. The wind turbines were not required to actively attempt to control voltage and frequency. Also, wind turbines were often disconnected from the grid when abnormal operating conditions occurred. For reliable supply from the wind systems, it is required to find appropriate solutions for maintaining good dynamic performance of the power systems with large amount of wind power infeed. This necessitates proper modeling of the integrated Wind-AC system to reflect the proper system behavior. A proper control study requires accurate steady-state and dynamic models of wind systems, the generators and their accessories.

A large number of studies have been reported in the literature on system simulation and studies for single machine systems. For multimachine system studies, most researchers use simulation softwares like PSS/E, PSCAD/EMTDC, DigSilent from Power Factory, etc [15, 32, 34, 35]. The details of these packages are generally not accessible to the researchers and the extents of the modeling rigor are generally unknown.

Conventional multimachine system study considers the induction generator to be a source of real power absorbing reactive power from the network. The electrical transient, interconnection of the asynchronous and synchronous machine are often ignored for simplicity. This item requires a detailed investigation.

Various methods are reported in the literature for controlling the steady state and transient performance of the wind systems. These include pitch control on the turbine side, and reactive power control on the generator side. In many cases, the control strategies are inadequate or too complicated. Design of simple and efficient controllers to enhance the system performance is always a matter of interest to the researchers. In addition, exploration of controllers and control techniques in a multimachine asynchronous-synchronous system require special investigation.

1.5 RESEARCH OBJECTIVES

The major objectives of this research are to study the impact of wind generation infeed on the AC power system, and to suggest control solutions in order to mitigate any ill-effect arising out of the interconnection. The first part of the objective will be attained through a detailed dynamic model of the integrated wind-AC system in time domain as well as frequency domain.

In the mitigation phase, various important existing control methods will be evaluated and a new method will be explored. Controls will be implemented which are local to the asynchronous generator. Some relatively newer methods being reported in the

above two aspects are application of short-term energy storage systems (ESSs). This research proposes to take a closer look at the possibility of introducing battery and supercapacitors as corrective dynamic tool. Feasibility of having both real and reactive power control with the support of ESS will be investigated analytically and then implemented for numerical simulation in both grid connected single machine and multimachine system.

In view of the above, this research proposes to do the following:

a) Develop dynamic model of a wind turbine induction generator system feeding an infinite bus system
b) Extend the model to include the wind-generator model feeding a multi-machine conventional power system
c) Study the impact of integrating wind system to the electrical grid through simulation of the single machine as well as the multi-machine systems.
d) Study the performance of the applied controls for dynamic enhancement of the single machine as well as multi-machine systems.

1.6 THESIS OUTLINE

Chapter 2 of the thesis presents a summary of the related literature. Chapter 3 develops a dynamical model of wind-generator system connected to infinite bus. Simulation results and control strategies to improve dynamic performance of grid connected wind generator are given in Chapter 4. Nonlinear and linearized models of multimachine AC power system comprising of asynchronous and as well as synchronous

generators is presented in Chapter 5. Simulation studies of the multimachine system are reported in Chapter 6, and Chapter 7 presents the control methods to enhance the system. Finally, Chapter 8 concludes the salient findings of this research.

CHAPTER 2

LITERATURE REVIEW

This chapter summarizes some of the salient studies performed on the analyses of integrated asynchronous wind systems in power systems. Dynamic performance improvement and power system stabilization with wind power infeed is considered in particular. Different aspects of modeling a wind generation system and the type of simulations as reported in the literature have been reviewed.

2.1 WIND GENERATION SYSTEMS

The development of various wind turbine concepts during the last two decades has been mainly in two streams – aerodynamic power control, and speed control. At high wind speed, aerodynamic power to the wind turbine is controlled basically in three ways *viz*, stall, pitch, or active stall. Depending on the wind turbine concepts, the type of associated generator and connection arrangement to the grid varies. Thus several types of wind generation system exist, three of them are very common [36]. The first type is a fixed-

speed wind turbine system using a multi-stage gearbox and a standard squirrel-cage induction generator (SCIG), directly connected to the grid. The second type is a variable-speed wind turbine system with a multi-stage gear box and a doubly fed induction generator (DFIG), where the power electronic converter feeding the rotor winding has a power rating of about 30% of the generator capacity; the stator winding of the DFIG is directly connected to the grid. The third category is also variable speed but of direct-driven (gearless) wind turbine type equipped with low-speed high-torque synchronous generator (SG) and full-scale power electronic converter. Permanent magnet synchronous generator (PMSG) also received considerable attention in wind generation application because of its attractive feature that eliminates excitation circuitry associated with synchronous generator or external excitation system with induction generator [37]. Both, low-speed and high-speed PMSGs exist for gearless and with gear coupling with the wind turbine [38].

Induction generators with fixed-speed wind turbines are operated in a narrow range (about 1% around the synchronous speed) and the speed is almost fixed to the grid frequency. Stall control or active-stall method is usually used for power control at higher wind speed. For a fixed-speed system, wind speed fluctuations are directly translated into electromechanical torque variations. Thus, the turbulence of the wind will result in power variations that affect the power quality of the grid [39]. For a variable-speed wind turbine the generator is controlled by power electronic equipment, which makes it possible to control the rotor speed. In this way the power fluctuations caused by wind variations can be more or less absorbed by changing the rotor speed [40] and thus power variations originating from the wind conversion and the drive train can be reduced. Hence, the

power quality impact caused by the wind turbine can be improved compared to a fixed-speed turbine [41].

2.2 WIND GENERATION SYSTEM MODELING

To study the impact of wind generation on electrical power system behavior and to study the power, frequency and voltage variation during different disturbances, adequate models are needed. Modeling of the entire wind generation system consists of individual component models of wind speed, wind turbine, drive-train, induction generator, transmission-line and load. Depending on the type of simulations conducted, several modeling approaches exist as mentioned below.

2.2.1 Wind speed model

Generation of electric power using wind turbines is characterized by the variability of the wind speed. The technical barriers relate primarily to the electrical grid transmission and distribution networks' ability to operate in a stable way when subject to variable power input. To evaluate the feasibility of wind power generation, the most important thing is to know how wind speed varies. The probabilistic models are usually used for such purpose [42].

The wind that hits the rotor of a wind turbine varies with time and space due to the tower shadow and other spatial effects [43]. Depending on what types of simulations are conducted, the wind model is adapted to facilitate simulations and make them as realistic as possible. When situations are simulated that only lasts for a few seconds, like transient

fault ride-through and power system stabilization, the natural wind variations are neglected [15]. When a whole wind farm is simulated, as opposed to a single wind turbine, the spatial wind speed variations that a rotor blade experiences during one revolution are neglected. These variations cancel each other out when several wind turbines are aggregated [44]. Sørensen *et all* showed that the assessment of power quality from wind farms depends on appropriate representation of the wind speed [45]. In wind farms, the turbulence spatial correlation must be included.

2.2.2 Wind Turbine and Drive-Train Model

The shaft system provides a coupling between the turbine and the generator rotors. In the most cases, the shaft systems contain a gearbox and are characterized by a relatively soft coupling. This soft coupling is expressed by relatively low values of the shaft stiffness. Therefore the shaft systems are generally represented with the two-mass models rather than with the lumped-mass models [13, 14, 46]. The two-mass model predicts fluctuations of the electrical and the mechanical parameters of the wind turbine and its generator at transient events in electric power networks. The natural frequency of such fluctuations is the shaft torsional mode. Such fluctuations are absent when applying the lumped-mass model. The two-mass model also predicts a larger over-speeding of fixed-speed wind turbines than with use of the lumped-mass model. This is important in voltage stability investigations because excessive over-speeding leads to voltage instability.

Some simple models of variable speed turbines neglect the aerodynamics and the mechanical dynamics of the wind turbine [47]. This might be justifiable when operation

with small signal disturbances is considered. However, if large disturbances in the grid upset the wind turbine, a detailed model of the wind turbine system is essential, even if its generator is connected to the grid via a full-scale converter. A detailed wind turbine model is even more important for fixed speed wind turbines with directly grid-connected squirrel cage induction generators. There the turbine dynamics are directly reproduced in the grid as variations in power and voltage. More advanced models of wind turbine systems include an aerodynamic model with the dynamic stall effect, a mechanical model which represents the turbine drive train as a two-masses, stiffness and damping system, and a detailed wind model [45, 48].

2.2.3 Induction Generator Model

The dynamic model of an induction machine (IM) is usually presented by means of a so called fifth-order model that represents IM by a system of five general differential equations of an idealized induction machine [49]. In some power system studies, it is desirable to reduce the complexity of the system by using reduced-order models that can be obtained by assuming some of the derivatives as being equal to zero [50]. For example, a third-order model of IM is obtained by neglecting the stator flux transients [51].

A common induction generator (IG) model is the so-called “voltage behind transient reactance model” which is widely used in the analysis of power system faults [52, 53]. In the case of transient stability studies, it is rather common to reduce the fifth-order model to a third-order model [54, 55]. However, as concluded by Akhmatov [46], using third-order models may result in too-low transient currents during disturbances,

which may lead to inaccurate results, especially when the transient behavior of a wind power system during a grid fault is being studied.

2.3 Aggregation of Multiple Wind Turbines

Aggregated representation of wind-farms with many wind turbines has been a topic of research in recent years. For simulating larger systems, an aggregation of several wind turbines and wind farms is favored, to increase simulation speed and to reduce computational resources. Such aggregations can be done on the whole wind turbine model and the spatial variation of the wind speed [56, 57].

Large grid-connected wind farms have many wind turbines usually with identical generator data and identical mechanical parameters for the shaft systems and aerodynamic rotors. Modeling details of such wind farms depend on the target of investigations. Detailed models with representation of all wind turbines in the wind farm, all the transformers connecting the wind turbine generators to the internal network of the wind farm, are applied to investigate if there is a risk of mutual interaction between the wind turbines and problems related to the internal network of the wind farm such as power losses, internal faults in the wind farm and protection [46]. For the investigations like IG terminal voltage stability or rotor speed stability, the focus is on the collective response of the large wind farm to a short-circuit fault in the transmission grid. In this case, an aggregated model of the large wind farm is commonly used where the whole wind farm is represented by a single [58] or few wind mill equivalents [56]. The power capacity of the equivalent is re-scaled for reaching the total capacity of the whole wind farm. For the

aggregated wind-turbine model to be acceptable, it must retain the relevant dynamic characteristics with respect to the grid similar to the totality of individual turbines in the wind park. Such characteristics can be the behavior of the slip, voltage and power oscillations of the aggregated model in steady-state conditions, as well as in abnormal conditions [57].

2.4 MULTIMACHINE SYSTEMS STUDY

The procedure for transient as well as dynamic stability assessment of all-ac multimachine power system is well established [59, 60]. Techniques for the construction of system dynamic model and types of analyses to be carried out are well defined [61, 62]. However, this is an area which has not been explored sufficiently for the multimachine power systems including synchronous generators (SGs) and induction generators (IGs).

Due to wide spread adoption of commercially available various simulation softwares, the development of multimachine power system dynamic model including synchronous generator and asynchronous wind generator has not been paid much attention. A general multimachine power system model is presented in [63], and transient stability of an isolated two machine diesel-wind power system was assessed [64]. Recently, a two-machine system model is presented in [18] where the synchronous machine is represented by very simple one-axis model and the doubly fed induction machine (DFIG) is represented by simplified third-order model.

In recent years, a number of studies have been carried out to examine the possibility of maintaining system stability of power system with wind power infeed. Some of these studies dealt with a very simplified system comprising of one SG and one IG along with infinite bus [53,65,66], while the others used various types of commercial power system dynamic simulation softwares like PSS/E [34], PSCAD/EMTDC [32], DigSilent [15], Mudapack [16], etc. These softwares are generally closed type and hence are not advantageous for other researchers. Results were posted using these softwares in time-domain simulations [15, 32, 65] as well as on frequency domain [16, 17]. The general observation is that under normal conditions or for smaller disturbances wind generators provide well damped response.

The transient fault behavior a part of the Danish power grid and the power networks in several Spanish regions were investigated in references [67,68], respectively using large disturbance model. The incidence of transient voltage collapse of the wind generator was investigated in relation to the location of fault, as well as size of nearby synchronous generator. Larger wind farm in a neighborhood of smaller synchronous generator is more vulnerable to voltage collapse in the event of fault in the system as the wind farm is expected to receive little reactive power support from the synchronous generator.

Voltage stability has been pointed out as another problem to large integration of wind power because wind farms demand reactive power. Freitas *et al* [69,70] presented a preliminary investigation on the influence of induction generators on the small disturbance voltage stability of distribution systems by using time-domain nonlinear

dynamic simulations. The system stability margin is analyzed through PV curves. Simulation results show that the influence can be positive or negative, depending on the operating point of the induction generator. Usually, the higher the machine loading, the worse the impact is on the voltage stability margin.

The impact on voltage quality, power characteristic and grid frequency is dependent on the turbine type considered [71, 72]. Such findings are not only based on theoretical considerations, but have been confirmed by measurements [73, 74]. The inherent variability of wind power causes wind turbines to exhibit power fluctuations and cause flicker in the grid. In more critical operating conditions wind turbines can even compromise voltage stability in the grid [75]. It has been found though, that the operation of wind turbines itself is also affected by variations in grid voltage, voltage imbalance, variation in system frequency and voltage distortion [45].

2.5 DYNAMIC PERFORMANCE IMPROVEMENT

During a short-circuit fault output electrical power and electromagnetic torque of the wind turbine are significantly reduced due to depressed terminal voltage of the wind generator, whereas the mechanical torque may be still applied to the wind turbine. Consequently, the turbine and generator will accelerate because of the torque unbalance. As the speed of IG increases, it demands more reactive power which aggravates terminal voltage recovery. To enhance transient stability different methods have been suggested focusing on voltage recovery and speed control.

2.5.1 Conventional Techniques

Reactive power support during fault has been proposed using various FACTS devices [76-79]. SVC and STATCOM are considered as the prospective candidate for this. Braking resistor control for fault ride-through has also been proposed in [80] to control active power during fault. Since relation between aerodynamic power and blade pitch angle is highly nonlinear, a varieties of control methods have been reported like PI control [21], fuzzy-logic based control [19], minimum variance control [20].

For a rotor-resistance-controlled induction generator, in addition to the reactive power support, the rotor resistance control can also be used to improve the stability. For a certain machine speed, the rotor resistance may be controlled to present a higher electromagnetic torque which will improve the opportunity of system recovery by reducing the acceleration. Therefore, the dynamic slip-controlled generator-based-pitch-controlled wind turbine may be controlled through two ways: dynamic slip control and pitch control. It is possible for the wind turbine to adjust the electromagnetic torque by dynamic slip control and to change the aerodynamic torque by pitch control [76].

2.5.2 Recent Trends – use of Bulk Energy Storage System (ESS)

Although STATCOM has been identified as the fastest responding device that can assist in improving the power quality and stability of the wind farm [31], its capability is limited to reactive power control only. To overcome this problem STATCOM with energy storage systems have been emerged as more promising devices for power system applications [81], as they have both real and reactive power control capabilities.

Among numerous types of existing ESS four are most common, which are: battery, supercapacitor, superconducting magnetic storage (SMES), and flywheel. Each of the systems realizes the same goal, however, the manner in which they store energy is quite different and consequently, their modeling and control differs significantly. Various factors need to be considered when choosing the type of energy storage system including: size, rating, speed, and cost. Some storage devices are better suited for larger ratings and the speed of exchange of energy also typically differs. Table 2.1 summarizes the characteristics of the different technologies based upon information presented in [82].

TABLE 2.1: Summary of short-term energy storage system characteristics

Technology	Energy Equations	Energy Cost ($/kWh/year)	Power Cost ($/kW/year)	Storage Time	Round Trip Effici-ency
Lead Acid Battery	$E(t) = E_o + \int v(t)i(t)dt$	69	91	60-300 min	63%
Super Capacitors	$E(t) = \frac{1}{2}CV_{sc}^2$	711	6	0.006-6 min	86%
SMES	$E(t) = \frac{1}{2}L_{smes}V_{smes}^2$	370,000	59	0.006-6 min	21%
High Speed Flywheel	$E(t) = \frac{1}{2}J\omega_{fw}^2$	96	1.2	0.006-6 min	89%

The two most promising *short-term* storage devices – flywheels and supercapacitors – both offer similar characteristics and are both suitable for wind energy applications. But flywheels are physically large and involves numerous safety and maintenance issues.

The supercapacitor technology relies on charging the electrochemical double layer arising from surface reactions at very high surface bipolar electrodes [83]. This capacitor is a very complex physical device in which charge is stored in a double layer formed at the interface between a large surface material such as activated carbon and a liquid electrolyte [84, 85]. It can store significant amount of energy and quickly release it. Their main application is for short term “power boost” type applications where they can release large amount energy quickly, and then recharge with a smaller current. It has high power density, wide temperature range, long life (lifecycle millions of time), and offers excellent performance. As it has both real and reactive power control capabilities, supercapacitors can be applied to transient and dynamic stability enhancement of power system [86].

In wind power application, STATCOM with battery energy storage system (BESS) is used to level the power fluctuations by charging and discharging operation [87]. Also, during sag or fault the BESS unit can be used to boost the stability margin by absorbing active power from the wind farm. To enhance transient stability margin further incorporation of braking resistor along with BESS has been suggested [33]. But BESS is based on chemical process and thus it has problems such as low response speed and short service life.

Recently, supercapacitors have also attracted the attention in the area of renewable energy [88]. However, most of the studies are limited to power smoothing of and terminal voltage regulation of both fixed and variable speed wind generators [32, 82, 89]. Wei Li and Geza Joos [90] used a supercapacitor hybrid energy storage system to mitigate power fluctuation of a wind farm. Breban *et al* [91] demonstrated expremently that the use

supercapacitor energy storage device in hybrid wind/microhydro power system can increase the maximum power yield.

CHAPTER 3

WIND GENERATOR SYSTEM MODEL

To study dynamic behavior of the wind-generator system as well as to design a suitable control system for dynamic performance improvement, a proper mathematical representation of the entire system considering all relevant components is very important. A complete dynamical model of wind-generator system connected to infinite bus is presented in this chapter. This is followed by frequency domain analysis.

3.1 SINGLE MACHINE INFINITE BUS SYSTEM

Fig 3.1 shows the variable speed wind turbine cage-generator system considered in this study. The system consists of a horizontal axis wind-generator connected to power grid through a set of converter-inverter-filter circuits, a step-up transformer (Tr), and the transmission line. The local load and excitation capacitor are located at the generator terminal. The models for the different components of the wind-generator system are given in the following.

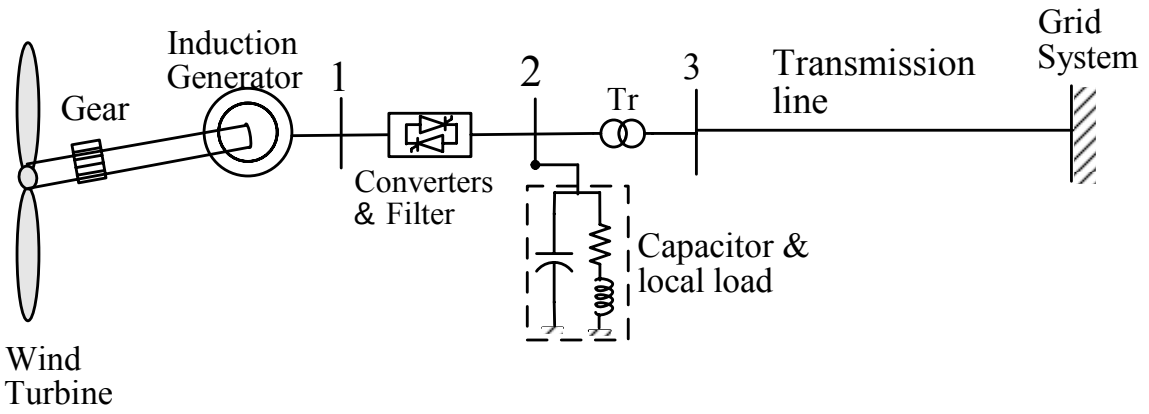

Figure 3.1: Wind generation system connected to an infinite bus.

3.2.1 **Wind Turbine Model**

The mechanical power output (P_m) of a wind turbine is related to the wind speed V_ω by [22],

$$P_m = \frac{1}{2}\rho A.C_p(\lambda,\beta).V_\omega^3 \tag{3.1}$$

Here, ρ is the air density and A is the swept area by the turbine blades. The power coefficient C_p (λ,β) depends on both blade pitch angle β and tip speed ratio, λ. The tip-speed ratio λ, which is the ratio of linear speed at the tip of blades to the speed of wind, is expressed as:

$$\lambda = \frac{\Omega R}{V_w} \tag{3.2}$$

where, R is wind turbine rotor radius and Ω is the mechanical angular velocity. Typical C_p-λ curves for the pitch angle changing from 0 to 20° are shown in Fig.3.2.

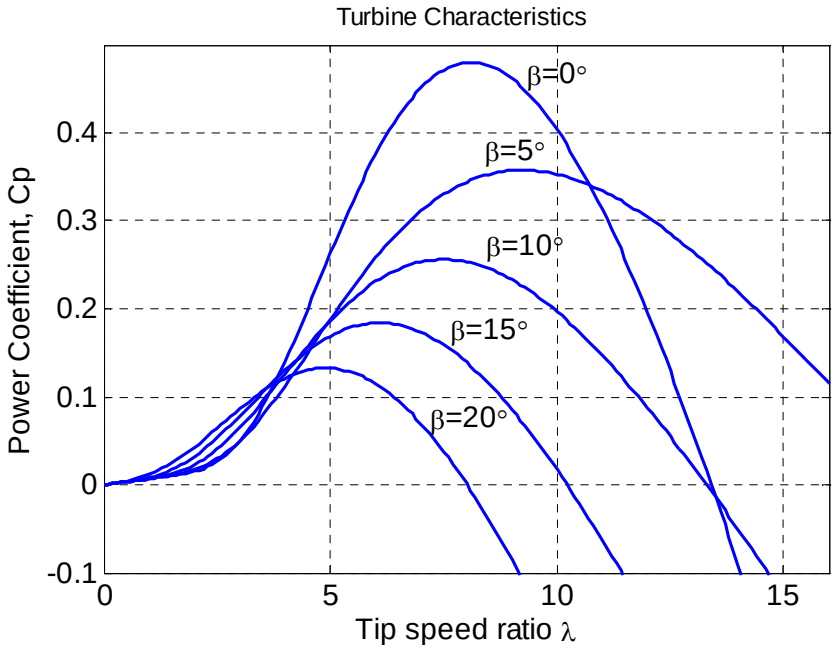

Figure 3.2: Typical power coefficient vs tip speed ratio plot

Expressions of C_p as a function of λ and β as employed in [92] are,

$$C_p(\lambda,\beta) = 0.5176\left(\frac{116}{\lambda_i} - 0.4\beta - 5\right)e^{\frac{-21}{\lambda_i}} + 0.0068\lambda$$
$$\frac{1}{\lambda_i} = \frac{1}{\lambda + 0.08\beta} - \frac{0.035}{\beta^3 + 1} \qquad (3.3)$$

Figure 3.3 shows the power-speed characteristics curves of a typical wind turbine for various wind velocities.

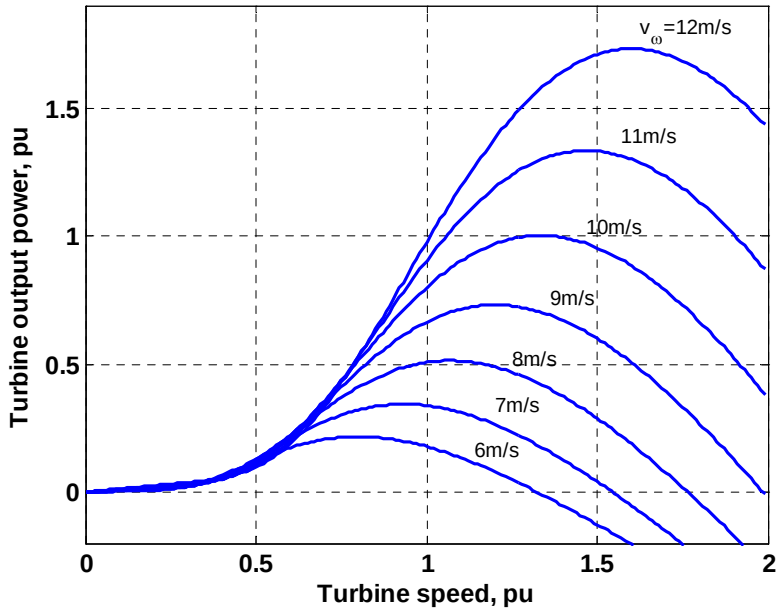

Figure 3.3: Speed vs. power output characteristics of a wind turbine

3.2.2 The Wind Profile

Wind speed simulation is one of the first steps for the wind generation model. Wind speed changes continuously and its magnitude are random over any interval. For simulation of randomly changing wind speed probability distribution of the random number should be known. The average wind speed is usually considered constant for some intervals (say about 10 minutes). The fluctuations during such intervals can be considered to be combination of constant and sinusoidal variation around the mean speed, V_m. A typical formula is [93].

$$V_\omega = V_m[1 - 0.2\cos(\frac{2\pi t}{20}) - 0.5\cos(\frac{2\pi t}{600})] \tag{3.4}$$

The wind gust can be simulated by varying the magnitude and frequency of the sinusoidal fluctuation. A typical wind profile for mean wind speed of 9 m/s is given in Fig. 3.4.

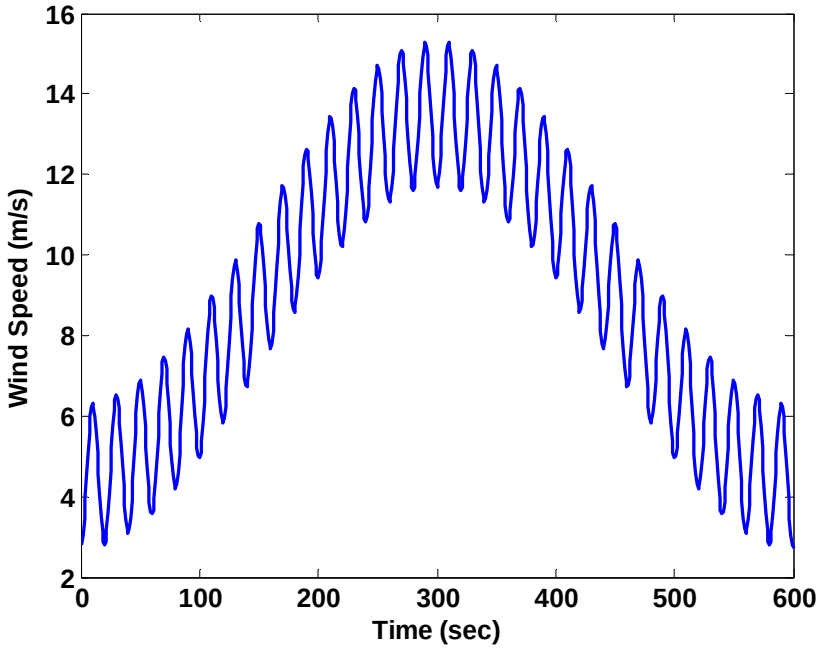

Figure 3.4: Wind profile over a period of 10 minutes

3.2.3 Drive-train model

Two-mass model is adopted here as much higher inertia wind turbine rotor is connected to the low inertia IG rotor with a relatively soft shaft. The dynamic equations of the two-mass representation are expressed as-

$$2H_t \frac{d\omega_t}{dt} = T_m - T_g - D_t\omega_t \tag{3.5}$$

$$2H_g \frac{d\omega_r}{dt} = T_g - T_e - D_g\omega_r \tag{3.6}$$

$$\frac{d\theta_s}{dt} = \omega_b(\omega_t - \omega_r) \tag{3.7}$$

The mechanical torque of the turbine rotor, T_m, and the mechanical torque applied to the generator rotor shaft, T_g, are:

$$T_m = \frac{P_m}{\omega_t} \tag{3.8}$$

$$T_g = K_s\theta_s + D_s(\omega_t - \omega_r)\omega_b \tag{3.9}$$

where θ_s is the shaft twist angle, K_s is the shaft stiffness, and D_s is the damping coefficient. The subscript *t*, *g* and *s* refer to the turbine and generator and shaft quantities respectively. T_e is the generator output torque.

3.2.4 **Induction Generator Model**

The induction generator is modeled as an equivalent voltage source, $E' = e'_d + je'_q$, behind the transient impedance, $Z' = r_s + jx'$. It is derived from the voltage-current-flux relations originally developed for induction motor [49]. In this thesis generator convention is used *i.e.* current flowing from machine towards grid is considered positive. The three-phase voltage equations of the induction machine are transformed into a synchronously rotating *d-q* frame with the *d*-axis is aligned with the stator voltage and the

q-axis is leading the *d*-axis. The detailed derivation is given in Appendix A. The dynamical equations relating voltage and current along the synchronously rotating *d-q* axes of the stator and rotor circuits, respectively, are given by –

$$\dot{i}_{ds} = -\frac{1}{x'}\left[\frac{1}{T'_o}(x_s - x') + \omega_b R_s\right] i_{ds} + \omega_e i_{qs} + (1-s)\frac{\omega_e}{x'} e'_d - \frac{1}{T'_o x'} e'_q - \frac{\omega_b}{x'} v_{ds} + \frac{x_m \omega_b}{x_r x'} v_{dr} \tag{3.10}$$

$$\dot{i}_{qs} = -\omega_e i_{ds} - \frac{1}{x'}\left[\frac{1}{T'_o}(x_s - x') + \omega_b R_s\right] i_{qs} + \frac{1}{T'_o x'} e'_d + (1-s)\frac{\omega_e}{x'} e'_q - \frac{\omega_b}{x'} v_{qs} + \frac{x_m \omega_b}{x_r x'} v_{qr} \tag{3.11}$$

$$\dot{e}'_d = -\frac{1}{T'_o}\left[e'_d - (x_s - x') i_{qs}\right] + s\omega_b e'_q - \frac{x_m}{x_{rr}} \omega_b v_{qr} \tag{3.12}$$

$$\dot{e}'_q = -\frac{1}{T'_o}\left[e'_q + (x_s - x') i_{ds}\right] - s\omega_b e'_d + \frac{x_m}{x_{rr}} \omega_b v_{dr} \tag{3.13}$$

where $x' = x_s + \dfrac{x_m x_r}{x_m + x_r}$; $\quad x_{rr} = x_m + x_r$; $\quad T'_o = \dfrac{x_m + x_r}{\omega_b R_r}$

$$e'_d = -\frac{x_m}{x_m + x_r} \psi_{qr}; \qquad e'_q = \frac{x_m}{x_m + x_r} \psi_{dr}$$

The slip s used in the above equations is defined as,

$$s = \frac{\omega_s - \omega_r}{\omega_s} \tag{3.14}$$

The symbols R, x, Ψ, ω, and s denote resistance, reactance, flux linkage, angular speed, and rotor slip respectively. The subscript s, r and b refer to the stator, rotor and base quantities respectively.

The electromagnetic torque is computed as:

$$T_e = e'_d i_{ds} + e'_q i_{qs} \tag{3.15}$$

The subscripts d and q stands for direct and quadrature axis values (in pu) respectively.

3.2.5 **Transmission line and load model**

Fig 3.5 shows the load and line model of the system is shown in Fig 3.1. V_t and V_B represent IG terminal voltage and infinite bus voltage respectively. Transformer and transmission line impedances are lumped together and represented as $z_1 = (R+jX)$. Compensating capacitor and local load are lumped together and is represented by the admittance term $Y_{11} = g_{11} + jb_{11}$.

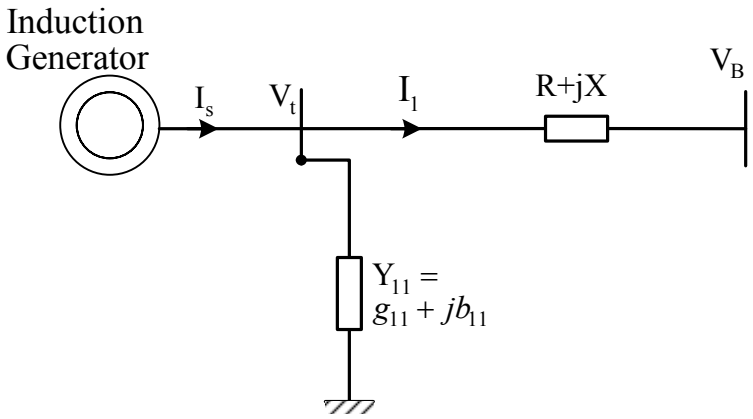

Figure 3.5: Line and load representations.

Induction generator terminal voltage is given by-

$$\bar{V}_t = \bar{V}_B + (\bar{I}_s - \bar{V}_t Y_{11}) z_1 \tag{3.16}$$

Writing voltages and current in their d-q components *i.e.* $V_t = v_{ds} + jv_{qs}$; $I_s = i_{ds} + ji_{qs}$; $V_B = V_{Bd} + jV_{Bq}$ and solving for v_{ds} & v_{qs} gives

$$\begin{bmatrix} v_{ds} \\ v_{qs} \end{bmatrix} = [C][A]\begin{bmatrix} i_{ds} \\ i_{qs} \end{bmatrix} + [C]\begin{bmatrix} V_{Bd} \\ V_{Bq} \end{bmatrix} \tag{3.17}$$

Where,

$$C = inv\big(I + [AB]\big); \qquad A = \begin{bmatrix} R & -X \\ X & R \end{bmatrix}; \quad \text{and} \quad B = \begin{bmatrix} g_{11} & -b_{11} \\ b_{11} & g_{11} \end{bmatrix}$$

3.2 NONLINEAR SYSTEM MODEL INCLUDING STATOR TRANSIENTS

For closed form dynamic representation, the turbine power output given in Fig 3.3 has to be expressed as an analytic function of the generator rotor speed or slip. For a certain wind velocity, a polynomial function has been generated through curve fitting methods using MATLAB functions '*polyfit*'. For example, for a wind velocity of 9m/sec, the expression for the power output as a function of speed n (rpm) is obtained as,

$$\begin{aligned} P_m = & -2.102\times10^{-13}n^6 + 1.305\times10^{-9}n^5 - 2.965\times10^{-6}n^4 \\ & + 28.750\times10^{-4}n^3 - 1.030n^2 + 143.348n - 4033.626 \end{aligned} \tag{3.18}$$

Differential equations (3.5) – (3.13) along with algebraic equation (3.17) can be arranged to give closed form state equations:

$$\dot{x} = f(x) \tag{3.19}$$

where,

$$x = [i_{ds} \;\; i_{qs} \;\; e'_d \;\; e'_q \;\; s \;\; \omega_t \;\; \theta_s]'.$$

The time constants of the converter circuit are not included in the model.

3.3 NONLINEAR SYSTEM MODEL NEGLECTING STATOR TRANSIENTS

In dynamic modeling, the stator current and flux transients can be neglected because of the relatively short time constant [14, 59]. ,

If stator transients are neglected then the derivatives terms in equations (3.10) & (3.11) become zero, which after some algebraic manipulations yield –

$$\begin{bmatrix} v_{ds} \\ v_{qs} \end{bmatrix} = -\begin{bmatrix} R_s & -x' \\ x' & R_s \end{bmatrix}\begin{bmatrix} i_{ds} \\ i_{qs} \end{bmatrix} + \begin{bmatrix} e'_d \\ e'_q \end{bmatrix} \tag{3.20}$$

Since i_{ds} & i_{qs} are now algebraic variables, they need to be represented in terms of state variable e'_d , & e'_q. Eliminating v_{ds} & v_{qs}, (3.17) and (3.20) can be solved for i_{ds} & i_{qs} in terms of state variables e'_d , e'_q , as

$$\begin{bmatrix} i_{ds} \\ i_{qs} \end{bmatrix} = [E]\begin{bmatrix} e'_d \\ e'_q \end{bmatrix} - [E][C]\begin{bmatrix} V_{Bd} \\ V_{Bq} \end{bmatrix} \tag{3.21}$$

Where,

$$E = inv\big([D] + [CA]\big); \qquad \text{and} \quad D = \begin{bmatrix} R_s & -x' \\ x' & R_s \end{bmatrix} \tag{3.22}$$

Combining (3.21) with the differential equations (3.5) – (3.13) the closed-form system model can be written as:

$$\dot{x} = f(x) \tag{3.23}$$

Where $x = [e'_d \;\; e'_q \;\; s \;\; \omega_t \;\; \theta_s]'$.

3.4 INITIAL VALUE COMPUTATION

Initial values of the wind-generator system are determined from the steady-state equations. At steady-state derivatives of (3.10) - (3.13) become zero. This gives steady-state equations as:

$$\left.\begin{aligned} v_{ds} &= -R_s i_{ds} + x' i_{qs} + e'_d \\ v_{qs} &= -R_s i_{qs} - x' i_{ds} + e'_q \end{aligned}\right\} \tag{3.24}$$

$$\left.\begin{aligned} \frac{x_m^2}{x_{rr}} i_{ds} + \frac{x_{rr}}{r_{rr}} s e'_d + e'_q &= \frac{x_m}{r_{rr}} v_{dr} \\ \frac{x_m^2}{x_{rr}} i_{qs} - e'_d + \frac{x_{rr}}{r_{rr}} s e'_q &= \frac{x_m}{r_{rr}} v_{qr} \end{aligned}\right\} \tag{3.25}$$

For a targeted value of power generation P_g, and expected terminal voltage V_t, steady-state torque-slip relation is solved to find operating slip s_o and reactive power absorbed (Q_{go}) by the induction generator at no-load condition. This Q_{go} is usually compensated locally and required capacitive susceptance (b_{11}) is estimated. Now for a given values of local load (g_{11}), and residual voltage v_{dr} & v_{qr}, (3.16), (3.24) & (3.25) are solved simultaneously to yield the steady values of i_{ds}, i_{qs}, e'_d, e'_q v_{ds}, and v_{qs}.

3.5 SIMULATION OF THE SINGLE MACHINE SYSTEM

To test acceptability of the reduced order model non-linear time-domain simulations are performed and compared the same with the full-order model. Fig 3.6 and Fig 3.7 show

the response of slip (Δs), and stator current (I_s) respectively, to a 15% input torque pulse applied for 0.15 sec; whereas Fig 3.8 shows response of electromagnetic torque (T_e) to a three-phase fault at the infinite bus for a duration of 75ms. Comparisons of responses show that there is no significant difference between the two models. Effect of high frequency stator transient is hardly noticeable. The oscillations settle within 2.5 sec after the fault is cleared.

The overall observation is that there is no significant difference between the two models particularly in the low frequency oscillation range. This is because the mechanical dynamics or the low frequency modes are not coupled with the stator transient mode. Moreover damping ratio of this high frequency mode is quite high. Thus neglecting the stator electrical transients will not significantly affect the performance of the system related to the electromechanical or, mechanical modes of the system.

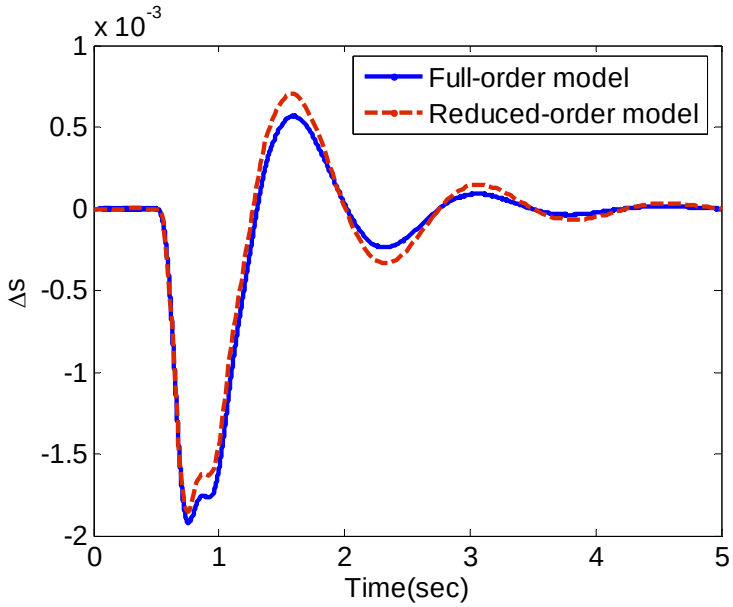

Figure 3.6: Rotor slip (Δs) response to 15% input torque pulse is applied for 0.15sec.

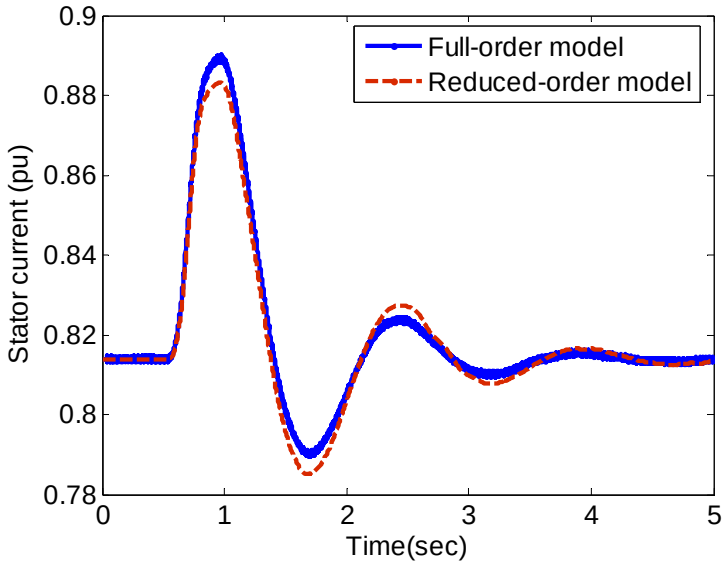

Figure 3.7: Stator current response to a 15% input torque pulse is applied for 0.15sec.

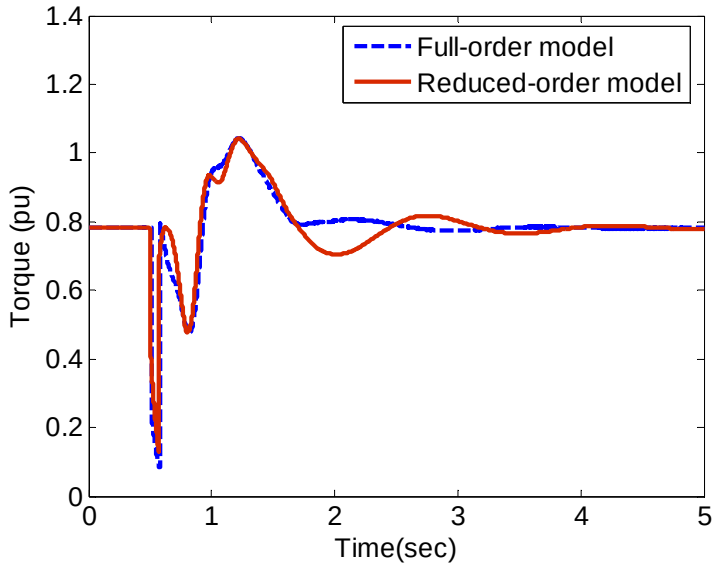

Figure 3.8: Responses of electrical torque to a three-phase fault of 75ms duration at the infinite bus.

3.6 EIGENVALUE ANALYSIS

Table 3.1 shows the system eigenvalues for the base case operating point of the wind generator system, P_g = 0.75 pu, slip *s* = - 0.0127, V_s = 1.0497 pu, mean wind-speed = 10 m/s. It also shows modal oscillation frequency, damping ratio and dominant states for different modes. Dominant states are identified by observing the participation factors as shown in Table 3.2.

TABLE 3.1: System Eigenvalues for the base case with full-order induction generator model

Eigenvalue $\lambda = \sigma \pm j\omega$	Oscillation frequency $f = \frac{\omega}{2\pi}$, Hz	Damping ratio $\xi = \frac{-\sigma}{\sqrt{\sigma^2 + \omega^2}}$	Dominant states (contribution in %)	
λ_1= - 687.56 ± j1590.9	253.2	0.3967	Stator electrical	i_{ds} = 49.79, i_{qs} = 49.76
λ_2= -4.3121± j24.533	3.9	0.173	Rotor electro-mechanical	e'_q = 41.6, s = 42.23
λ_3= -6.4443	0	1	Rotor electrical	e'_d =78.78
λ_4= -1.0555 ± j4.1953	0.6677	0.244	Turbine mechanical	ω_t = 42.44 θ_s = 36.56

Operating point: slip *s* = - 0.0127, P_g = 0.75, V_s = 1.0497

It is observed that the base case has four stable modes, three of which are oscillating at different frequency. The high frequency mode is associated with the stator electrical dynamics. The medium-frequency mode is mainly associated with the rotor electrical (e'_q) and mechanical dynamics (rotor speed, ω_r). And the low-frequency mode

of about 0.67 Hz is associated with the mechanical dynamics of the turbine (ω_t, θ_s). The non-oscillating mode is associated with the rotor electrical dynamics (e'_d). The mechanical mode is the dominant mode. It has a very low frequency (~0.6677 Hz) with a reasonable damping ratio 0.244. The electromechanical mode has a low frequency and a damping ratio of 0.173. The stator electrical mode has highest damping ratio (0.3967), and has very high frequency which is out of the range of interest. Table 3.2 shows that this mode is almost decoupled from the other modes.

TABLE 3.2. Participation Factors for the base case

	Pids	Piqs	Ped	Peq	Pslip	Pωt	Pθs
λ1	0.4979	0.4976	0.0021	0.0021	0.0003	0	0
λ2	0.0011	0.0031	0.0717	0.416	0.4223	0.0031	0.0828
λ3	0.0001	0.0008	0.7878	0.1829	0.0103	0.0057	0.0124
λ4	0.0004	0.0002	0.0555	0.1343	0.0196	0.4244	0.3656

3.7 ANALYSIS OF SYSTEM INSTABILITY

To determine effective controller for a system to enhance its stability, it is very important to diagnose the critical mode i.e. mode responsible for initiating system instability [94]. Degree of coupling between different modes, and the role of each mode in system stability would provide added information. To examine these, eigenvalues for different

generator loadings (P_g) are determined and their variations are carefully observed as described below.

The considered generator loadings are: 0.15, 0.25, 0.35, 0.45, 0.55, 0.65, 0.75, 0.85, 0.95, 1.1, 1.2, 1.25, and 1.5 pu. Z_{line} is kept constant to its base-case value (X=0.55pu, R=0.1pu). For each loading, steady-state condition is established by adjusting susceptance b_{11} such that the generator terminal voltage is approximately 1.05 pu. Modes of calculated eigenvalues are identified and contributions of individual state-variable to the modes are determined through participation factor method. Compilations of this information are presented graphically through Figs 3.9 – 3.11. Fig 3.9 shows the contour of eigenvalues with increased generator loading. Fig 3.10 shows percentage contribution of individual state-variable to the modes at different loadings. Fig 3.11 shows the variation of individual mode damping-ratio and oscillation frequency with loading.

From Fig 3.9, it can be seen that both λ_1 and λ_2 move away from the imaginary axis as the loading increases. This means that higher the loading the more stable these modes are. Fig 3.11 shows that their damping ratio increases as the generator loading increases. Fig 3.10 shows that states predominantly contributing to λ_1 are stator currents i_{ds} and i_{qs}. Participation from other states to this mode is almost negligible. States significantly participating to mode λ_2 are s and e'_q. At light loading s dominates whereas at higher loading e'_q starts dominating. The changeover of their influence on λ_2 is reflected in frequency of oscillation as shown in Fig 3.11 which is better from stability point of view.

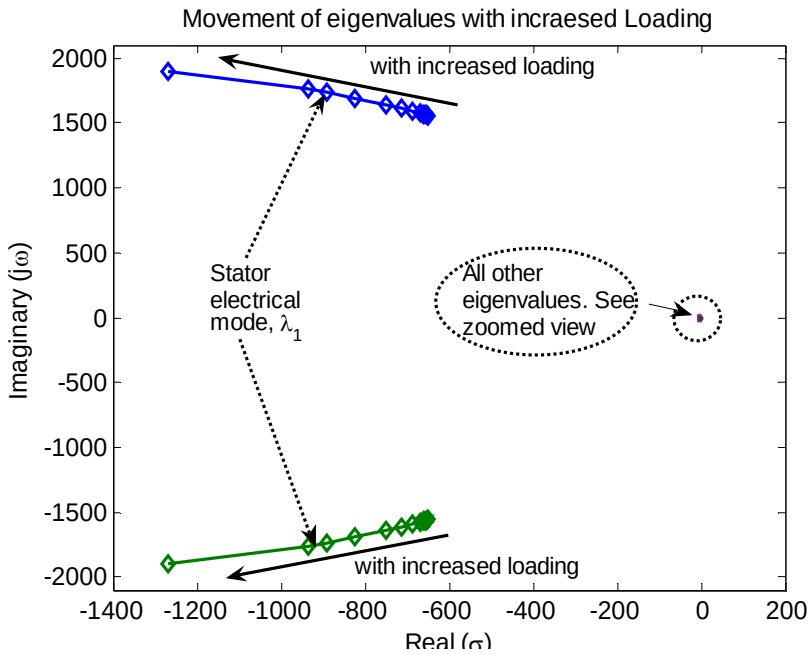

(a)

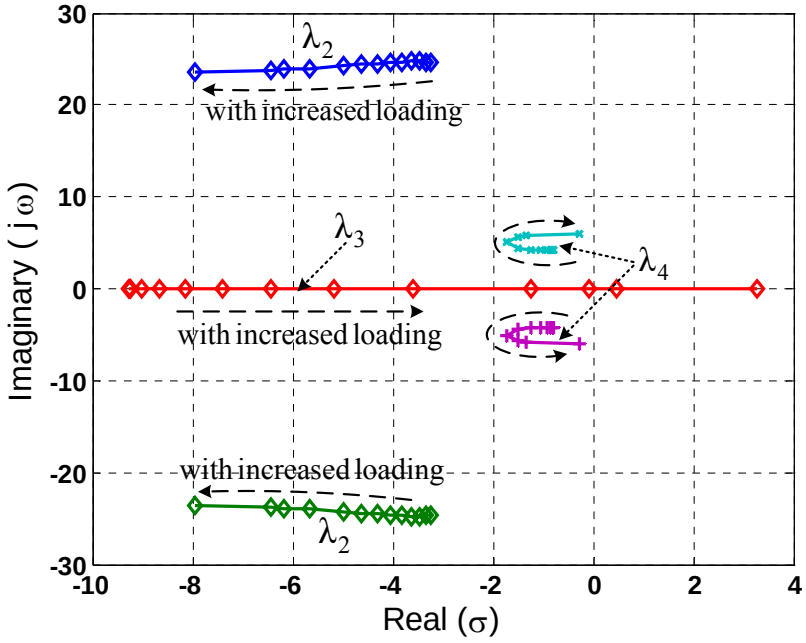

(b)

Figure 3.9: Contour of eigenvalues with the increase of generator loading (a) original plot (b) zoomed view of the portion shown in Fig 3.9(a).

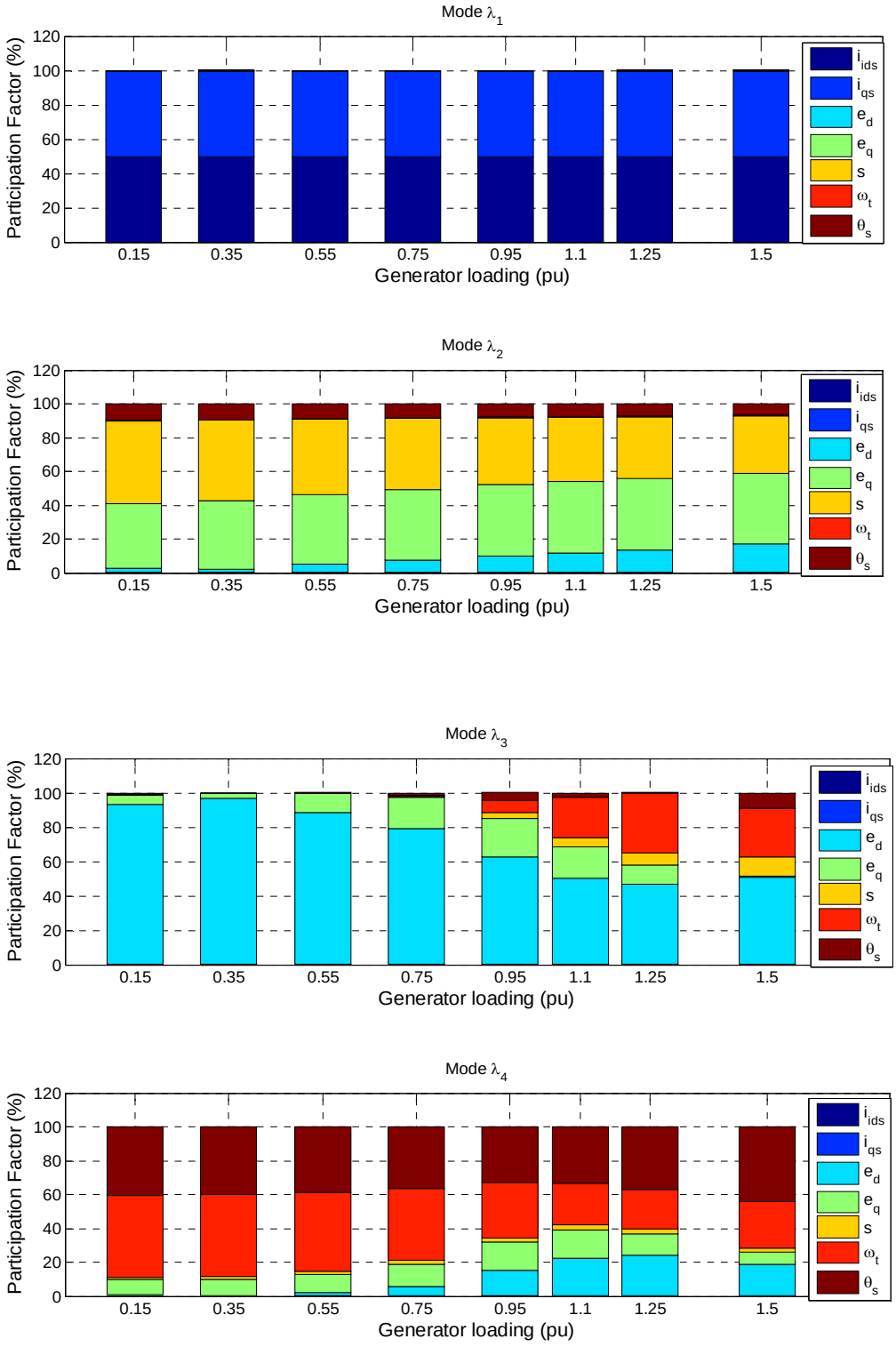

Figure 3.10: Percentage contribution of different states to modes at different generator loading.

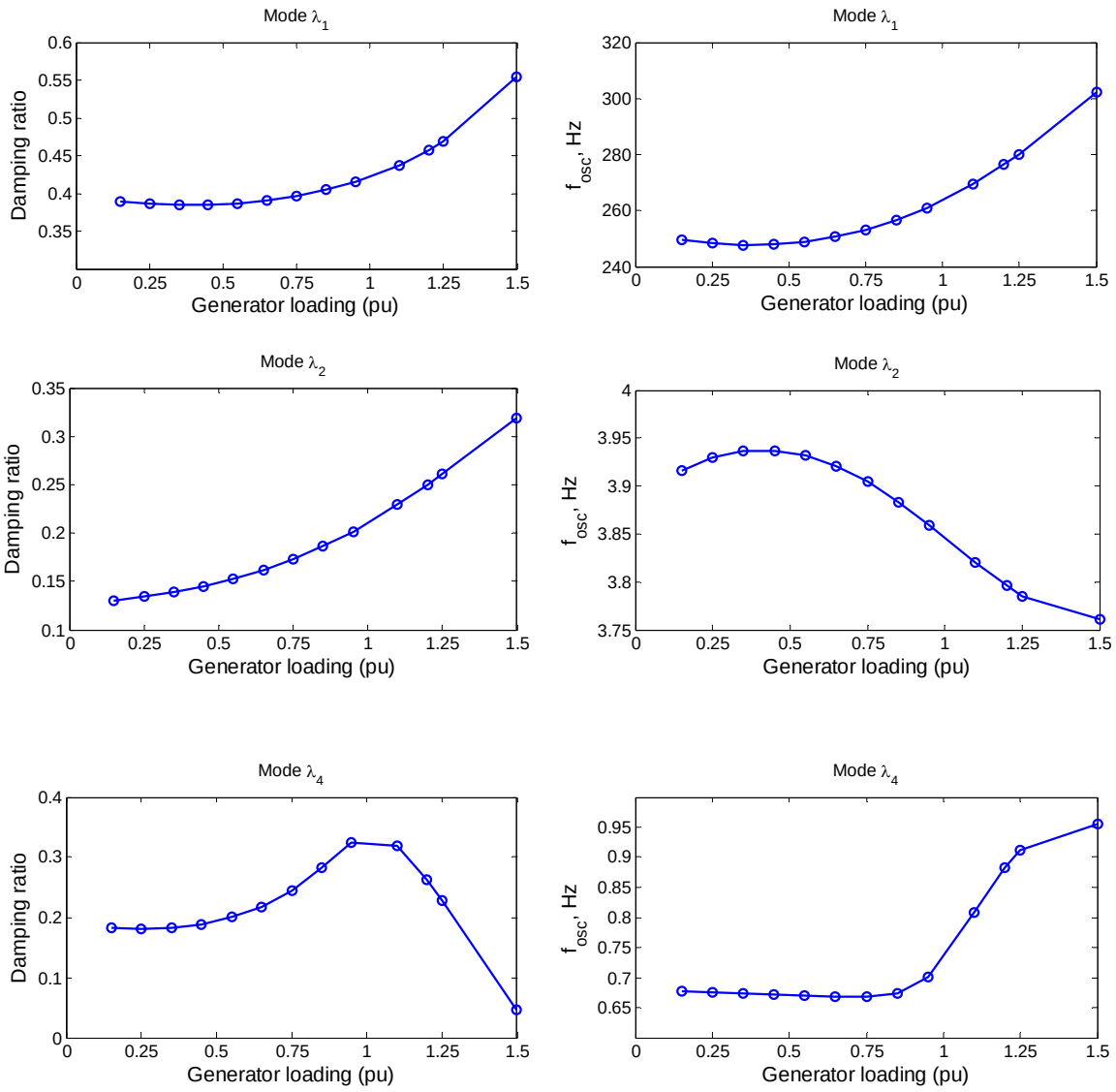

Figure 3.11: Variation of individual mode damping and oscillation frequency ratio with generator loading.

Fig 3.9 also shows that, the contour of non-oscillating mode λ_3 moves towards the imaginary axis as the loading is increased, thus deteriorating system stability. At loading around 1.25 pu, λ_3 becomes positive, thus putting entire system in an unstable state. As can be seen from Fig 3.9(b), for loading 0.15pu to 1.2 pu, λ_4, moves away from the imaginary axis.

Beyond 1.2 pu, λ_4 changes its direction, thus worsening system stability. This gives the indication on safe operating regime, which for the present case is below 1.0pu. The mode initiating system instability is λ_3. Fig 3.10 shows that, the state contributing to this mode is predominantly e'_d at lower loading upto 1.0 pu. Beyond 1.0pu participation from e'_d drops sharply and participations from ω_t, θ_s, and s start increasing. Fig 3.11 shows that beyond 1.0 pu damping ratio of λ_4 drops sharply whereas frequency of oscillation increases rapidly indicating that the system is heading towards instability. Thus, it can be concluded that λ_4 is responsible for system instability which is triggered by λ_3. To preserve system stability the contribution from e'_d to mode λ_3 should be maintained when the machine is operated at loading below 1.0 pu.

As, $e'_d = -\frac{x_m}{x_{rr}}\Psi_{qr}$, also, $\left.\begin{aligned} v_{ds} &= -R_s i_{ds} + x' i_{qs} + e'_d \\ v_{qs} &= -R_s i_{qs} - x' i_{ds} + e'_q \end{aligned}\right\}$

these indicate that any control that provides quick re-establishment of rotor flux or terminal voltage would the most effective means of averting instability following a disturbance.

As it is also observed, at the verge of system instability, the state ω_t becomes more active and its participation to mode λ_3 gets higher. This implies that, ω_t could also be another controlling variable for stabilization of the system.

CHAPTER 4

WIND GENERATOR SYSTEM CONTROL

Wind turbine driven variable speed induction generators are vulnerable to transient disturbances like wind gusts and faults on the system. As wind turbines mostly do not take part in voltage and frequency control, changes in turbine input and load may cause oscillations in frequency and voltage, leading to eventual voltage collapse. This is primarily attributed to the lack of support adaptive excitation to the system [95]. The transient under-performance can normally be compensated for by blade pitch-angle control on the turbine side, and voltage, current and power control on the generator side. Dynamic reactive power support using SVC and STATCOM has also been identified as an effective means for preventing voltage collapse. In this research, two more schemes for dynamic performance enhancement have been explored. These are –

(i) Variable susceptance excitation control

(ii) Dynamic active and reactive power compensation using STATCOM supported by bulk energy storage devices

Both battery energy storage system (BESS) and supercapacitor based energy storage system (SCESS) have been considered. Investigation of dynamic performance of both schemes (i) & (ii) have been presented in this chapter. Through detailed dynamic modeling of entire wind generation system, simulation studies have been carried out considering different contingencies.

4.1 VARIABLE SUSCEPTANCE EXCITATION CONTROL

Following transient disturbances, the reactive power demand of induction generator jumps sharply due to large variations in slip. The fixed capacitor located at the generator terminal cannot normally cater for the reactive power demand during the transient period. Thus, external supports are required for the ride through of these transients. An excitation adaptation scheme using the control of variable susceptance exhibits very good potential for quick damping of many transients arising from changes in turbine input and generator load.

The variable susceptance can be obtained by controlling a static VAR system through the firing angle control of the thyristors. The controller is connected to the grid side as shown in Fig 4.1. It contains a fixed capacitor (FC) needed for normal excitation of the induction generator. If additional capacitor excitation is required, the thyristor switched capacitor (TSC) is switched in. A reduction in capacitance is achieved by switching in the thyristor controlled reactor (TCR) into the circuit. For control purposes, the static VAR system described above is represented through a gain K_{SE} and time constant T_{SE} in the block diagram of Fig. 4.2 [96].

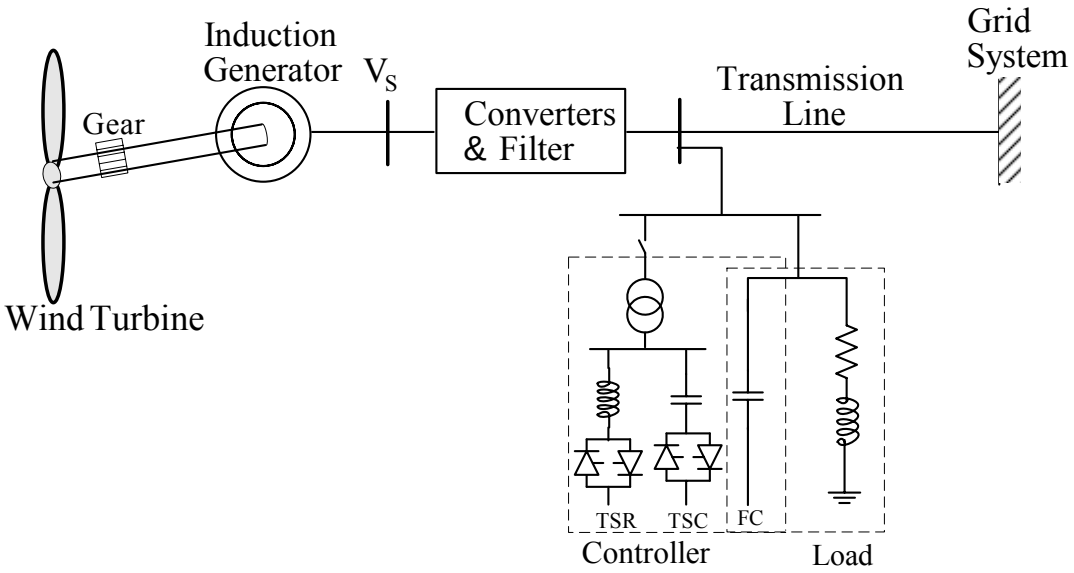

Figure 4.1: Variable susceptance controller configuration

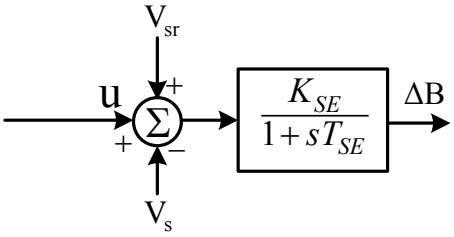

Figure 4.2: Functional block diagram of the susceptance control

The controller compares the generator terminal voltage (V_s) with a reference signal (V_{sr}) and injects susceptance (ΔB) at the terminal to keep proper excitation of the system. The TSC is switched ON when the output voltage of the induction generator (V_s)

is less than the desired or reference value (V_{sr}). The dynamic equations for the control block can be written as,

$$\frac{d\Delta B}{dt} = -\frac{1}{T_{SE}}\left[K_{SE}(V_s - V_{sr}) + \Delta B\right] + \frac{K_{SE}u}{T_{SE}} \tag{4.1}$$

From Fig 4.2 it can be observed that the susceptance injected by the control circuit is automatically adjusted depending on the terminal voltage of the induction generator. Thus, the thyristor controlled circuit injects capacitive/inductive reactance to the system depending on the system requirement, so as to maintain the generator terminal voltage constant. This in turn, will limit the excursion of other transients in the system.

4.1.1 PID Control of Susceptance

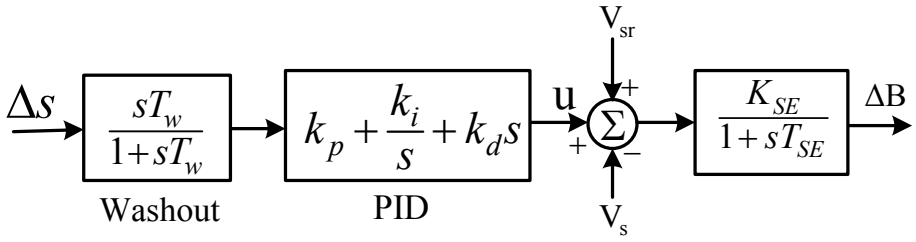

Figure 4.3: Functional block diagram of the susceptance control with PID

Further enhancement of the transient profile may be achieved by introducing additional control (u) to the thyristor control circuit as shown in Fig. 4.2. A PID control as shown in Fig 4.3 is explored for further transient performance improvement. An additional washout blocks the unwanted signal in the steady state. Though various other

controllers may have been used for generating the auxiliary control u, the PID has been used here because of its widespread use in industry and because of the ease in tuning its parameters. The input to the controller is considered to be the variation in slip of the generator.

The transfer function of the PID controller is

$$G_c(s) = K_P + \frac{K_I}{s} + K_D s \tag{4.2}$$

The parameters of the PID controller are found through a pole-placement technique for optimal damping [95]. The steps involved in determining the gain parameters are:

a) The nonlinear wind generation system equations (3.23) along with controller differential equation (4.1) are linearized around a nominal operating point. Selecting the proper output variable y, the linearized system equations are written as,

$$\begin{aligned} \dot{x} &= Ax + Bu \\ y &= Cx \end{aligned} \tag{4.3}$$

b) For a specific location of eigenvalue λ it can be shown that,

$$\frac{\lambda T_w}{1+\lambda T_w}\left[K_P + \frac{K_I}{\lambda} + K_D\lambda\right] = \frac{1}{C(\lambda I - A)^{-1}B} \tag{4.4}$$

Placing the eigenvalues at desired locations to provide adequate damping to the system, (4.4) can be solved for the values of K_P, K_I and K_D.

4.1.2 Eigenvalue Analysis and PID Controller

In the absence of auxiliary control u, the eigenvalues of the linearized system are: [-4.1729 ± j24.6476, -9.0023±j5.8799, -0.9404±j4.1426]. The damping ratio of the least damped dominant pair of eigenvalues [-4.1729 ± j24.6476] is 0.1669. The PID controller is designed to move the eigenvalues to [-5.2594 ± j24.7214], corresponding to a damping ratio of 0.2081. The gains of the PID controller K_P, K_I, and K_D are computed to be 10.4112, -6.2213, and -0.7485, respectively. The value of T_w, the washout time constant, considered to be 1.0. The gain and time constant of the first order controller block as shown in Fig 4.2 are K_{SE}=0.85, and T_{SE}=0.1, respectively.

4.1.3 Simulation Results

Grid connected wind turbine induction generation system shown in Fig. 4.1 was simulated to study the performance of variable susceptance controller. Wind generator system parameters are given in Appendix B. The transient performance of the system was tested through different disturbance scenarios for a nominal loading of 75%. The dynamic response of the system was investigated with following two scenarios –

(a) Wind generation system with no controller

(b) With variable susceptance (B) controller

4.1.3.1 Responses with Torque Pulse

Figs 4.4 - 4.5 show the variation of generator slip, and terminal voltage respectively, when the generator is subjected to a 50% torque pulse applied to the turbine shaft for only 0.75s. From the responses shown it is very clear that in the absence of any control the wind generator system voltage transients could be significant even for very small changes in the wind input. With this sudden increase in mechanical power input, induction generator accelerates and its speed reaches such a higher level that necessitates additional excitation adaptation (capacitive/inductive) to the stator circuits to develop required decelerating torque. Lack of this support, the slip of induction generator continues to grow and resulting collapse of terminal voltage.

However, in the presence of variable susceptance controller, the situation is tackled very effectively. The controller senses changes in the generator terminal voltage (V_s) and injects required susceptance (ΔB) to regulate the bus voltage at the reference level. Because of this B support, induction generator terminal voltage and slip return to the pre-disturbance state after a brief oscillation. The three plots in each figure are, (a) with no excitation control circuit, (b) with excitation control circuit, but no auxiliary control u, and (c) with additional PID in the excitation control circuit.

It can be observed from Figs 4.4 & 4.5 that the uncontrolled case leads to growing oscillation which would result in grid separation of the wind generator by the protective equipment. The excitation control, on the other hand, eliminates the transients quickly where the presence of PID controller improves the transient profile significantly. As such,

in the rest of the studies only PID assisted excitation control will be considered when it comes to the susceptance control case.

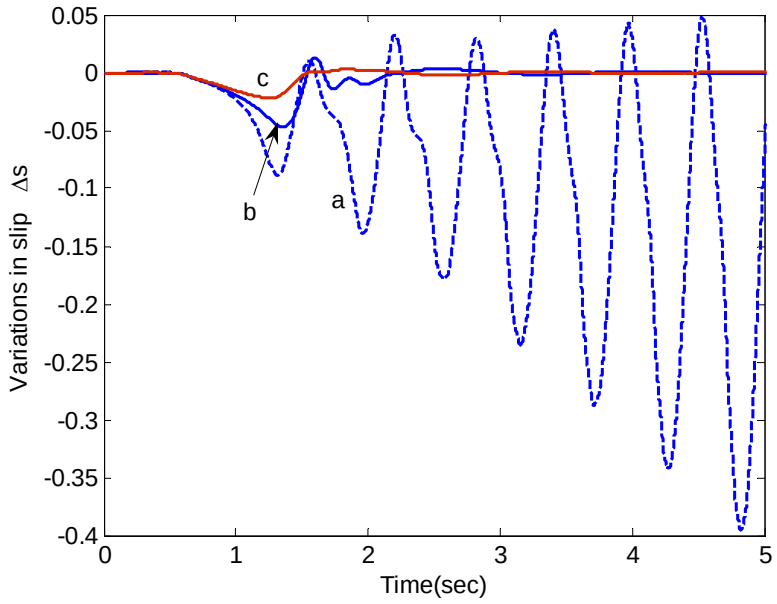

Figure 4.4: Induction generator rotor slip variation when a 50% torque pulse is applied for 0.75 sec, with (a) no excitation control circuit, (b) automatic excitation control, but no u, and (c) additional PID control with 'b'.

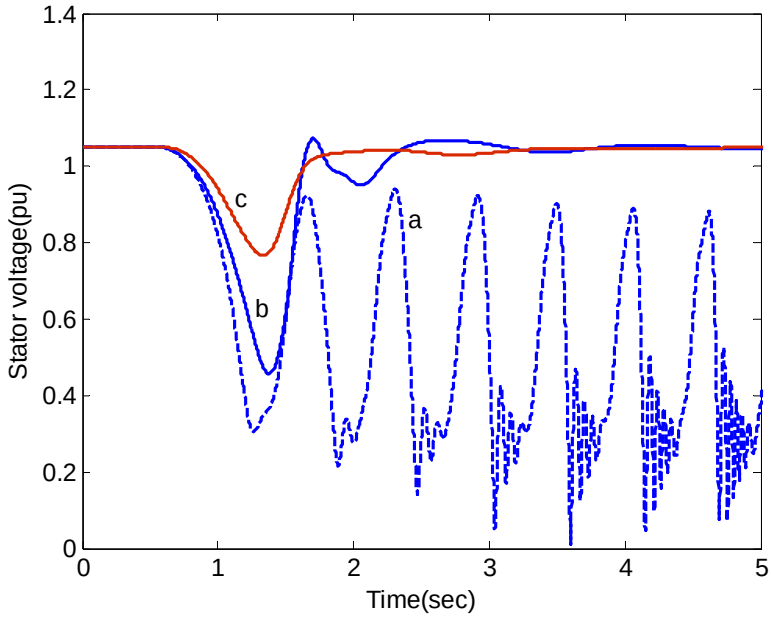

Figure 4.5: Induction generator terminal voltage variation corresponding to Fig. 4.4.

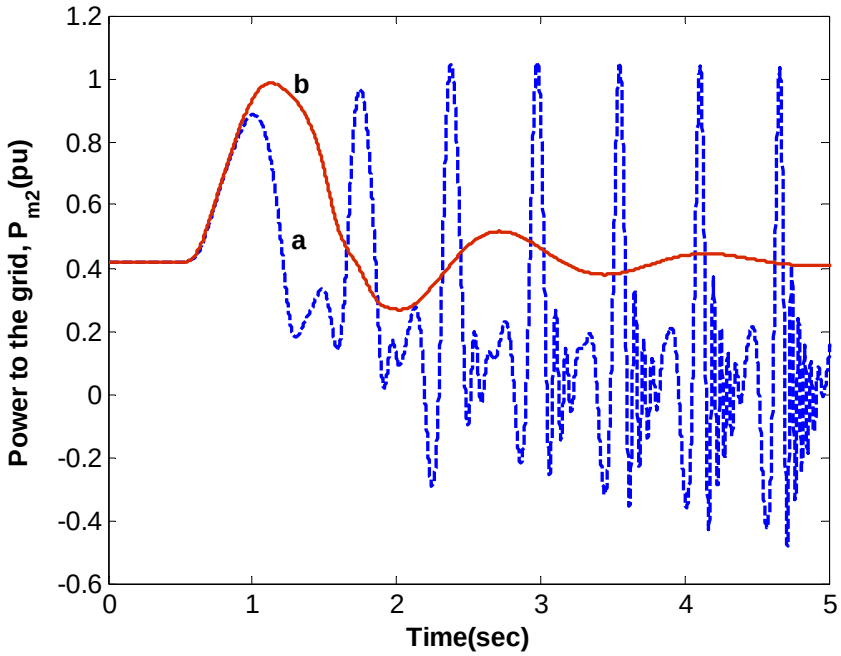

Figure 4.6: Variation in real power delivered to the grid when a 50% torque pulse is applied for 0.75 sec, with (a) no susceptance control circuit, (b) PID assisted susceptance control.

In the presence of local load, only about 0.428 pu power is available for the delivery to the grid. Fig 4.6 shows the variation in real power delivered to the grid (P_{m2}) following the 50% torque pulse. In the absence of susceptance adaptation circuit, power output from the generator becomes highly oscillatory which is reflected in P_{m2}. However, with the aid of variable susceptance control circuit the generator can continue to deliver prescribed power to the grid.

4.1.3.2 Responses with Torque Step

An increase in wind speed corresponding to a torque step of 30% was simulated to observe the transient phenomenon in the system. Figs.4.7 and 4.8 show the variations of induction electromagnetic torque (T_e) and slip (Δs) respectively, following the 30% step change in turbine power. It is clear that the generator system cannot cope with this change, and as such oscillations continue to grow. This will lead to eventual disconnection of the system when the rotor speed will exceed a certain set limit. Observe that incorporation of the variable susceptance control helps to stabilize the oscillations, which will provide enough space for new loads to be switched in the stator network. The susceptance control circuit releases the required capacitive excitation as shown in Fig. 4.9.

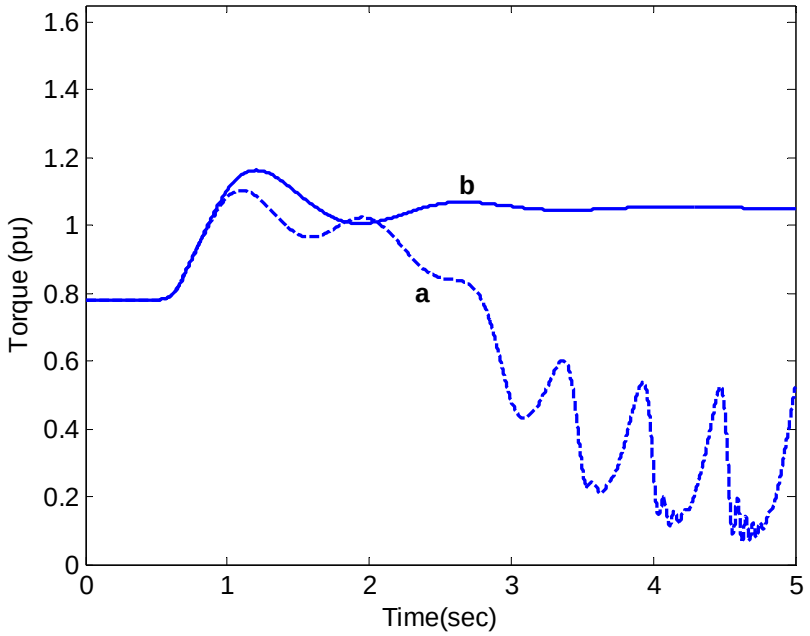

Figure. 4.7. Induction generator electromagnetic torque variations following a 30% step change in turbine power, with (a) no control, and (b) proposed susceptance control.

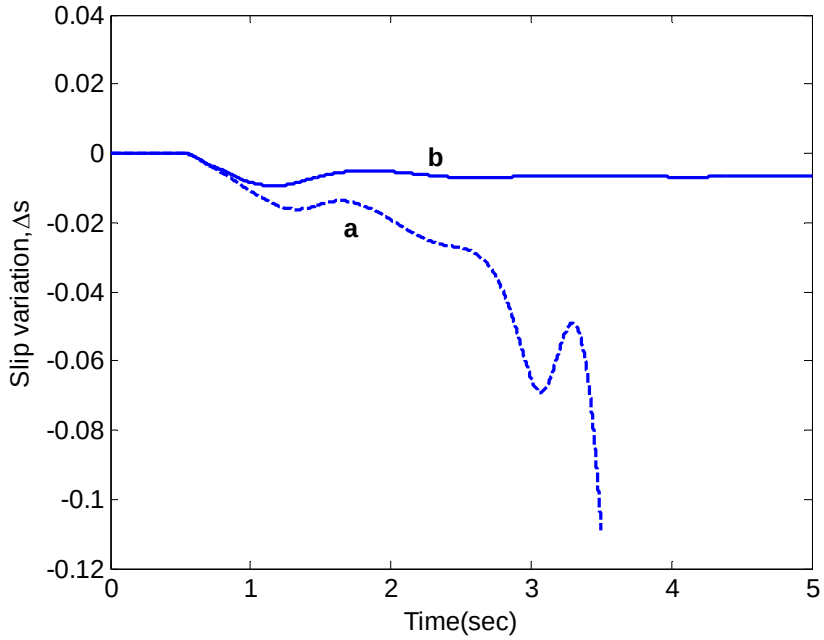

Figure 4.8. Induction generator slip variations following a 30% step change in turbine power, with (a) no control, and (b) proposed susceptance control.

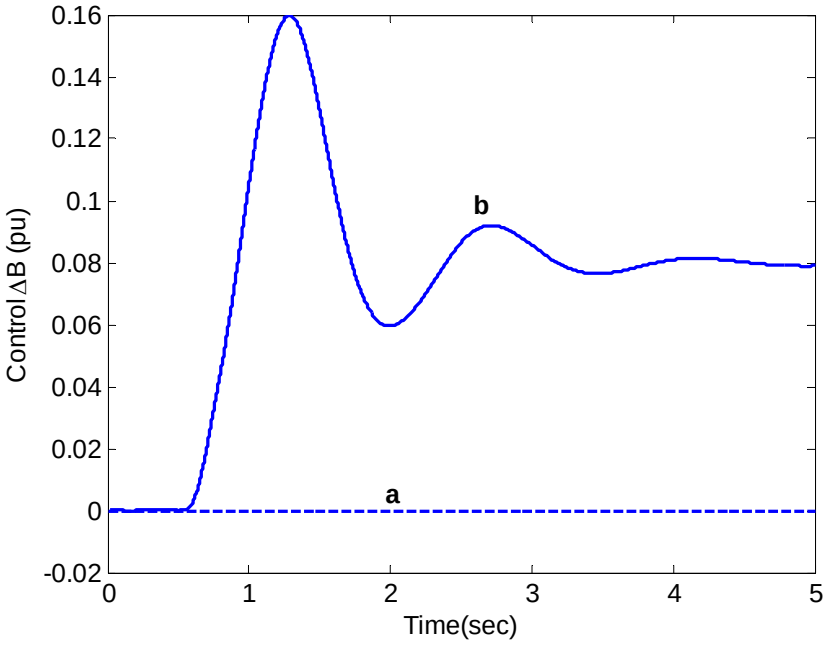

Figure 4.9. Changes in the capacitive excitation following a 30% step change in turbine power, with (a) no control, and (b) proposed susceptance control.

4.1.3.3 Responses with Three-phase Fault

For a three-phase fault on the grid for 150 ms, the transient responses are shown in Figs 4.10 – 4.12. They display the changes in generator slip (Δs), stator voltage variations, and variations in electromagnetic torque, respectively. As can be observed from the slip variations, in the absence any control the generator would need to be isolated. Incorporation of the variable susceptance control restores the generator voltage fairly quickly, and machine speed and power output return to normal, as are exhibited in Figs. 4.10-4.12. The improvement in the transient response is ascribed to the adaptation of the needed susceptance as shown in Fig 4.13.

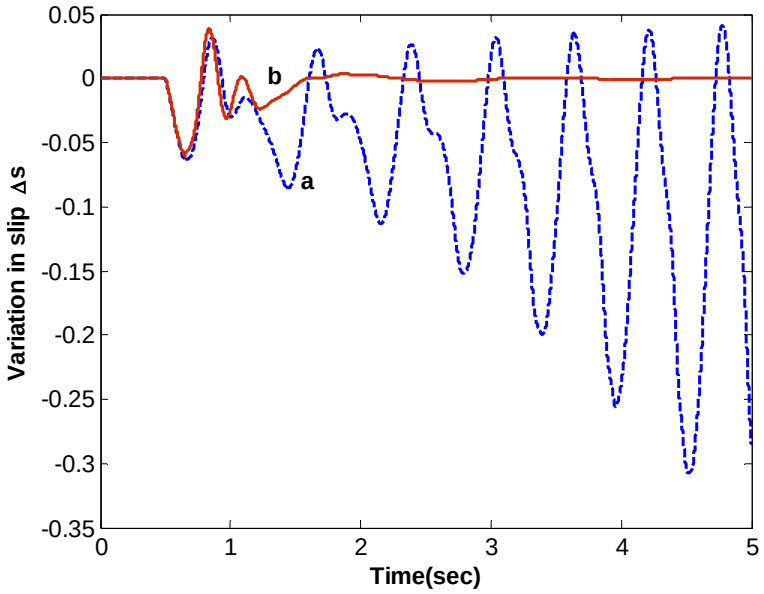

Figure 4.10: Variation in rotor slip (Δs) following momentary three-phase of 150ms duration, with (a) no susceptance control circuit, (b) PID assisted susceptance control.

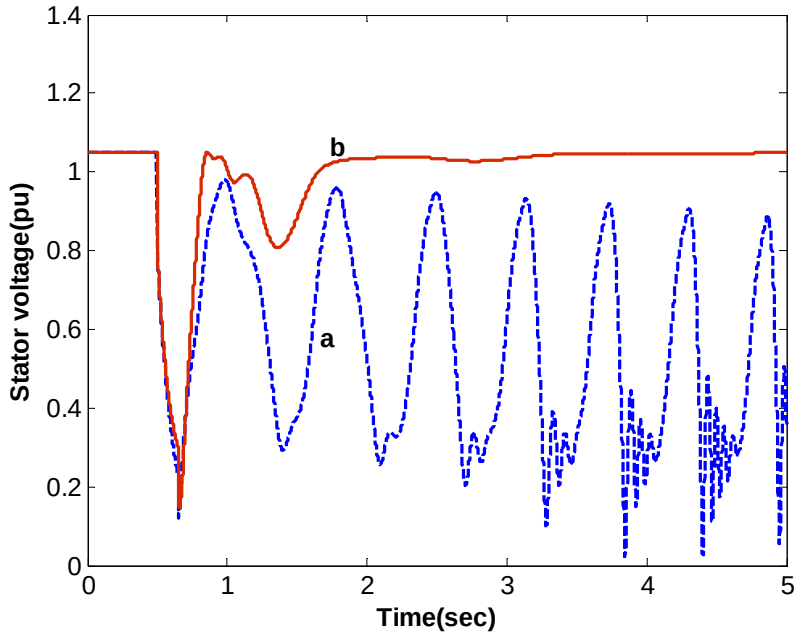

Figure 4.11: Generator terminal voltage variation corresponding to Fig. 4.10.

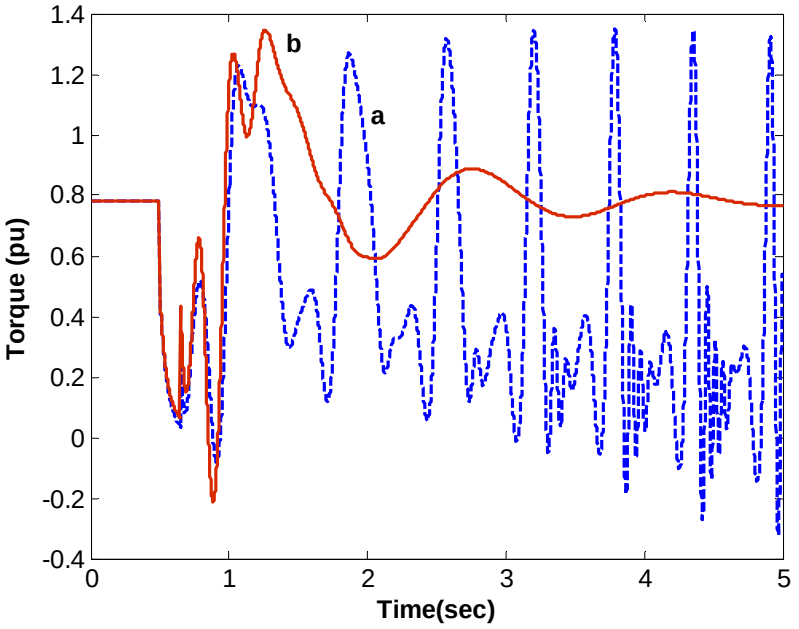

Figure 4.12: Variation in electromagnetic torque corresponding to Fig. 4.10.

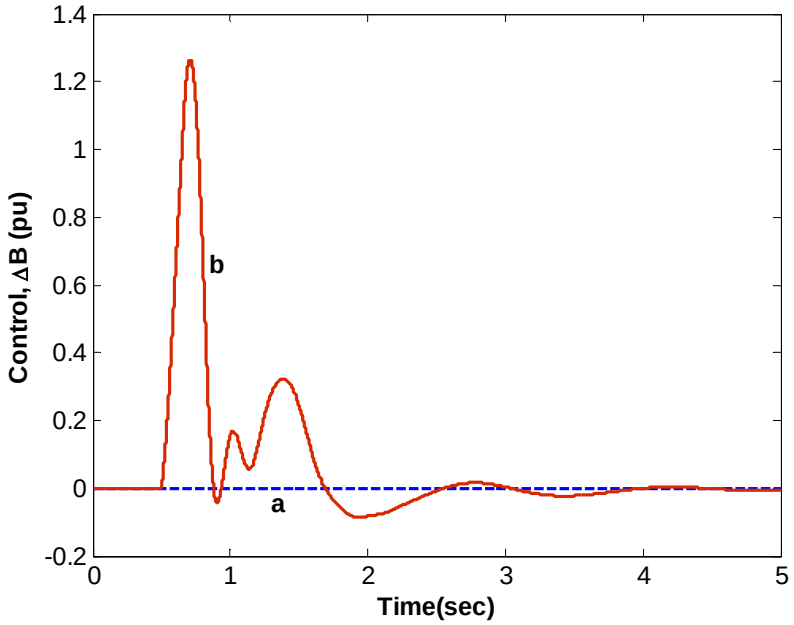

Figure 4.13: The variation of the susceptance controller output (ΔB) corresponding to Fig. 4.10.

From the responses shown in Figs 4.4 – 4.13, it is observed that variable susceptance controller is well capable of suppressing transients arising from turbine input change and/or generator load change. In the presence of such controller, many shutdown and reconnection events can be averted, and wind generator system can return to the steady-state operation smoothly. However, such controller has some operational limitations. It controls generator terminal quantities like voltage, current, or torque through the modulation of circuit parameters such as inductance or capacitance. Since these circuit parameters are passive devices, resulting control on electrical quantities takes place indirectly and is slower. This in turn causes large first swing in the response of many terminal quantities, particularly V_s as shown in Fig 4.5 & 4.11.

A variable susceptance controller basically provides reactive power (Q) compensation. It merely affects the active power flow indirectly by regulating the voltage at the point of connection with the transmission line. By adding up the provision for real power (P) compensation, the transient performance of wind generation system can further be enhanced, in particular the variations in slip (Δs) and P_{m2}. One way to have both P & Q control is STATCOM with bulk energy storage device. A common STATCOM consists of a voltage source inverter (VSI) and a DC voltage source (usually a DC capacitor). Because a DC capacitor is not a bulk energy storage device, a common STATCOM does not have the ability of active power compensation. If a bulk energy storage device is connected to the DC capacitor, the power regulation ability of a common STATCOM can be expanded to both reactive and active power compensation. Since STATCOM is also an active device, its prospect for transient performance enhancement of wind generation system is quite high.

Among the possible energy storage devices are: battery, supercapacitor, SMES (superconducting magnetic storage), fuel cell. In this work the following two energy storage devices have been considered –

- Battery energy storage system (BESS), and
- Supercapacitor energy storage system (SCESS)

4.2 STATCOM WITH BULK ENERGY STORAGE SYSTEM

A STATCOM is a shunt connected FACTS device that can generate a balanced set of three-phase sinusoidal voltages at the fundamental frequency, with rapidly controllable

amplitude and phase angle. By injecting a current of variable magnitude and almost in quadrature with the line voltage, at the point of connection with the transmission line, a STATCOM can inject reactive power to the power system.

The single machine infinite bus system considered in Fig. 3.1 is assumed to be installed with a STATCOM at the generator end through a step-down transformer (Tr) as shown in Fig. 4.14. The two control variables are: modulation index (m) and phase angle (Ψ), defined by VSC PWM. The VSC generates a variable AC voltage V_{st} whose magnitude is controlled by m. The main advantage of the STATCOM over other FACTS devices is that the STATCOM current I_{st} can be directly controlled through voltage V_{st} [97].

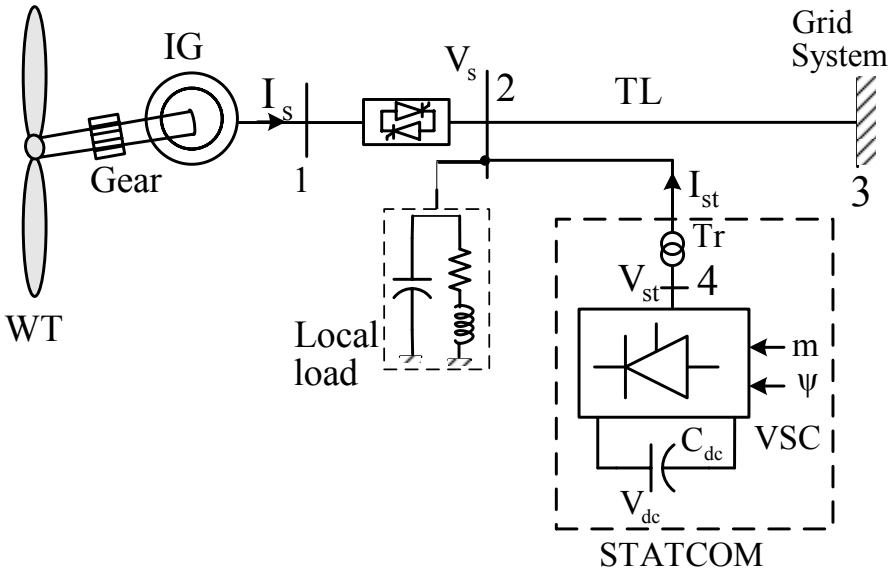

Figure 4.14: Wind generation system with STATCOM

The STATCOM is modeled as a controllable voltage source $V_{st} = mV_{dc}\angle\Psi$, where V_{dc} is the dc-link voltage. The dynamic voltage-current relationship of the STATCOM including the converter transformer is obtained from,

$$L_{st}\frac{dI_{st}}{dt} + R_{st}I_{st} = V_{st} - V_s \tag{4.5}$$

Here, R_{st} and L_{st} are the resistance and inductance of the STATCOM including the converter transformer, respectively. The above can be broken up to synchronously rotating d-q frames to yield two differential equations involving i_{std} and i_{stq}. i_{std} and i_{stq} are respectively the d axis and q axis components of I_{st}. Expressing them in per unit representation they will be of the form,

$$\frac{di_{std}}{dt} = \omega_b\left(-\frac{R_{st}}{L_{st}}i_{std} + \frac{\omega}{\omega_b}i_{stq} + \frac{mV_{dc}}{L_{st}}\cos(\psi+\theta_s) - \frac{V_s}{L_{st}}\cos\theta_s\right) \tag{4.6}$$

$$\frac{di_{stq}}{dt} = \omega_b\left(-\frac{\omega}{\omega_b}i_{std} - \frac{R_{st}}{L_{st}}i_{stq} + \frac{mV_{dc}}{L_{st}}\sin(\psi+\theta_s) - \frac{V_s}{L_{st}}\sin\theta_s\right) \tag{4.7}$$

The dynamics of the dc link voltage V_{dc} is given by [30]

$$\frac{dV_{dc}}{dt} = -\frac{m}{C_{dc}}\left(i_{std}\cos(\psi+\theta_s) + i_{stq}\sin(\psi+\theta_s)\right) \tag{4.8}$$

Here, θ_s is the phasor angle of V_s. The corresponding phasor angle of V_{st} is $(\psi + \theta_s)$.

4.2.1 STATCOM with Battery Energy Storage System

STATCOM provides the option of interfacing energy storage device or real power source across the dc-link capacitor [98]. Fig. 4.15 shows the section of such a STATCOM with battery energy storage system (STATCOM/BESS), which is connected to the system bus 2 corresponding to Fig. 4.14. The battery is represented by an ideal DC voltage source V_{batt}, and a resistor R_b. R_b can also account for any loss in the inverter. The battery is represented by this simple model because of the fact that STATCOM/BESS is used here to improve system's transient stability. In this short period of the system transient, there should be no significant variation to the potential of the battery.

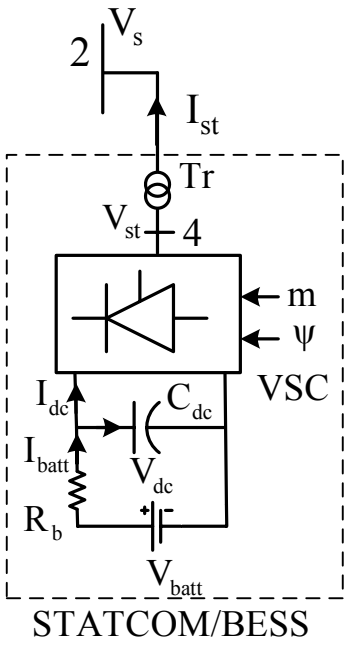

Figure 4.15: STATCOM with battery energy storage system

Applying KCL on the dc side of the STATCOM, the dynamic equation of the dc link voltage V_{dc} is can be obtained as (details in Appendix C)

$$\frac{dV_{dc}}{dt} = -\frac{m}{C_{dc}}\left(i_{std}\cos(\psi+\theta_s) + i_{stq}\sin(\psi+\theta_s)\right) + \frac{V_{batt}-V_{dc}}{R_b C_{dc}} \tag{4.9}$$

The other two equations (4.6) & (4.7) are also applicable to STATCOM/BESS.

4.2.2 STATCOM with Supercapacitor Energy Storage System

Fig. 4.16 shows the section of the STATCOM with supercapacitor energy storage system (STATCOM/SCESS), which is connected to the system bus 2 corresponding to Fig. 4.14. The SCESS comprises the supercapacitors, and a bi-directional DC-DC buck-boost converter to control the charge and discharge of the supercapacitor module. The operation of buck-boost converter is controlled by varying the duty ratio (D_r) of the switches S_1 & S_2.

The supercapacitor is modeled by an ideal capacitance and an equivalent series resistance (ESR) as shown in Fig. 4.17. The ESR accounts for resistive losses in the dielectric, plate material, and electrolytic solution. The actual capacitance and ESR are dependent on terminal voltage, voltage charge rate, current, and temperature. However, within the capacitor's working region, fixed value capacitance and ESR can accurately model a real supercapacitor.

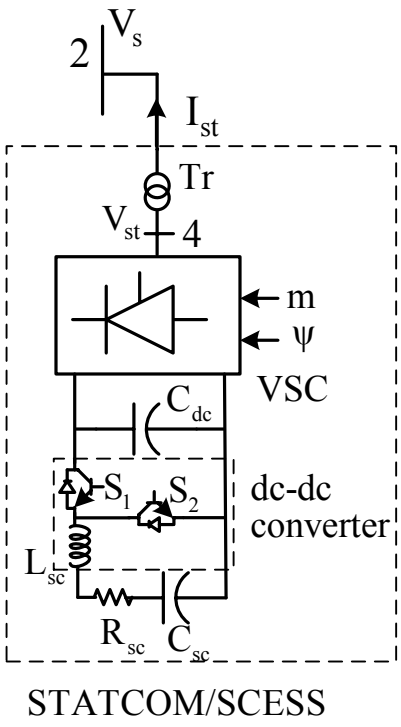

Figure 4.16: STATCOM with supercapacitor energy storage system

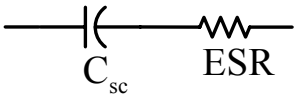

Figure 4.17: Supercapacitor model

Similar to (4.9), by applying KCL on the dc side of the STATCOM, the dynamic equation of the dc link voltage V_{dc} is can be obtained as (details in Appendix C)

$$\frac{dV_{dc}}{dt} = -\frac{m}{C_{dc}}\left(i_{std}\cos(\psi+\theta_s) + i_{stq}\sin(\psi+\theta_s)\right) - \frac{D_r I_{sc}}{C_{dc}} \tag{4.10}$$

where I_{sc} is the supercapacitor current. Supercapacitor voltage *Vsc* is given by-

$$V_{sc} = E_{sc} + R_{sc} I_{sc}; \quad \text{with } I_{sc} = C_{sc} \frac{dE_{sc}}{dt} \tag{4.11}$$

The other two equations (4.6) & (4.7) remain unchanged for STATCOM/SCESS model.

4.3 THE COMPOSITE SYSTEM MODEL

In all three systems shown in Fig 4.14 - 4.16, the STATCOM is considered to be a current source, injecting current I_{st} to the line. Referring to Fig 4.14, the STATCOM current I_{st} is linked with rest of the system through

$$V_s = V_B + (R + jX)(I_s + I_{st} - V_s(g_{11} + jb_{11})) \tag{4.12}$$

where (R+jX) represents the impedance of the transmission line, and (g_{11}+jb_{11}) represents the admittance of the local load including capacitance required for normal excitation at steady-state. Writing voltage and current phasors in d-q components, (4.12) can be solved for v_{ds} & v_{qs}, and substituting these in (3.24) gives the expression for stator current components (i_{ds} & i_{qs}) in terms of state variables as

$$\begin{bmatrix} i_{ds} \\ i_{qs} \end{bmatrix} = [K_1] \begin{bmatrix} e'_d \\ e'_q \end{bmatrix} + [K_2] \begin{bmatrix} i_{std} \\ i_{stq} \end{bmatrix} + [K_3] \begin{bmatrix} V_{Bd} \\ V_{Bq} \end{bmatrix} \tag{4.13}$$

Here, K_1, K_2, and K_3 are matrices which depend on system impedances and admittances. Combining (4.13) with the differential equations (3.5) – (3.13), (4.6) – (4.9) gives the closed-form state model of wind generation system supported by STATCOM/BESS as-

$$\dot{x} = f(x,u) \tag{4.14}$$

Here, x is the vector of states $[e'_d, e'_q, s, \omega_t, \theta_t, i_{std}, i_{stq}, V_{dc}]^T$, and u is the control variable $[m, \psi]^T$.

For the case of STATCOM/SCESS, (4.9) is replaced by (4.10) & (4.11), which gives states and control vectors in (4.14) as

$$x = [e'_d, e'_q, s, \omega_t, \theta_t, i_{std}, i_{stq}, V_{dc}, E_{sc}]^T \quad \text{and } u = [m, \psi, D_r]^T.$$

4.4 STATCOM ESS CONTROL

At steadystate, the STATCOM/ESS is considered floating *i.e.* $I_{st} = 0$. At the contingency period, STATCOM/ESS controller injects necessary real and/or reactive power to bring the system to normal steady-state condition. The amount of real and reactive power injected by the STATCOM is given by –

$$\begin{aligned} P_{st} &= V_s \cos\theta_s i_{std} + V_s \sin\theta_s i_{stq} \\ Q_{st} &= V_s \sin\theta_s i_{std} - V_s \cos\theta_s i_{stq} \end{aligned} \tag{4.15}$$

For this dual power control, it is necessary to have independent control of P_{st} and Q_{st} so that the controllers can inject needed real and/or reactive power in a decoupled manner. The decoupled P – Q control strategy is obtained by defining a new set of STATCOM currents as –

$$I_{st}^{new} = I_{st} e^{-j\theta_s}$$

This makes

$$P_{st} = V_s i_{std}^{new};\ \text{and}\quad Q_{st} = -V_s i_{stq}^{new} \tag{4.16}$$

P_{st} and Q_{st} can then be controlled independently by i_{std}^{new} and i_{stq}^{new}.

4.4.1 Decoupled P - Q Control

From (4.16) it can be observed that P_{st} depends on i_{std} and Q_{st} depends on i_{stq}. Thus, realizing P-Q decoupled control means realizing i_{std}, i_{stq} decoupled control. With I_{st}^{new}, (4.6), and (4.7) can be written as [26]:

$$\frac{d}{dt}\begin{bmatrix} i_{std}^{new} \\ i_{stq}^{new} \end{bmatrix} = \omega_b \begin{bmatrix} -\frac{R_{st}}{L_{st}} & 0 \\ 0 & -\frac{R_{st}}{L_{st}} \end{bmatrix} \begin{bmatrix} i_{std}^{new} \\ i_{stq}^{new} \end{bmatrix} + \begin{bmatrix} u_1 \\ u_2 \end{bmatrix} \tag{4.18}$$

where

$$\begin{bmatrix} u_1 \\ \\ u_2 \end{bmatrix} = \omega_b \begin{bmatrix} \frac{\omega}{\omega_b} i_{stq}^{new} + \frac{mV_{dc}}{L_{st}} \cos\psi - \frac{V_s}{L_{st}} \\ \\ -\frac{\omega}{\omega_b} i_{std}^{new} + \frac{mV_{dc}}{L_{st}} \sin\psi \end{bmatrix} = \omega_b \begin{bmatrix} \frac{\omega}{\omega_b} i_{stq}^{new} + \frac{e_{xd}}{L_{st}} - \frac{V_s}{L_{st}} \\ \\ -\frac{\omega}{\omega_b} i_{std}^{new} + \frac{e_{xq}}{L_{st}} \end{bmatrix} \tag{4.19}$$

Defining

$$e_{xd} = mV_{dc}\, cos\,\psi \quad \text{and} \quad e_{xq} = mV_{dc}\, sin\,\psi$$

Equation (4.19) can be written as

$$\begin{aligned} e_{xd} &= \frac{L_{st}}{\omega_b}(u_1 - \omega i_{stq}^{new}) + V_s \\ e_{xq} &= \frac{L_{st}}{\omega_b}(u_2 + \omega i_{std}^{new}) \end{aligned} \tag{4.20}$$

$$m = \frac{\sqrt{e_{xd}^2 + e_{xq}^2}}{V_{dc}} \quad \text{and} \quad \psi = \tan^{-1}\left(\frac{e_{xq}}{e_{xd}}\right) \tag{4.21}$$

Equation (4.18) shows that i_{std} and i_{stq} (*new*) respond to u_1 and u_2 respectively, through a simple first-order transfer function, with no crosscoupling. Thus providing decoupled control of i_{std} and i_{stq}. The control rule of equation (4.19) is thus completed by defining the feedback loops and PI compensation as follows:

$$u_1 = \left(k_{p1} + \frac{k_{i1}}{s} \right)\left(i_{std}^{*} - i_{std} \right)$$
$$u_2 = \left(k_{p2} + \frac{k_{i2}}{s} \right)\left(i_{stq}^{*} - i_{stq} \right) \qquad (4.22)$$

The inverter voltage vector is controlled through the m and ψ defined in (4.21). A block diagram of the control scheme is presented in Fig. 4.18.

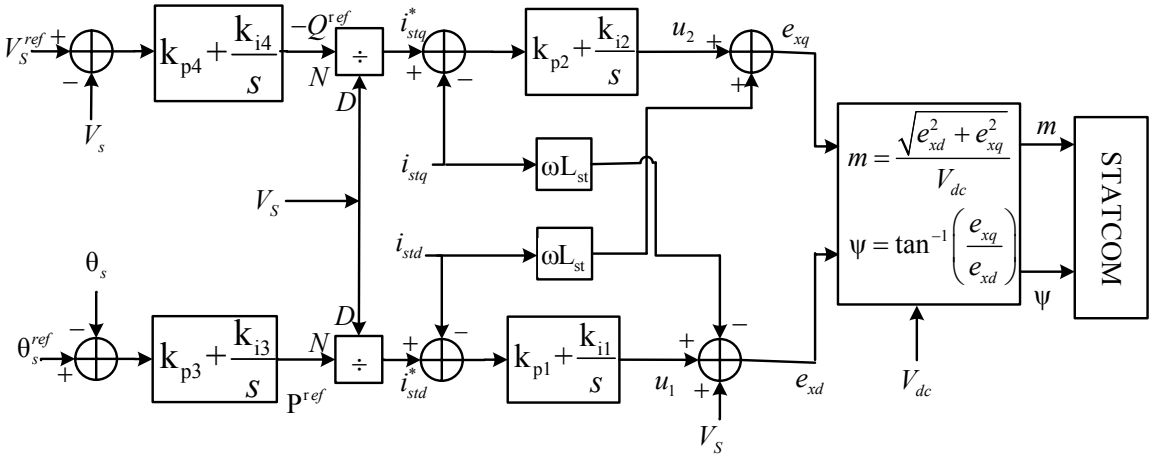

Figure 4.18: Block diagram for the decoupled P – Q control scheme of STATCOM.

4.4.2 Generation of P^{ref} and Q^{ref} for the STATCOM Controller

Among the control objectives are (i) to regulate voltage at bus 2 by injecting/absorbing required reactive power, and (ii) to minimize variations in real power delivered to the grid P_{m2}. Q^{ref} is generated by sensing the deviation of voltage magnitude at bus 2 *i.e* ($V_s^{ref} - V_s$) where V_s^{ref} is the predisturbance voltage magnitude. Similarly, P^{ref} is generated by sensing

the deviation of bus voltage angle i.e (θ_s^{ref} - θ_s), where θ_s^{ref} is the pre-disturbance bus voltage angle. PI controllers used to ensure zero steady-state error. Fig. 4.18 shows the generation of P^{ref} and Q^{ref}. Corresponding i_{std}^{ref} and i_{stq}^{ref} are generated using (4.16).

4.4.3 DC-DC Converter Control with the Supercapacitor Circuit

The charging and discharging of supercapacitor is controlled by varying the duty-ratio (D_r) of the switches S_1 & S_2 associated with dc-dc converter. As shown in Fig. 4.16, the main circuit of the bidirectional dc-dc converter (buck-boost converter) contains three energy storage components i.e. the dc-link capacitor (C_{dc}), the choke (L_{sc}) and the super capacitors (C_{sc}). Among the objectives of the control are: (i) to regulate the dc-link voltage with energy stored in the supercapacitor (SC), and (ii) to keep the SC voltage V_{sc} in its desired operating range. These are achieved through the use of two controllers (i) dc-link voltage controller, and (ii) SC current controller as shown in Fig. 4.19.

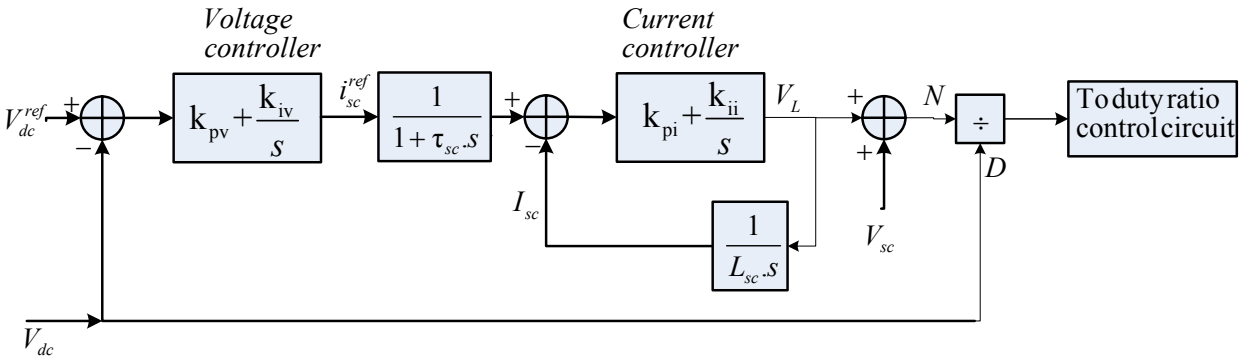

Figure 4.19: Block diagram for the DC-DC converter control scheme.

The measured dc-link voltage (V_{dc}) is compared to the reference V_{dc}^{ref} and the error is taken into the PI voltage controller which outputs the reference currents I_{sc}^{ref}. The voltage reference for the converter V_{pwm}^{ref} is obtained as the sum of SC voltage V_{sc} and the inductor voltage reference V_L^{ref} obtained from the current loop PI controller. Mathematically it can be expressed as –

$$(V_{dc}^{ref} - V_{dc})(k_{pv} + \frac{k_{iv}}{s}) = I_{sc}^{ref} \tag{4.23}$$

$$(I_{sc}^{ref} - I_{sc})(k_{pi} + \frac{k_{ii}}{s}) = V_L^{ref} \tag{4.24}$$

$$(V_L^{ref} + V_{sc}) = V_{pwm}^{ref} \tag{4.25}$$

$$Duty\,ratio,\ D_r = \frac{(V_L + V_{sc})}{V_{dc}} \tag{4.26}$$

The response of current controller must be fast enough with good reference tracking capability. Following the design procedure suggested in [99], the gain values of current controller are calculated.

4.5 SIMULATION RESULTS

4.5.1 STATCOM with BESS

STATCOM supported wind generation system shown in Fig 4.14 was simulated to study the performance of the decoupled P – Q compensation scheme. BESS is considered as the source of real power compensation. It is assumed that BESS can supply 0.5 pu of power during discharging and can absorb 0.15 pu power during charging *i.e.* $P_{st}^{max} = 0.5\text{pu}$ and $P_{st}^{min} = -0.1\text{pu}$. The dynamics of the BESS is neglected. The transient performance of the system was tested through different disturbance scenarios for a nominal loading of 75%. The dynamic response of the system was investigated with following three scenarios –

(a) Wind generation system with no control

(b) With STATCOM and Q control only

(c) With STATCOM/BESS and both P – Q control

4.5.1.1 Responses with Wind Gust

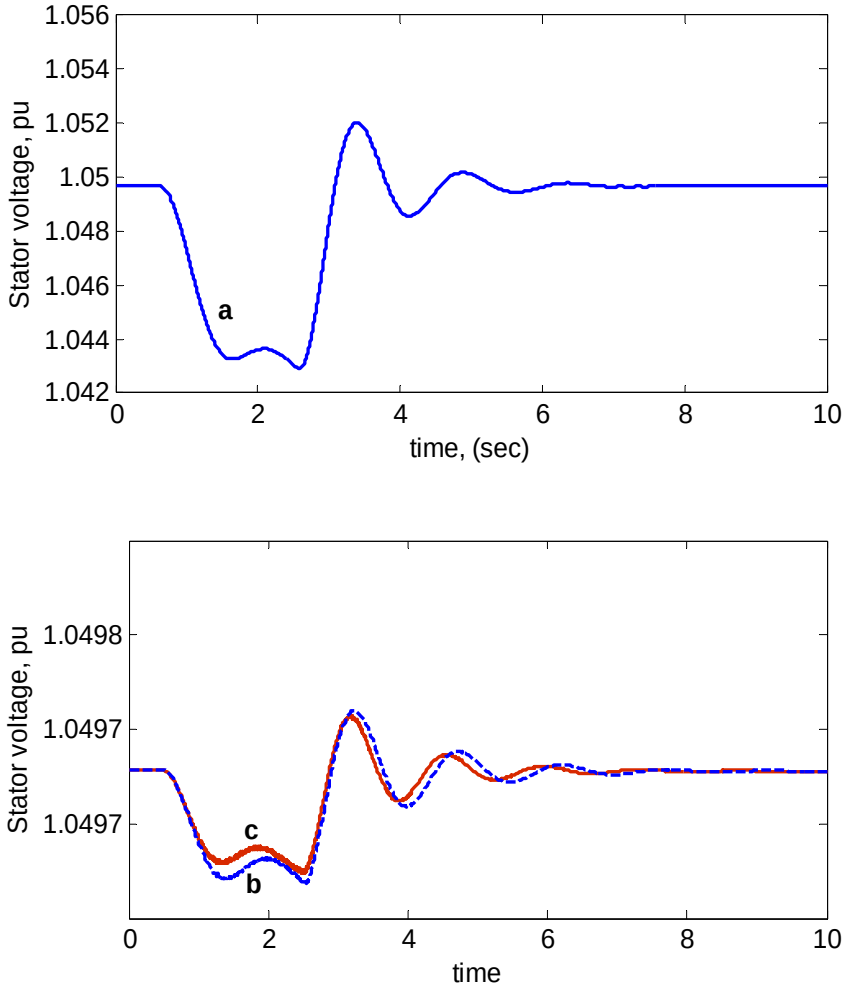

Figure 4.20: Induction generator terminal voltage variations following a short 2 sec wind gust applied to the generator model. The nominal load is 75%. (a) without control (b) with STATCOM Q control (c) with STATCOM/BESS both P & Q control.

Figs. 4.20 and 4.21 show the variations of generator terminal voltage and power delivered to the grid, respectively when subjected to a wind gust for 2sec. The wind gust model considered is given in (3.4). It can be observed that the transient peak becomes quite high

even for this short duration gust. Incorporation of STATCOM/BESS suppresses these variations to a very negligible value. The Q controller eliminates the terminal voltage variations by injecting required reactive power (Q_{st}), whereas the P controller cancels out the variations in real power (P_{m2}) delivered to the grid as shown in Figs. 4.20 & 4.21 respectively. The variations of injected real power (P_{st}) is shown in Fig. 4.22. P_{st} is in phase opposition with the ripples of P_{m2}, thus nullify the variations. The voltage responses with (b) & (c) are almost same. This demonstrates the decouple nature of the controller.

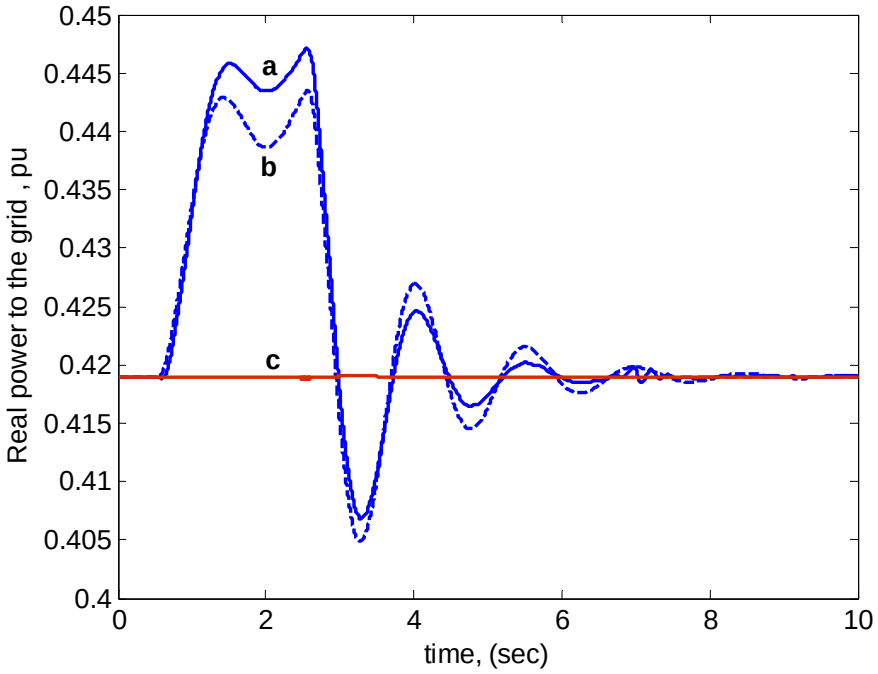

Figure 4.21: Variations of induction generator delivered power to the grid (P_{m2}) following a short 2 sec wind gust applied to the generator model. The nominal load is 75%. (a) without control (b) with STATCOM Q control (c) with STATCOM/BESS both P & Q control.

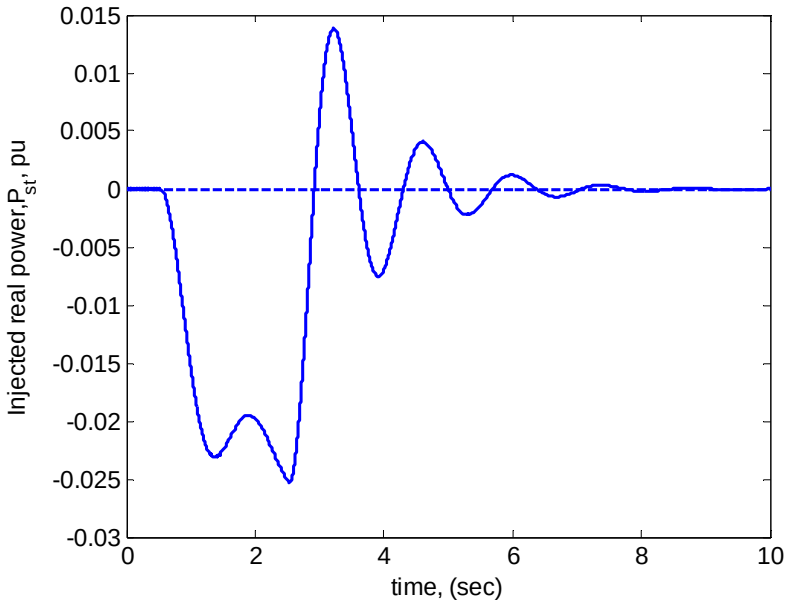

Figure 4.22: Injected real power by the STATCOM/BESS P controller (P_{st}) following a short 2 sec wind gust applied to the generator model. The nominal load is 75%. (a) without control (b) with STATCOM Q control (c) with STATCOM/BESS both P & Q control.

4.5.1.2 Wind Power Smoothing

One of the main problems of wind energy is power fluctuations due to wind speed variations. The wind energy is not only intermittent but also fluctuating. Therefore, wind power cannot be dispatched the same as other power sources. Power fluctuations, in systems with high wind power penetration, causes frequency deviations as well as voltage deviation in the grid.

The decoupled P – Q control based STATCOM/BESS can suppress wind power fluctuations and help delivery of smoothed power to the grid. To demonstrate this, a randomly varying wind speed is generated as shown in Fig 4.23 using (4.27) [42, 45].

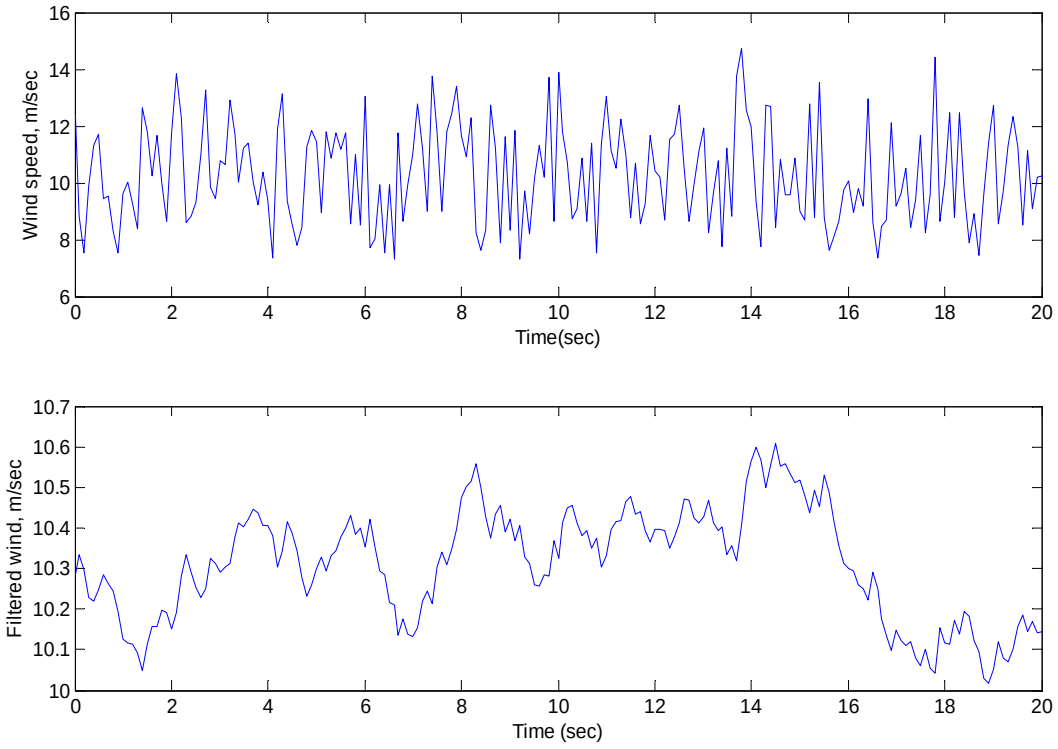

Figure 4.23: Wind speed variations for 20 sec (i) actual wind speed (ii) filtered wind speed.

$$v_w = mean\ speed \times (1 + (-\ln(r)/c)^{\frac{1}{k}}) \tag{4.27}$$

Where, r is a random number (0,1), k, c are respectively scale and shape parameters of the Weibull distribution. Here $c = 4$; $k = 2$, and mean wind speed is 10 m/sec.

Usually this high frequency wind gets partially filtered over the rotor surface of the large wind turbines. The considered low-pass filter is as shown in Fig 4.24 [34]. Fig 4.25 shows the corresponding wind generated power delivered to the grid. It can be seen that without controller the delivered power could be highly fluctuating in nature

especially for conventional fixed-speed wind turbine. However, with the proposed STATCOM/ESS the wind power fluctuation is minimized substantially.

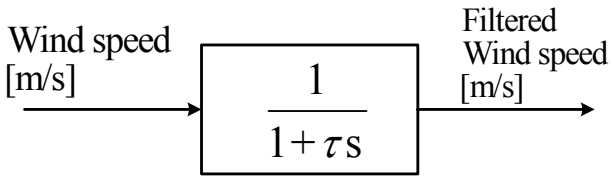

Figure 4.24: Low pass filter for including the smoothing of high-frequency wind speed variations over the rotor surface.

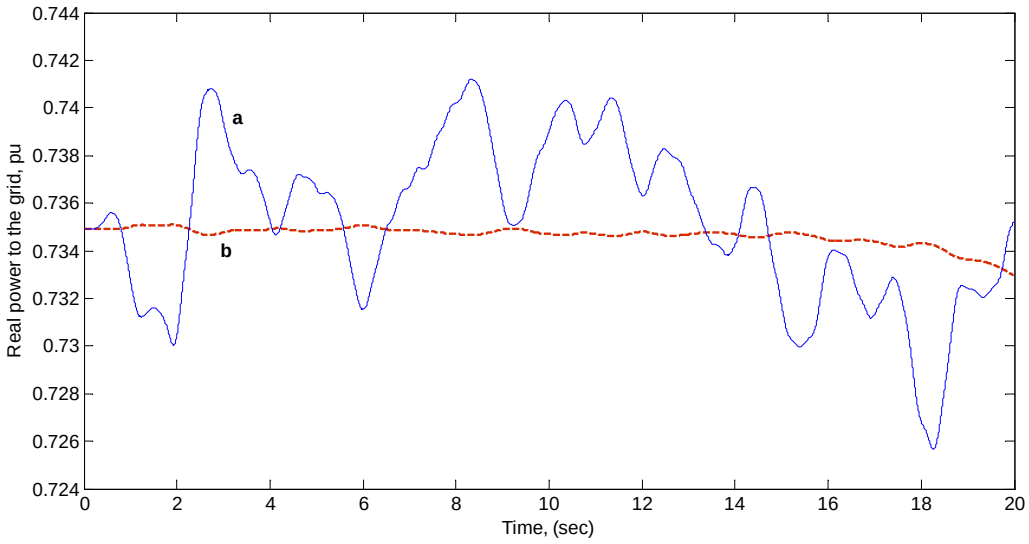

Figure 4.25: Wind power delivered to the grid (a) without STATCOM/BESS, and (b) with STATCOM/BESS

4.5.2 STATCOM with SCESS

To investigate the performance of STATCOM/SCESS, same wind generation system as mentioned in section 4.5.1 was simulated when it was supported by STATCOM/SCESS as shown in Fig. 4.16. The dynamic response of the system was investigated with following three scenarios –

(a) Wind generation system with no control

(b) With STATCOM and Q control only

(c) With STATCOM/SCESS and both P – Q control

4.5.2.1 Responses with Three-phase Fault

Figs 4.26 - 4.28 show the variations in generator slip, terminal voltage, and power delivered to the grid respectively, with a three-phase fault on the grid for 150ms. Since the uncontrolled responses are already mentioned in section 4.1.3.3, responses with (i) Q control only, and (ii) both P & Q control are brought up here. From the responses it can be observed that both STATCOM with Q control only, and STATCOM/SCESS having both P & Q control, prevent terminal voltage collapse. Thus, wind generator remains in operational in the event of such grid fault. The superiority of responses in the presence of P controller is obvious. It almost eliminates the variations in slip (Δs) as depicted in Fig. 4.26, and quickly resumes the delivery of real power to the grid as can be seen from Fig. 4.28. The amount of injected real power (P_{st}) is shown in Fig. 4.29, where the negative sign indicates absorption.

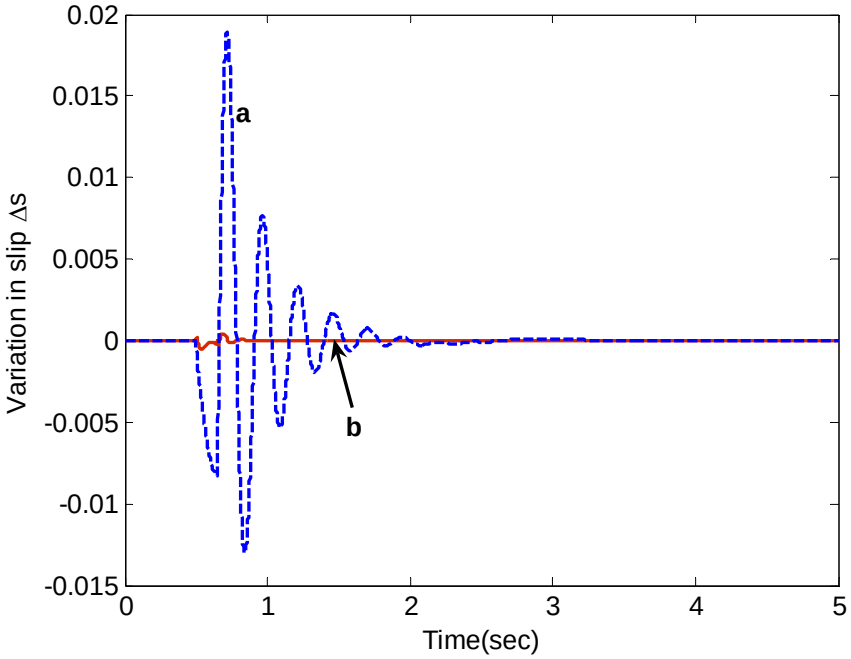

Figure 4.26: Variation in rotor slip (Δs) following momentary three-phase of 150ms duration, with STATCOM/SCESS (a) Q control only, (b) both P & Q control (solid line).

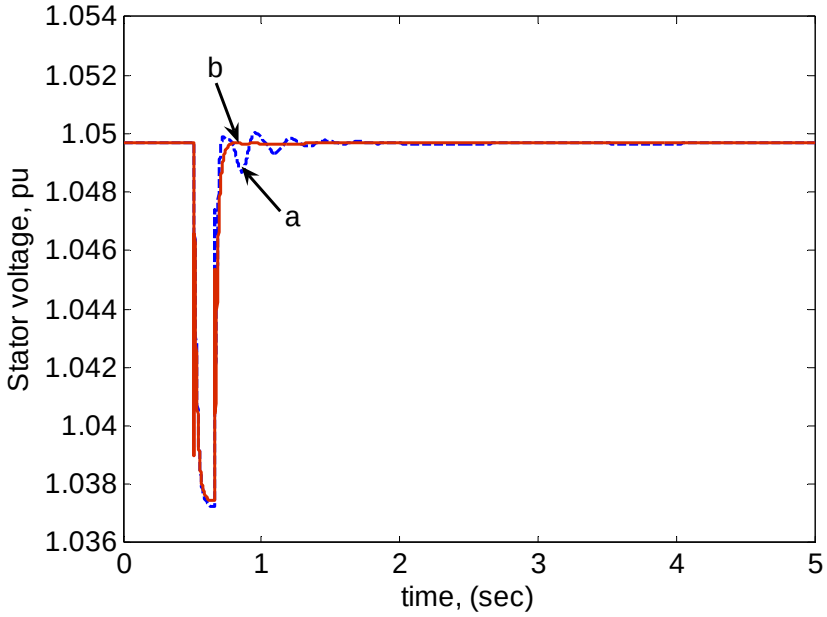

Figure 4.27: Variation in generator terminal voltage corresponding to Fig. 4.26.

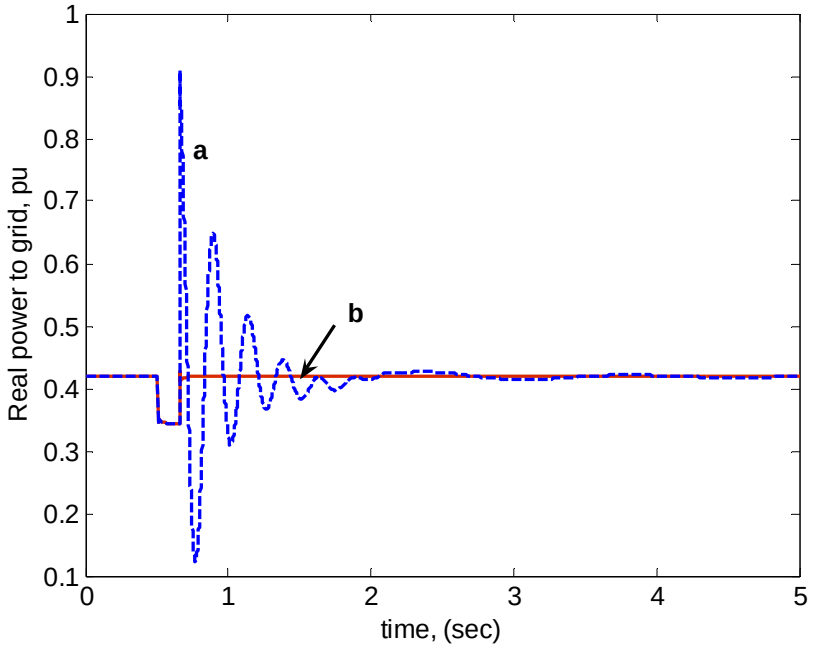

Figure 4.28: Variation in real power delivered to the grid corresponding to Fig. 4.26.

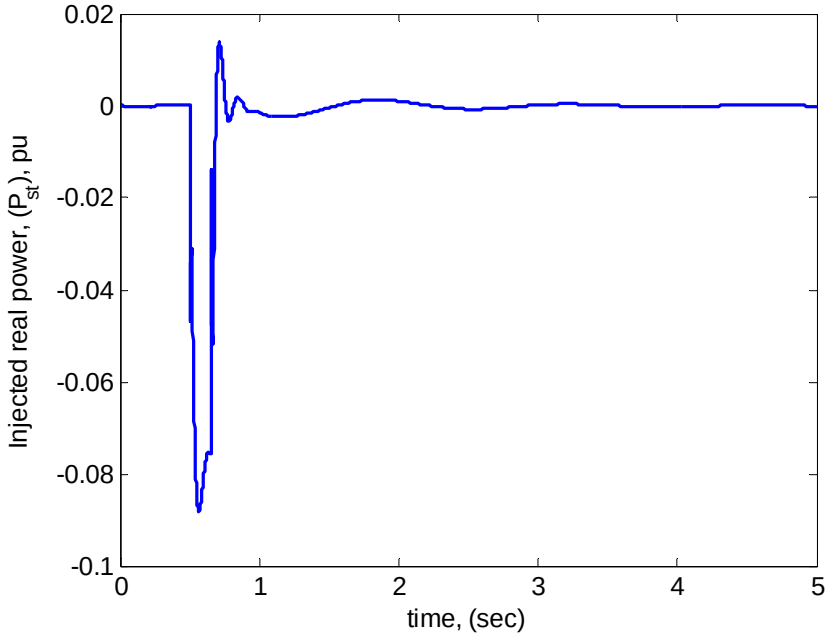

Figure 4.29: Real power injection by the P controller (P_{st}) in the event of grid fault.

4.5.3 PERFORMANCE COMPARISON OF THREE CONTROL STRATEGIES

In the previous sections, it is demonstrated that all three control strategies: (i) variable susceptance (B) control, (ii) STATCOM Q control, and (iii) STATCOM/ESS P & Q control, are well capable of suppressing transients arising from mid level disturbances. In this section, the performance of three different control strategies have been compared with regard to longer duration of three-phase fault (625ms) at the grid. Although some other disturbances could have been considered, but this fault conditions have been stipulated in the grid code issued by the US Federal Energy Regulatory Commission (FERC) for the examination of Low Voltage Ride-through (LVRT) capability of wind farm [100]. This code stipulates that the wind generator has to remain connected to the power system if the voltage remains at a level greater than 15% of the nominal voltage for a period that does not exceed 0.625 sec as shown in Fig 4.30 [Appendix D].

A three-phase fault is simulated at the infinite bus is simulated which is cleared after 625ms. The performance of the controllers are displayed through the transient responses of generator slip variations (Δs), terminal voltage variations, and variations in electromagnetic torque developed respectively as shown in Figs 4.31– 4.34. As seen from these Figs, variable susceptance controller is incapable of withstanding such large disturbance, thus lacks the capability in meeting the LVRT requirement. Whereas with either STATCOM Q control or with STATCOM/ESS P & Q control, the situation is tackled very effectively. However, the performance of control strategy (iii) *i.e.* STATCOM/ESS both P & Q control, has been seen to be always superior. The main credit goes to STATCOM's reactive power (Q) controller which promptly restores the terminal voltage by injecting required reactive power (Q_{st}). Because the STATCOM tries

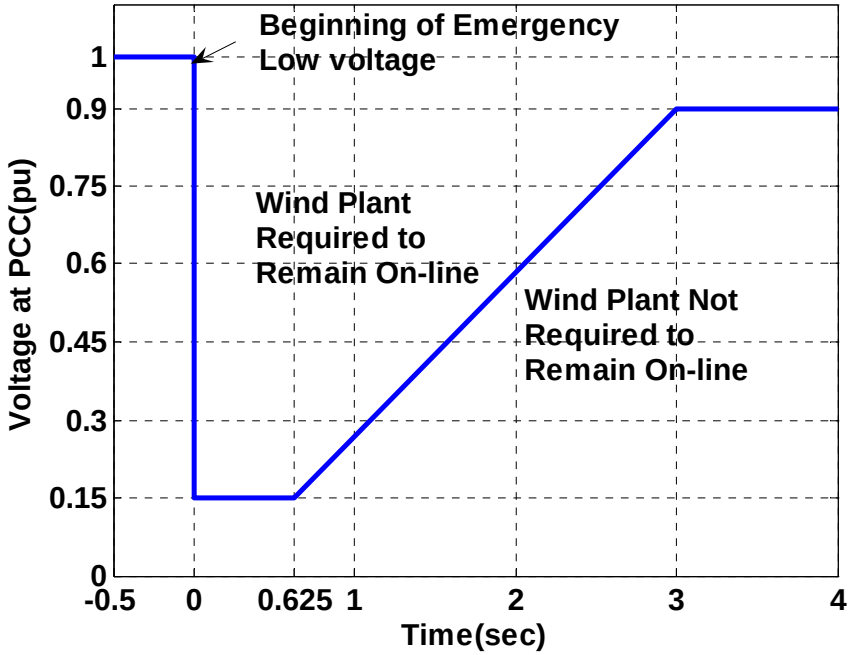

Figure 4.30: Low voltage ride through standard set by FERC, USA [100].

to maintain the bus voltage dynamically, the voltage profile in Fig 4.32 shows very little deterioration whatsoever. As depicted in Fig 4.34, whether Q controller is acting alone or with P controller, it injects almost same amount of reactive power ($Q_{st} \approx 1.85$ pu) to restore the terminal voltage. This demonstrates the functionality of P & Q controllers in decoupled manner. However, P controller enhances the performance of STATCOM/ESS by eliminating the transients in the variables like slip (Δs), electromagnetic torque (Te), above all real power delivered to the grid as shown in Fig 4. 35. The amount of injected real power by the P controller (P_{st}) is not that much (less than -0.1 pu) as depicted in Fig. 4.36. Since it is within the range of BESS, both STATCOM/BESS and STATCOM/SCESS would demonstrate similar performance. However, for some other

disturbance scenario, if P_{st} limit exceeds, then controller performance will degrade accordingly. Summary of simulation results for single machine infinite bus system is given in Table 4.1.

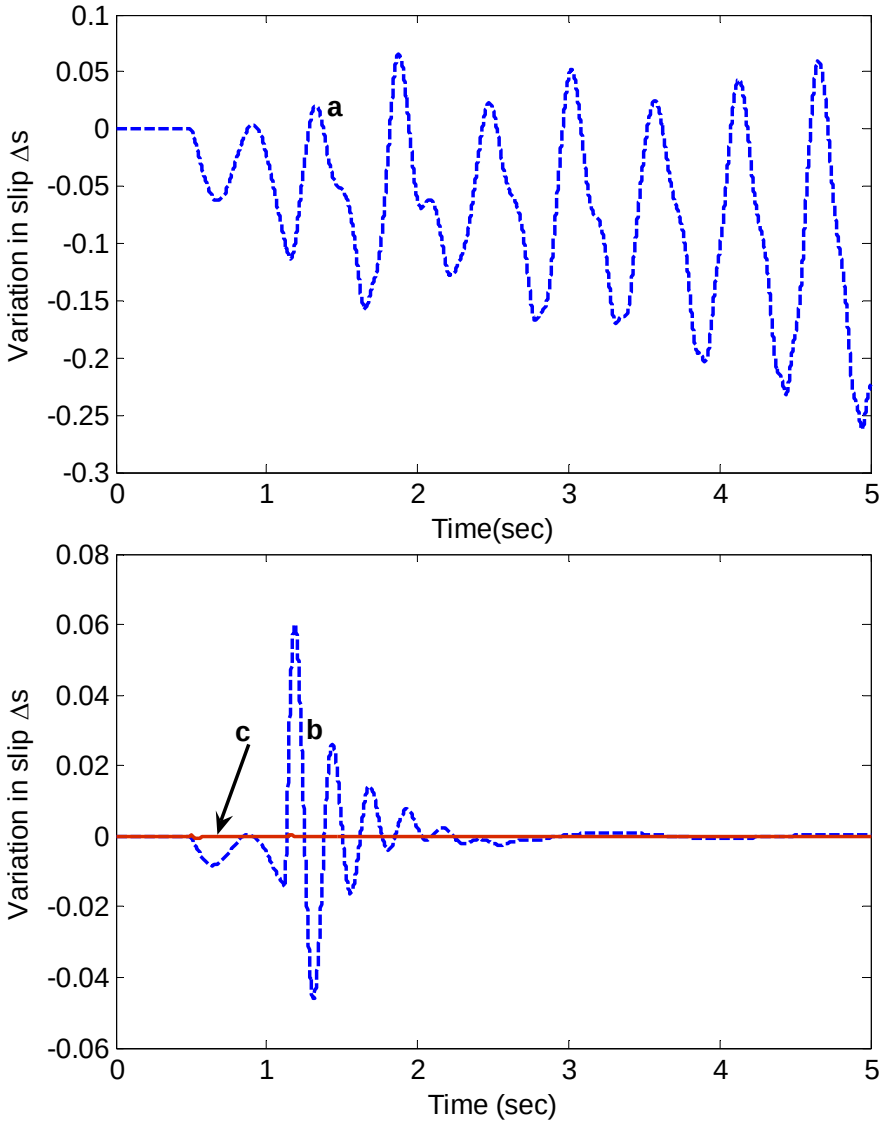

Figure 4.31: Induction generator slip variations (Δs) following three-phase fault of 625 ms duration (a) B control (b) STATCOM Q control, and (c) STATCOM/ESS P & Q control.

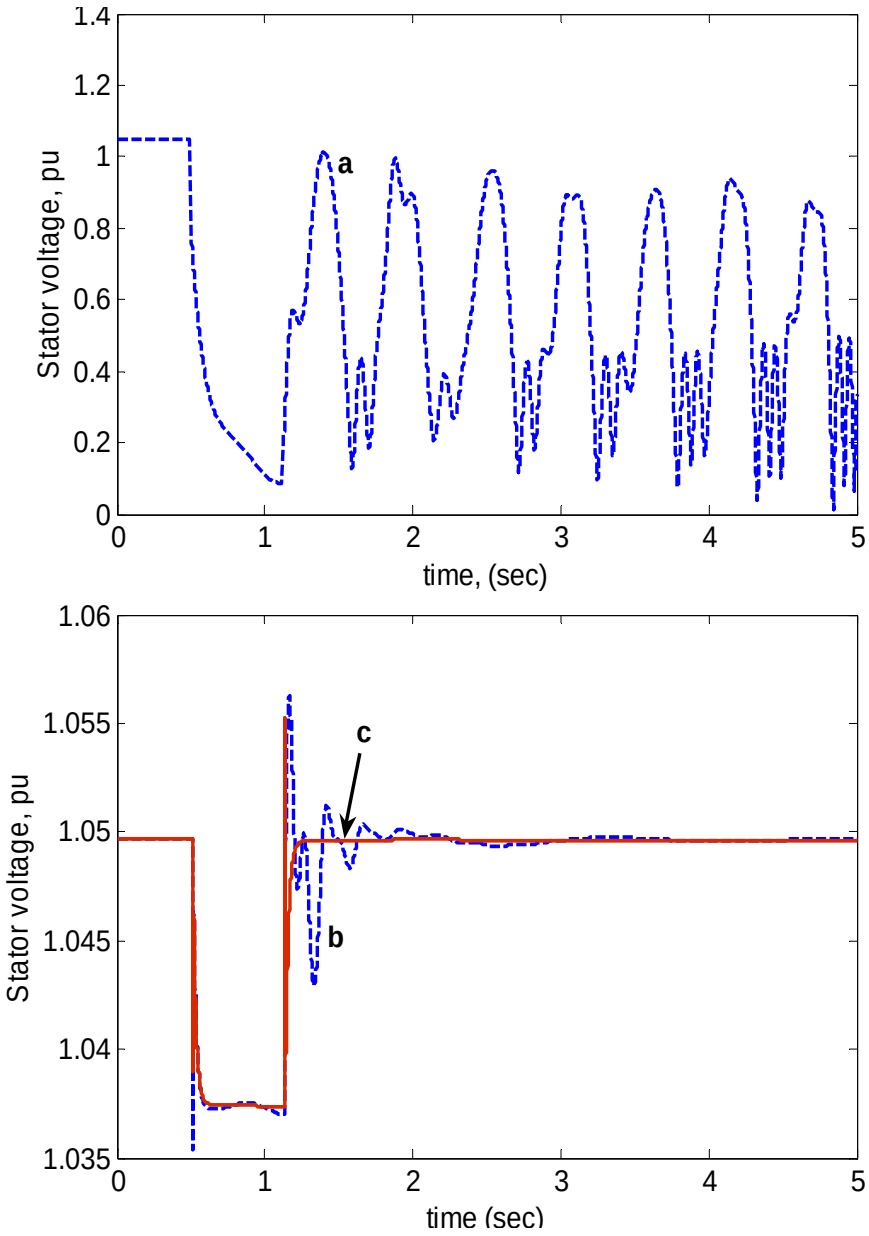

Figure 4.32: Induction generator terminal voltage variations corresponding to Fig 4.31.

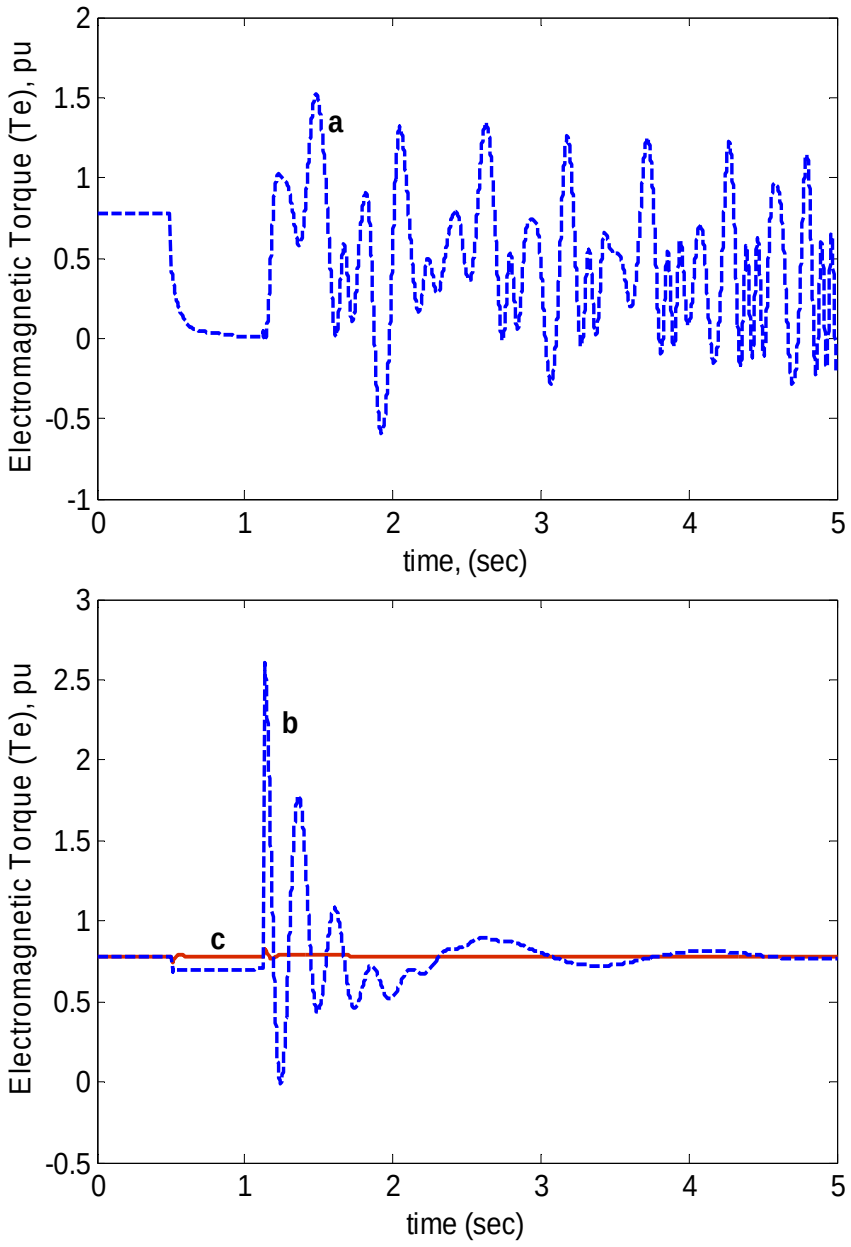

Figure 4.33: Induction generator electromagnetic torque variations corresponding to Fig 4.31.

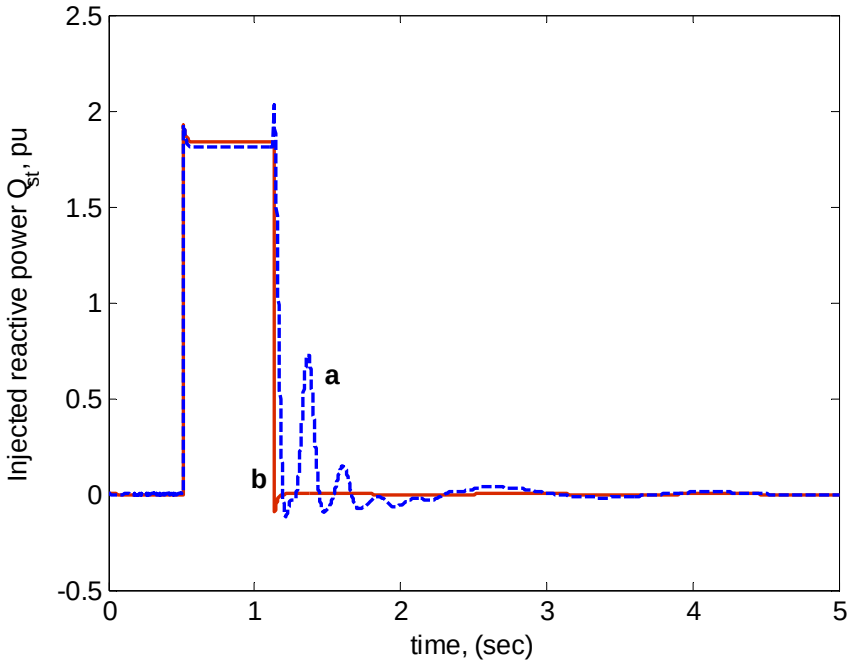

Figure 4.34. Injected reactive power (Q_{st}) by Q controller following three-phase fault of 625ms duration.

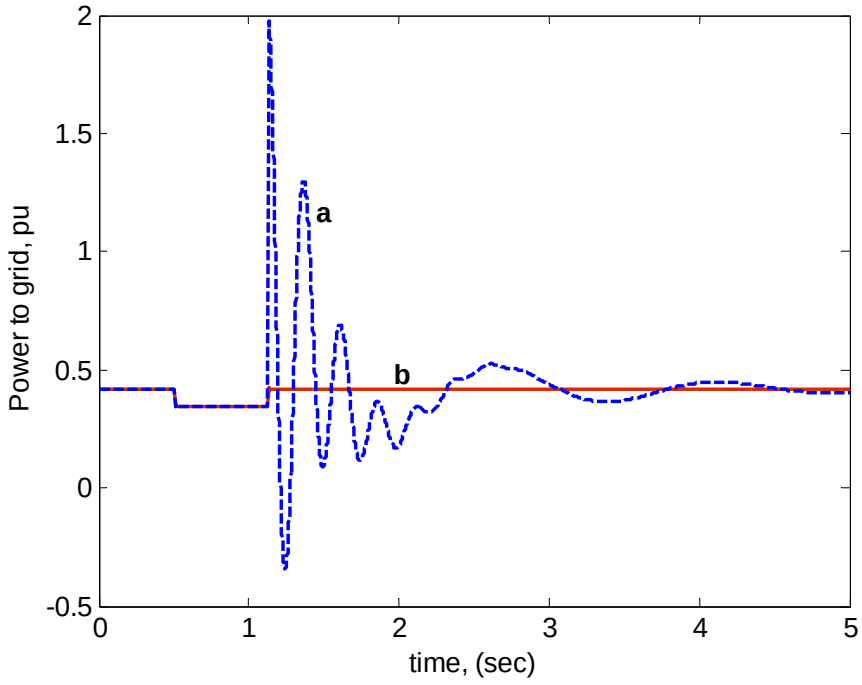

Figure 4.35: Real power delivered to the grid (P_{m2}) following three-phase fault of 625ms duration.

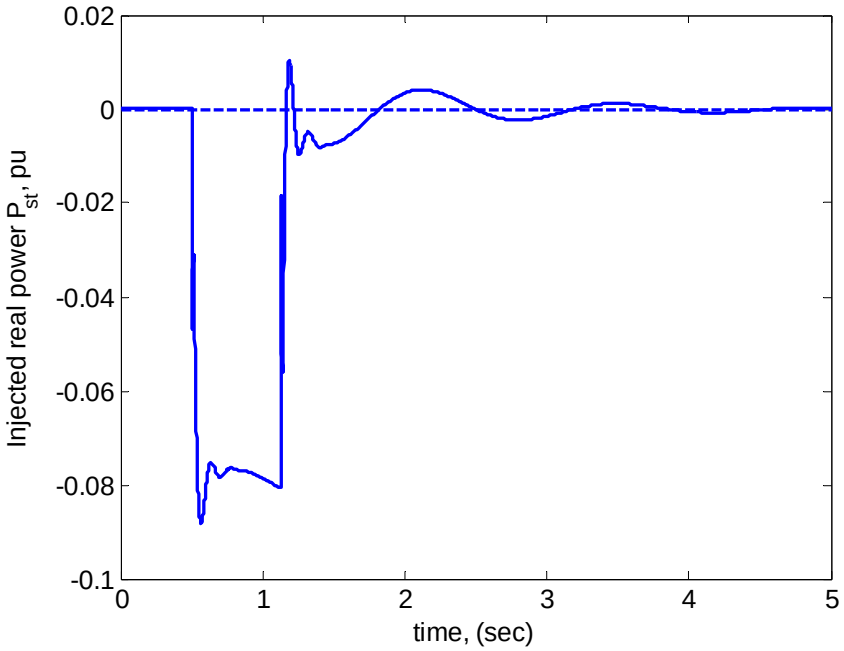

Figure 4.36: Injected active power (P_{st}) by P controller following three-phase fault of 625ms duration.

TABLE 4.1: Summary of simulation results for single machine infinite bus system

	Response of wind generation system with			
Disturbance type	**No control**	**Variable Susceptance control**	**STATCOM with Q control only**	**STATCOM with both P & Q control**
50% Torque pulse of 0.75sec duration	Unstable	* Stable * Larger transients exist in Vs & P_{m2}	*Stable *Larger transients exist in P_{m2}	*Stable *Transients in Vs & P_{m2} are eliminated almost totally
30% Torque step	Unstable	Stable	Stable	Stable
Wind gust for 2sec	Stable Large	*Stable *Larger transients exist in P_{m2}	*Stable *Larger transients exist in P_{m2}	*Stable *Transients in P_{m2} are eliminated almost totally
Three-phase fault of 150ms at grid connection point	Unstable	*Stable *Larger transients exist in slip, Vs & P_{m2}	*Stable *Larger transients exist in slip, Vs & P_{m2}	*Stable *Transients in slip, Vs & P_{m2} are eliminated almost totally
Three-phase fault of 625ms at grid connection point	Unstable	Unstable	*Stable *Larger transients exist in slip, Te and P_{m2}	*Stable *Transients in slip, Te & P_{m2} are eliminated almost totally

CHAPTER 5

WIND GENERATORS IN MULTIMACHINE POWER SYSTEM

A detailed nonlinear model of multimachine power system comprising of arbitrary number of synchronous generators, induction generators and loads is presented in this chapter. This is followed by a small-excursion linearized model. This model permits to formulate a multimachine power system of arbitrary topology with any number of interconnected synchronous and asynchronous generators.

5.1 GENERALIZED MULTIMACHINE SYSTEM CONFIGURATION

Wind farms may be located at different geographical areas having different wind conditions like different wind speed, air density. In addition, the size of wind turbines, and ratings of the induction generators may be different. Depending on the local conditions, induction generators operating slip at different wind farms may differ. Formulation of such wind farms along with the AC system is given below.

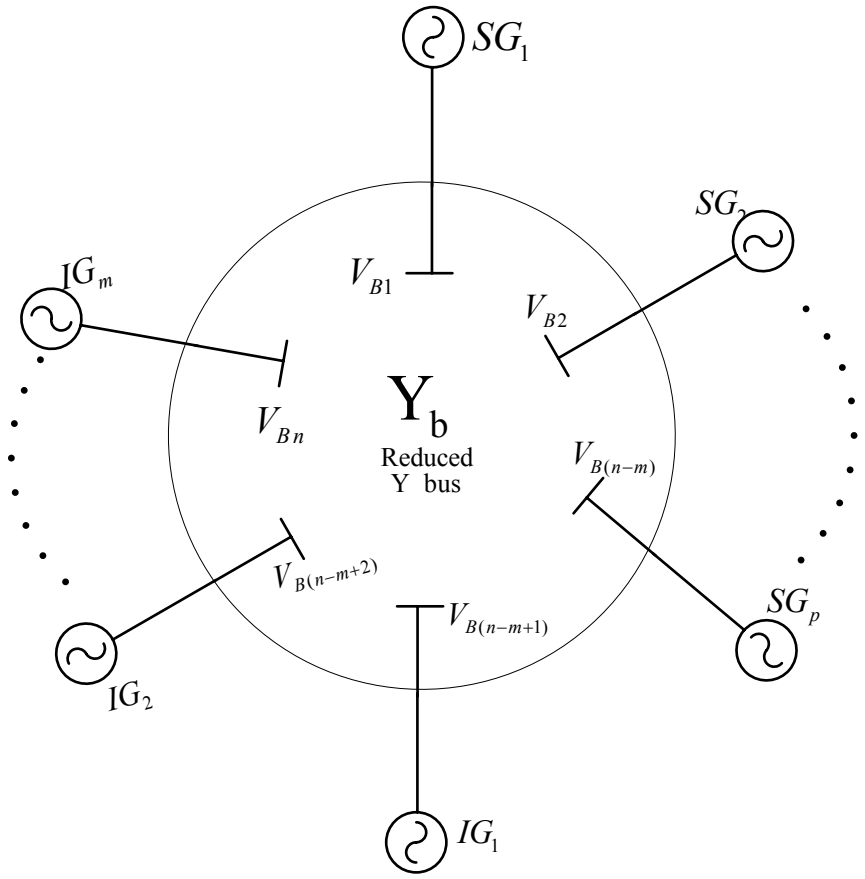

Figure **5**.1: A general multimachine AC system including several wind generators

Fig 5.1 shows a general multimachine power system where several wind farms are at different operating conditions. For the convenience of mathematical formulation and subsequent numerical simulation, machines (MCs) are numbered in such a way that the synchronous generators (SGs) come first and then the induction generators (IGs).

$$\left[MC_1, MC_2, MC_3, \ldots\ldots MC_p, MC_{p+1}, MC_{p+2}, \ldots\ldots MC_n\right]$$

$$= \left[SG_1, SG_2, SG_3, \ldots\ldots SG_p, IG_1, IG_2, \ldots\ldots IG_m\right]$$

Where, n = Total number of machines, (SG + IG)

m = Total number of wind farms i.e. equivalent induction generators (IGs)

p = (n – m) = Total number of synchronous generators (SGs)

It is considered that each generator has a local load ($Y_{11}=g_{11}+jb_{11}$) and connected to the network bus through a transmission line having impedance $Z_{Line} = R + jX$ as shown in Fig 5.2. Capacitive susceptance (b_c) required for the steadystate excitation of induction generator is considered to be included with b_{11}.

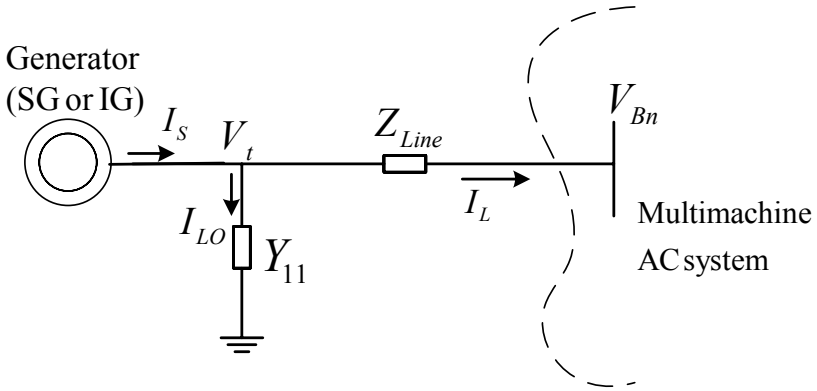

Figure **5**.2: Line and load modeling for each generator

5.2 LOAD AND LINE MODELING

For a realistic model of the load it is necessary to estimate qualitatively and quantitatively its composition, the nature of the load components and their percentage in the total load. In the simplest but common case, the whole load or part of this can be modeled as an

impedance $Z_L = R_L + j\omega L_L$. When the active load P_L and reactive load Q_L are known at steady state, the values of resistance and reactance can be obtained from the relation,

$$P_L + jQ_L = |V_t|^2 Y_L^* \tag{5.1}$$

The * denotes the conjugate of the load admittance Y_L.

The transmission line components and loads are considered to be in quasi-static state whose voltage current phasors are considered to be rotating at synchronous speed (ω_o) and written in network D-Q frame of reference. The network admittance matrix can be reduced to obtain Y_{red} with dimension $n \times n$, where n is the number of power system bus bars where current is injected. Eliminating all the load buses, the vector of currents injected to the network buses is given by:

$$I_{LN} = Y_{red} V_{BN} \tag{5.2}$$

Where I_{LN} is a vector of injected currents from the generators and V_{BN} is the resulting bus voltages. Separating the contributions from synchronous generators (sg) and induction generators (ig), the above can be written as –

$$\left[\begin{array}{c} I_{sg} \\ \hline I_{ig} \end{array}\right] = \left[\begin{array}{c|c} Y_1 & Y_2 \\ \hline Y_3 & Y_4 \end{array}\right] \left[\begin{array}{c} V_{sg} \\ \hline V_{ig} \end{array}\right] \tag{5.3}$$

5.3 SYNCHRONOUS GENERATOR MODEL

Considering transient saliency (*i.e.* $x'_d \neq x'_q$), each synchronous generator is represented by the following 5th order model

$$\dot{e}'_q = \frac{1}{T'_{do}}\left[E_{fd} - e'_q - (x_d - x'_d) i_{ds} \right] \tag{5.4}$$

$$\dot{e}'_d = \frac{1}{T'_{qo}}\left[-e'_d + (x_q - x'_q) i_{qs} \right] \tag{5.5}$$

$$\dot{\omega} = \frac{1}{2H}\left[T_m - T_e - T_D \right] \tag{5.6}$$

$$\dot{\delta} = \omega_b \Delta\omega = \omega_b(\omega - 1) \tag{5.7}$$

$$\dot{E}_{fd} = \frac{1}{T_A}\left[K_A(v_{ref} - v_t) - E_{fd} \right] \tag{5.8}$$

Where the stator voltage and currents are related through

$$\left.\begin{aligned} v_{ds} &= -r_s i_{ds} + x'_q i_{qs} + e'_d \\ v_{qs} &= -r_s i_{qs} - x'_d i_{ds} + e'_q \end{aligned}\right\}$$
$$v_t = \sqrt{{v_{ds}}^2 + {v_{qs}}^2} \tag{5.9}$$

The electromagnetic torque (T_e) and damping torque (T_D) are computed as (5.10) and (5.11) respectively

$$T_e = e'_d i_{ds} + e'_q i_{qs} + (x'_q - x'_d) i_{ds} i_{qs} \tag{5.10}$$

$$T_D = D(\omega - 1) = D\Delta\omega \tag{5.11}$$

Note that generator output currents i_{ds} and i_{qs} are non-state variable and they have to be expressed in terms of the quantities of the rest of the network.

5.4 INDUCTION GENERATOR MODEL

For induction generator, reduced order model as described in Chapter 3, is considered in the multimachine modeling for ease of aggregation/ inclusion with the other components of the multimachine system. The model equations are rewritten here as below -

$$\dot{e}'_q = -\frac{1}{T'_o}\left[e'_q + (x_{ss} - x')i_{ds} \right] - s\omega_b e'_d + \frac{x_m}{x_{rr}}\omega_b v_{dr} \tag{5.12}$$

$$\dot{e}'_d = -\frac{1}{T'_o}\left[e'_d - (x_{ss} - x')i_{qs} \right] + s\omega_b e'_q - \frac{x_m}{x_{rr}}\omega_b v_{qr} \tag{5.13}$$

$$\left.\begin{aligned} v_{ds} &= -r_s i_{ds} + x' i_{qs} + e'_d \\ v_{qs} &= -r_s i_{qs} - x' i_{ds} + e'_q \end{aligned}\right\} \tag{5.14}$$

$$T_e = e'_d i_{ds} + e'_q i_{qs} \tag{5.15}$$

Neglecting damping terms the two-mass model of the drive-train can be simplified as:

$$2H_t \frac{d\omega_t}{dt} = T_m - K_s\theta_s \tag{5.16}$$

$$2H_g \frac{d\omega_r}{dt} = K_s\theta_s - T_e \tag{5.17}$$

$$\frac{d\theta_s}{dt} = \omega_b(\omega_t - \omega_r) \tag{5.18}$$

The symbols are as used in Chapter 3.

Models of the various components of the asynchronous-synchronous system presented have to be linked together and solved to study the dynamic behavior of the system. Since the equations for the various components are written in their own 'frame of reference', they have to be converted to a common frame. The inclusion of the asynchronous devices often poses a challenge. In more general case of a power system the transmission network is not neglected and an arbitrary number of synchronous generators and/or asynchronous machines are connected at each bus bar. The difference between the machine reference frames implies normally a large amount of consecutive intermediate calculations in order to calculate machine stator currents. The intermediate calculations are eliminated by inclusion of general transformation matrix.

In a multimachine all-AC system, the individual machine equations in their own d-q are related to the network frame D-Q quantities through the relationship

$$[M]_{DQ} = [T][M]_{dq} \tag{5.19}$$

M may be either *V* or *I*. The transformation matrix *T* is [62]

$$T_1 = \begin{bmatrix} e^{j(\delta_1 - \frac{\pi}{2})} & & & \\ & e^{j(\delta_2 - \frac{\pi}{2})} & & \\ & & \ddots & \\ & & & e^{j(\delta_{(n-1)} - \frac{\pi}{2})} \end{bmatrix} \tag{5.20}$$

Note that both synchronous machine d-q frames as well as the network D-Q frames are considered to rotate at synchronous speed.

The induction generator d-q coordinates are in arbitrary reference frames. Since it is arbitrary, the d-axis can be assumed to be aligned with the stator voltage (Machine Frame) with the network coordinates (Network Frame), or some other suitable references [49, 62]. The asynchronous induction generator equations can be integrated with the synchronous devices through the T_1 matrix given in (5.20) with the introduction of induction generator angle δ satisfying the relationship,

$$\delta_i = \frac{\pi}{2} + arg(V_i) \tag{5.21}$$

The phasor diagram showing the definitions of the rotor angles for the synchronous as well as the induction machines are shown in Fig 5.3 below.

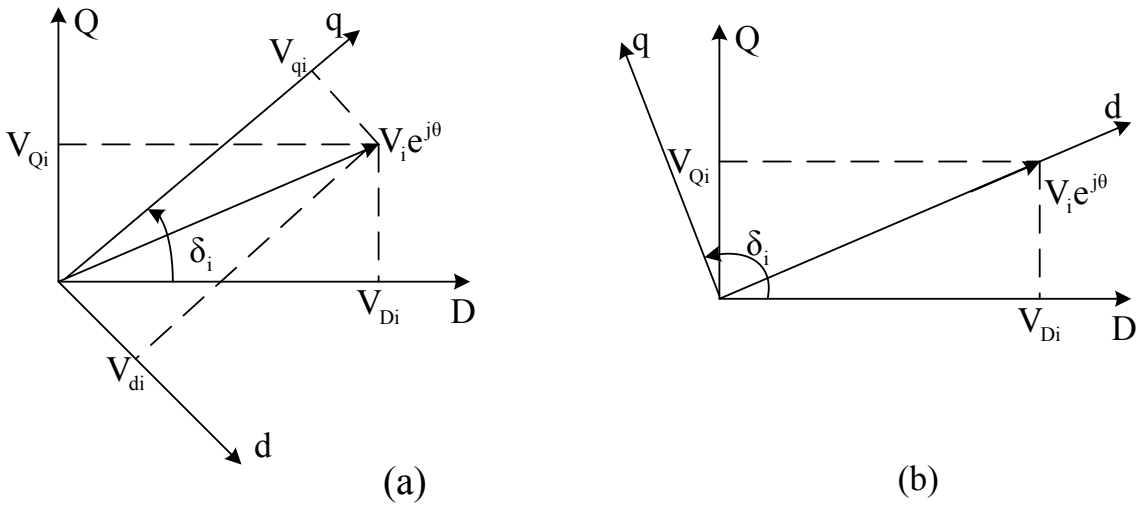

Figure 5.3: Graphical representation of the relation between network (D-Q) and machine (d-q) reference frames of (a) synchronous and (b) asynchronous machines

Observe that rotor angle δ of both synchronous as well as induction machines is the angle between the D-axis of the network frame and q-axis of each machine. As in the case of synchronous system, the induction generator angle can be obtained from the relationship,

$$\dot{\delta} = \omega_o \Delta\omega_R \tag{5.22}$$

where $\Delta\omega_R = \frac{\omega_R - \omega_o}{\omega_o}$

One of the fundamental differences between the synchronous and asynchronous systems is that because of the synchronizing torque, the synchronous generator will be pulled together and they will stabilize at the common frequency following a contingency. The asynchronous machines, on the other hand, may not be able to restore original system frequency because of lack of synchronizing forces. This may let the machine settle at a

speed or slip other than nominal. This would mean the induction generator will continue to grow dragging asynchronous system frame. Since all the phasors will be drifting, it will have no impact on power flow (real and reactive) of the system. However, the phase drifts may continue to pump transients to synchronous devices in the system. It is for this reason that if asynchronous generators are to be integrated with multimachine system they need to be equipped with mechanical or electromechanical device for automatically controlling the speed by relating the input and output of the generator. For a constant setting of the speed changer the static increase in generator output is directly proportional to static frequency droop. After the primary control function, which brings the system to an equilibrium state with a permanent frequency error, a secondary control is needed which eventually establishes nominal rotational speed by eliminating the static frequency error. The device which performs action is called the frequency error signal integrator [105]. This of course, implies that the wind generation system should have auxiliary power source to supply the difference.

In order to keep the analysis simple at this stage, it is assumed that an addition power/frequency controller is not implemented. This will yield a constant δ angle for the induction generator, and its voltage current phasors can be expressed either in machine frame or network frame. In the subsequent analysis, the induction generators are expressed in their own arbitrary frames which align with the network (D-Q) frame. The transformation matrix T_1, contains only the synchronous generator rotor angles. Equation (5.3) can then be written as

$$\begin{bmatrix} I_{sg}^{dq} \\ I_{ig}^{dq} \end{bmatrix} = \begin{bmatrix} T_1^{-1} Y_1 T_1 & T_1^{-1} Y_2 \\ Y_3 T_1 & Y_4 \end{bmatrix} \begin{bmatrix} V_{sg}^{dq} \\ V_{ig}^{dq} \end{bmatrix} \tag{5.23}$$

Where,

$$I_{LN} = \begin{bmatrix} I_{sg}^{dq} \\ I_{ig}^{dq} \end{bmatrix}; \quad V_{BN} = \begin{bmatrix} V_{sg}^{dq} \\ V_{ig}^{dq} \end{bmatrix}; \quad Y_m = \begin{bmatrix} T_1^{-1} Y_1 T_1 & T_1^{-1} Y_2 \\ Y_3 T_1 & Y_4 \end{bmatrix}$$

Equation (5.23) can be written in more compact form as

$$I_{LN} = Y_m V_{BN} \tag{5.24}$$

Breaking I_{LN}, V_{BN}, Y_m into real and imaginary parts and collecting terms (5.24) can be written as

$$\begin{bmatrix} I_{LNd} \\ I_{LNq} \end{bmatrix} = \begin{bmatrix} G_m & -B_m \\ B_m & G_m \end{bmatrix} \begin{bmatrix} V_{BNd} \\ V_{BNq} \end{bmatrix} \tag{5.25}$$

In the following, generalized expression for the non-state variables i_{ds} and i_{qs} are obtained in terms of system states chosen. Once these are obtained, expression for current dependent variables like terminal voltage, power, *etc*. are derived in terms of state variables. The generalized procedure followed is :

i) Obtain the voltage-current relationship from the machine side

ii) Obtain those from the network side

iii) Solve the non-state quantities using (i) and (ii) simultaneously

Looking from the machine side

Current injected to the i^{th} network bus

$$I_L = I_s - V_t Y_{11} \tag{5.26}$$

Breaking I_L & I_S into d-q coordinates and writing $Y_{11} = g_{11} + jb_{11}$, we can get

$$\begin{bmatrix} i_{ds} \\ i_{qs} \end{bmatrix} = \begin{bmatrix} I_{Ld} \\ I_{Lq} \end{bmatrix} + \begin{bmatrix} g_{11} & -b_{11} \\ b_{11} & g_{11} \end{bmatrix} \begin{bmatrix} v_{ds} \\ v_{qs} \end{bmatrix} \tag{5.27}$$

Substitute (5.27) into the stator equation (5.9) and solve for v_{ds} and v_{qs} as

$$\begin{bmatrix} v_{ds} \\ v_{qs} \end{bmatrix} = [C_1] \begin{bmatrix} e'_d \\ e'_q \end{bmatrix} - [C_1 A_1] \begin{bmatrix} I_{Ld} \\ I_{Lq} \end{bmatrix} \tag{5.28}$$

Where,

$$C_1 = inv[I + A_1 B_1]$$

$$A_1 = \begin{bmatrix} r_s & -x'_q \\ x'_d & r_s \end{bmatrix}; \qquad B_1 = \begin{bmatrix} g_{11} & -b_{11} \\ b_{11} & g_{11} \end{bmatrix}.$$

The terminal voltage equation for i^{th} machine is,

$$V_B = V_t - z_{12} I_L \tag{5.29}$$

The above equation can be written in d-q coordinate as

$$\begin{bmatrix} V_{Bd} \\ V_{Bq} \end{bmatrix} = \begin{bmatrix} v_{ds} \\ v_{qs} \end{bmatrix} - \begin{bmatrix} R & -X \\ X & R \end{bmatrix} \begin{bmatrix} I_{Ld} \\ I_{Lq} \end{bmatrix} \tag{5.30}$$

Substitute v_{ds} & v_{qs} from (5.28) into (5.30) to get,

$$\begin{bmatrix} V_{Bd} \\ V_{Bq} \end{bmatrix} = [C_1] \begin{bmatrix} e'_d \\ e'_q \end{bmatrix} - [D_1 + C_1 A_1] \begin{bmatrix} I_{Ld} \\ I_{Lq} \end{bmatrix} \tag{5.31}$$

Where,

$$D_1 = \begin{bmatrix} R & -X \\ X & R \end{bmatrix}$$

Equation (5.31) is for individual machine and its d-q components can be separated as

$$\begin{aligned} V_{Bd} &= k_{11} e'_d + k_{12} e'_q - k_{21} I_{Ld} - k_{22} I_{Lq} \\ V_{Bq} &= k_{13} e'_d + k_{14} e'_q - k_{23} I_{Ld} - k_{24} I_{Lq} \end{aligned} \tag{5.32}$$

here, k_{11}, k_{12}, k_{13}, k_{14}, k_{21}, k_{22}, k_{23}, and k_{24} are scalars whose value depends on system impedances and admittances. For n number of machine buses, the vector of bus voltages can be written as

$$\begin{bmatrix} V_{BNd} \\ V_{BNq} \end{bmatrix} = \begin{bmatrix} K_{11} & K_{12} \\ K_{13} & K_{14} \end{bmatrix} \begin{bmatrix} E'_d \\ E'_q \end{bmatrix} - \begin{bmatrix} K_{21} & K_{22} \\ K_{23} & K_{24} \end{bmatrix} \begin{bmatrix} I_{LNd} \\ I_{LNq} \end{bmatrix} \tag{5.33}$$

Where,

$$V_{BNd} = [V_{Bd1}, V_{Bd2}, ...V_{Bdn}]^T; \quad V_{BNq} = [V_{Bq1}, V_{Bq2}, ...V_{Bqn}]^T;$$

$$E'_d = [e'_{d1}, e'_{d2}, ...e'_{dn}]^T; \quad E'_q = [e'_{q1}, e'_{q2}, ...e'_{qn}]^T;$$

$$I_{LNd} = [I_{Ld1}, I_{Ld2}, ...I_{Ldn}]^T; \quad I_{LNq} = [I_{Lq1}, I_{Lq2}, ...I_{Lqn}]^T;$$

K_{11}, K_{12}, K_{13}, K_{14}, K_{21}, K_{22}, K_{23}, and K_{24} are diagonal matrices whose elements are respectively k_{11}, k_{12}, k_{13}, k_{14}, k_{21}, k_{22}, k_{23}, and k_{24} of each machine as mentioned in (5.32).

Finally, substituting V_{BNd} and V_{BNq} from (5.33) into (5.25) we obtain

$$\begin{bmatrix} I_{LNd} \\ I_{LNq} \end{bmatrix} = [D_2 A_2 B_2] \begin{bmatrix} E'_d \\ E'_q \end{bmatrix} \tag{5.34}$$

Where,

$$D_2 = inv(I + A_2 C_2)$$

$$A_2 = \begin{bmatrix} G_m & -B_m \\ B_m & G_m \end{bmatrix}; \; B_2 = \begin{bmatrix} K_{11} & K_{12} \\ K_{13} & K_{14} \end{bmatrix}; \; C_2 = \begin{bmatrix} K_{21} & K_{22} \\ K_{23} & K_{24} \end{bmatrix}$$

By substituting (5.34) in (5.28) an expression for V_{ds} and V_{qs}, in terms of system states can be obtained as:

$$\begin{bmatrix} V_{ds} \\ V_{qs} \end{bmatrix} = f_1\left(\begin{bmatrix} E'_d \\ E'_q \end{bmatrix}\right) \tag{5.35}$$

Similarly, by substituting (5.34) & (5.35) in (5.27) an expression for I_{ds} & I_{qs} in terms of states can be obtained as

$$\begin{bmatrix} I_{ds} \\ I_{qs} \end{bmatrix} = f_2\left(\begin{bmatrix} E'_d \\ E'_q \end{bmatrix}\right) \tag{5.36}$$

The set of differential equations (5.4 – 5.8), (5.12 – 5.13), (5.16 – 5.18) and the algebraic equations (5.35) & (5.36) can be combined together to obtain state model of multimachine power system with wind infeed as:

$$\dot{x} = f(x) \tag{5.37}$$

where, $x = [E'_q \;\; E'_d \;\; \omega_r \;\; \delta \;\; E'_{fd} \;\; \omega_t \;\; \theta_s]^T$.

5.5 LINEARIZED MODEL OF MULTIMACHINE WIND GENERATOR SYSTEM

The linearization of the dynamic equations (5.4 - 5.8), (5.12, 5.13), (5.16 - 5.18) require small perturbation expressions for non-state variables i_{ds} and i_{qs}. Though closed form expressions of these variables have been obtained in the previous sections, obtaining the perturbation model directly is difficult, though not impossible. The reasons for this are:

(a) The transformation matrix T_1 required in formulating admittance matrix is δ dependant

(b) The coefficients of the state variables in the expressions for i_{ds} and i_{qs} are complicated expressions involving inverses of state dependent matrices. Getting small perturbation expressions for such terms is not easy.

The procedure used in linearization of the system equations goes back to the deriving equations of the multimachine system. The linearized model is then rebuilt from the fundamental voltage current relations.

5.5.1 Derivation of Stator Currents

Rewriting (5.23)

$$\begin{bmatrix} I_{sg}^{dq} \\ I_{ig}^{dq} \end{bmatrix} = \begin{bmatrix} T_1^{-1}Y_1T_1 & T_1^{-1}Y_2 \\ Y_3T_1 & Y_4 \end{bmatrix} \begin{bmatrix} V_{sg}^{dq} \\ V_{ig}^{dq} \end{bmatrix} \tag{5.38}$$

Here, T_1 matrix contains the state variable δ. Considering $\delta=\delta_0+\Delta\delta$, from (5.20) we can write

$$\Delta T_1 = j\begin{bmatrix} e^{j(\delta_{10}-\frac{\pi}{2})} & & \\ & \ddots & \\ & & e^{j(\delta_{sg0}-\frac{\pi}{2})} \end{bmatrix}\begin{bmatrix} \Delta\delta_1 & & \\ & \ddots & \\ & & \Delta\delta_{sg} \end{bmatrix} = jT_0\Delta\delta \tag{5.39}$$

Similarly,

$$\Delta(T_1^{-1}) = -j\begin{bmatrix} e^{-j(\delta_{10}-\frac{\pi}{2})} & & \\ & \ddots & \\ & & e^{-j(\delta_{sg0}-\frac{\pi}{2})} \end{bmatrix}\begin{bmatrix} \Delta\delta_1 & & \\ & \ddots & \\ & & \Delta\delta_{sg} \end{bmatrix} = -jT_0^{-1}\Delta\delta \tag{5.40}$$

From (5.38), (dropping the superscript *dq*)

$$\begin{aligned}\Delta I_{sg} = {} & \{T_0^{-1}Y_1T_0\Delta V_{sg} + T_0^{-1}Y_1(\Delta T_1)V_{sg0} + \Delta(T_1^{-1})Y_1T_0V_{sg0}\} \\ & + \{T_0^{-1}Y_2\Delta V_{ig} + \Delta(T_1^{-1})Y_2V_{ig0}\}\end{aligned} \tag{5.41}$$

Substituting (5.39) and (5.40) in (5.41) we can write

$$\Delta I_{sg} = m_1\Delta V_{sg} + m_3\Delta V_{ig} + m_2\Delta\delta \tag{5.42}$$

Similarly,

$$\Delta I_{ig} = m_4 \Delta V_{sg} + m_5 \Delta \delta + m_6 \Delta V_{ig} \tag{5.43}$$

Where,

$$m_1 = T_0^{-1} Y_1 T_0$$

$$m_2 = j\{(T_0^{-1} Y_1 T_0) diag(V_{sg0}) - diag((T_0^{-1} Y_1 T_0) V_{sg0}) - diag(T_0^{-1} Y_2 V_{sg0})\}$$

$$m_3 = T_0^{-1} Y_2$$

$$m_4 = Y_3 T_0; \quad m_5 = j(Y_3 T_0) diag(V_{sg0})); \quad m_6 = Y_4$$

Breaking the system voltages, currents, and the expressions for m_1, m_2, m_3, m_4, m_5, m_6 into *d-q* components, (5.42) and (5.43) can be expressed in a compact form,

$$\begin{bmatrix} \Delta I_d \\ \Delta I_q \end{bmatrix} = \begin{bmatrix} G_x & -B_x \\ B_x & G_x \end{bmatrix} \begin{bmatrix} \Delta V_d \\ \Delta V_q \end{bmatrix} + \begin{bmatrix} G_y \\ B_y \end{bmatrix} \Delta \delta \tag{5.44}$$

Where,

$$G_x = real\left(\begin{bmatrix} m_1 & m_3 \\ m_4 & m_6 \end{bmatrix}\right); \qquad B_x = imag\left(\begin{bmatrix} m_1 & m_3 \\ m_4 & m_6 \end{bmatrix}\right)$$

$$G_y = real\left(\begin{bmatrix} m_2 \\ m_5 \end{bmatrix}\right); \qquad B_y = imag\left(\begin{bmatrix} m_2 \\ m_5 \end{bmatrix}\right)$$

Repeating the steps of section 5.5, the perturbed generator terminal voltage equations are,

$$\begin{bmatrix} \Delta V_d \\ \Delta V_q \end{bmatrix} = \begin{bmatrix} -R_s & X_{q1} \\ -X_{d1} & -R_s \end{bmatrix} \begin{bmatrix} \Delta I_d \\ \Delta I_q \end{bmatrix} + \begin{bmatrix} \Delta E'_d \\ \Delta E'_q \end{bmatrix} \tag{5.45}$$

Where,

$$R_s = diag(r_s);\ X_{d1} = diag(x'_d);\quad X_{q1} = diag(x'_q)$$

Substituting (5.45) in (5.44), the expressions for the small perturbation of currents can be written as

$$\begin{bmatrix} \Delta I_d \\ \Delta I_q \end{bmatrix} = [D_3][A_3] \begin{bmatrix} \Delta E'_d \\ \Delta E'_q \end{bmatrix} + [D_3][C_3]\Delta\delta \tag{5.46}$$

Where,

$$D_3 = inv(I + A_3 B_3)\,; \qquad C_3 = \begin{bmatrix} G_y \\ B_y \end{bmatrix}$$

$$A_3 = \begin{bmatrix} G_x & -B_x \\ B_x & G_x \end{bmatrix}; \qquad B_3 = \begin{bmatrix} R_s & -X_{q1} \\ X_{d1} & R_s \end{bmatrix}$$

Substituting ΔI_d & ΔI_q, the d-q components of the perturbed stator voltage can be expressed as

$$\begin{bmatrix} \Delta V_d \\ \Delta V_q \end{bmatrix} = \left(I - [B_3 D_3 A_3]\right) \begin{bmatrix} \Delta E'_d \\ \Delta E'_q \end{bmatrix} - [B_3 D_3 C_3]\Delta\delta \tag{5.47}$$

5.5.2 Linearization of Machine Dynamic Equations

The small-perturbation equations of the generator internal voltage e'_d and e'_q of the synchronous generators are,

$$\Delta\dot{E}'_{qsg} = [diag(\frac{1}{T'_{do}})]\Delta E_{fd} - [diag(\frac{1}{T'_{do}})]\Delta E'_{qsg} - [diag(\frac{x_d - x'_d}{T'_{do}})]\Delta I_{dsg} \tag{5.48}$$

$$\Delta\dot{E}'_{dsg} = -[diag(\frac{1}{T'_{qo}})]\Delta E'_{dsg} + [diag(\frac{x_q - x'_q}{T'_{qo}})]\Delta I_{qsg} \tag{5.49}$$

While these for the induction generators are

$$\begin{aligned} \Delta\dot{E}'_{qig} = &-diag(\frac{1}{T'_o})\Delta E'_{qig} - diag(\frac{(x_{ss} - x')}{T'_o})\Delta I_{dig} - diag(s_o\omega_s)\Delta E'_{dig} \\ &- diag(\omega_s E'_{digo})\Delta\omega_r \end{aligned} \tag{5.50}$$

$$\begin{aligned} \Delta\dot{E}'_{dig} = &-diag(\frac{1}{T'_o})\Delta E'_{dig} - diag(\frac{(x_{ss} - x')}{T'_o})\Delta I_{qig} - diag(s_o\omega_s)\Delta E'_{qig} \\ &- diag(\omega_s E'_{qigo})\Delta\omega_r \end{aligned} \tag{5.51}$$

Note that, $\Delta\omega_r = -\Delta s$.

Substituting the expressions for ΔI_d and ΔI_q from (5.46) in the above, generalized form of the internal voltage equations for both the synchronous and induction generators can be written as,

$$\begin{bmatrix} \Delta \dot{E}'_q \\ \Delta \dot{E}'_d \end{bmatrix} = \begin{bmatrix} A_{s11} & A_{s12} \\ A_{s21} & A_{s22} \end{bmatrix} \begin{bmatrix} \Delta E'_q \\ \Delta E'_d \end{bmatrix} + \begin{bmatrix} A_{s13} & A_{s14} \\ A_{s23} & A_{s24} \end{bmatrix} \begin{bmatrix} \Delta \omega_r \\ \Delta \delta \end{bmatrix} + \begin{bmatrix} A_{s15} \\ 0 \end{bmatrix} \Delta E_{fd} \qquad (5.52)$$

The expressions for the coefficients A_{s11}, A_{s12}, A_{s13}, A_{s14}, A_{s15}, A_{s21}, A_{s22}, A_{s23}, A_{s24} are given in Appendix E.

The speed/swing equation of the generators contain a non-state term T_e. The small perturbation form of this equation is

$$\Delta T_e = i_{d0}\Delta e'_d + i_{q0}\Delta e'_q + \{e'_{d0} + (x'_q - x'_d)i_{q0}\}\Delta i_d + \{e'_{q0} + (x'_q - x'_d)i_{d0}\}\Delta i_q \qquad (5.53)$$

Substituting the expressions for ΔI_d and ΔI_q in (5.53), we write

$$-\frac{1}{M}\Delta T_e = A_{s31}\Delta E'_q + A_{s32}\Delta E'_d + A_{s34}\Delta\delta \qquad (5.54)$$

To get a closed form representation and also to get the small perturbation model, the wind turbine output T_m needs to be written as an explicit form which is a function of rotor speed. For a particular wind speed, the turbine output torque T_m *vs*. speed data is converted to an expression like the following through a curve fitting technique.

$$T_m(mech,\omega) = C(1)\times Speed^{Order} + C(2)\times Speed^{Order-1} + ... + C(Order)$$

where '*Order*' is the order of the polynomial. The perturbation of turbine torque is written as,

$$\Delta T_m(mech,\omega) = [C(1)\times Order \times Speed\,0^{Order-1} + C(2)\times(Order-1)\times Speed\,0^{Order-2}$$

$$+ ..... + C(Order-1)]\Delta Speed = C_T \Delta Speed \tag{5.55}$$

Substituting (5.54) & (5.55) in the small perturbation for of the speed equation,

$$\Delta\dot{\omega} = A_{s31}\Delta E'_q + A_{s32}\Delta E'_d + A_{s33}\Delta\omega + A_{s34}\Delta\delta + B_{u36}\Delta T_m \tag{5.56}$$

The expressions for the coefficients A_{s31}, A_{s32}, A_{s33}, A_{s34}, B_{u36}, are given in Appendix E.

The small perturbation form of rotor angle equation is

$$\Delta\dot{\delta} = A_{s43}\Delta\omega \tag{5.57}$$

The variation of terminal voltage equation is

$$\Delta v_t = \frac{v_{d0}}{v_{t0}}\Delta v_d + \frac{v_{q0}}{v_{t0}}\Delta v_q \tag{5.58}$$

Substituting Δv_d and Δv_q from (5.47) in (5.58) gives

$$-\frac{K_A}{T_A}\Delta v_t = A_{s51}\Delta E'_q + A_{s52}\Delta E'_d + A_{s54}\Delta\delta \tag{5.59}$$

The small perturbation form of field voltage equation is

$$\Delta \dot{E}_{fd} = \frac{1}{T_A}\left[K_A(\Delta v_{ref} - \Delta v_t) - \Delta E_{fd} \right] = \frac{K_A}{T_A}\Delta v_{ref} - \frac{K_A}{T_A}\Delta v_t - \frac{1}{T_A}\Delta E_{fd} \qquad (5.60)$$

Substitute (5.56) in (5.57) to get,

$$\Delta \dot{E}_{fd} = A_{s51}\Delta E'_q + A_{s52}\Delta E'_d + A_{s54}\Delta\delta + A_{s55}\Delta E_{fd} + B_{u55}\Delta v_{ref} \qquad (5.61)$$

Combining all the state equations, the linearized model of the entire system is given by

$$\dot{X} = A_{sys}X + BU \qquad (5.62)$$

where, $X = [\Delta E'_q \;\; \Delta E'_d \;\; \Delta\omega \;\; \Delta\delta \;\; \Delta E_{fd} \;\; \Delta\omega_t \;\; \Delta\theta_t]^T$ and $U = [\Delta T_m \;\; \Delta V_{ref}]^T$

The system matrix A_{sys} is given in Appendix E.

CHAPTER 6

SIMULATION RESULTS FOR THE MULTIMACHINE SYSTEM

This chapter presents simulation studies for the multimachine system model developed. The following cases have been considered:

- A 4 machine 12 bus system
- 10 machine 39 bus New England system

6.1 COMPUTATIONAL PROCEDURE FOR MULTIMACHINE SYSTEM

With the generation and load data along with transmission line parameters, load-flow analysis was carried-out to determine bus voltage and power injected into each bus at steady-state. In the load flow analysis, the induction generator (IG) is represented as a PV bus [106]. With the load-flow solution, steady-state analysis is performed to determine initial slip and reactive power consumed by the IG [46]. At the IG terminal appropriate

reactive power is provided by a fixed capacitor such that at steady-state the induction generator operates at unity power factor mode (i.e. Q_{ig}=0). Also, with the obtained loadflow solution, the generators are initialized by solving its set of differential-algebraic equations with all time derivatives set equal to zero. The steps followed in the simulation procedure are shown in the flow diagram of Fig. 6.1. In this diagram the symbol ig stands for induction generator. Y_{bf}, Y_{df} and Y_{pf} represent reduced Y_{bus} of the network at before fault, during fault and post fault respectively. All types of damping were disregarded to obtain worse scenario.

6.2 SIMULATION OF 4-MACHINE 12-BUS SYSTEM

The multimachine system shown in Fig. 6.2 was simulated for studying the dynamic performance of the system. Time-domain simulations were carried out with the multimachine non-linear model developed in Chapter 5. For dynamic analysis, the following two cases were considered -

(a) All the four machines in the system are synchronous generators

(b) Machine at bus # 4 is replaced by an equivalent wind generator.

For comparison purposes, a base case is considered where all the four machines in the system are synchronous generators, i.e. a synchronous generator of equivalent capacity replaces the machine at bus 4. Generation and load data for the base case are given in Appendix B. Line data and generator parameters are also provided there.

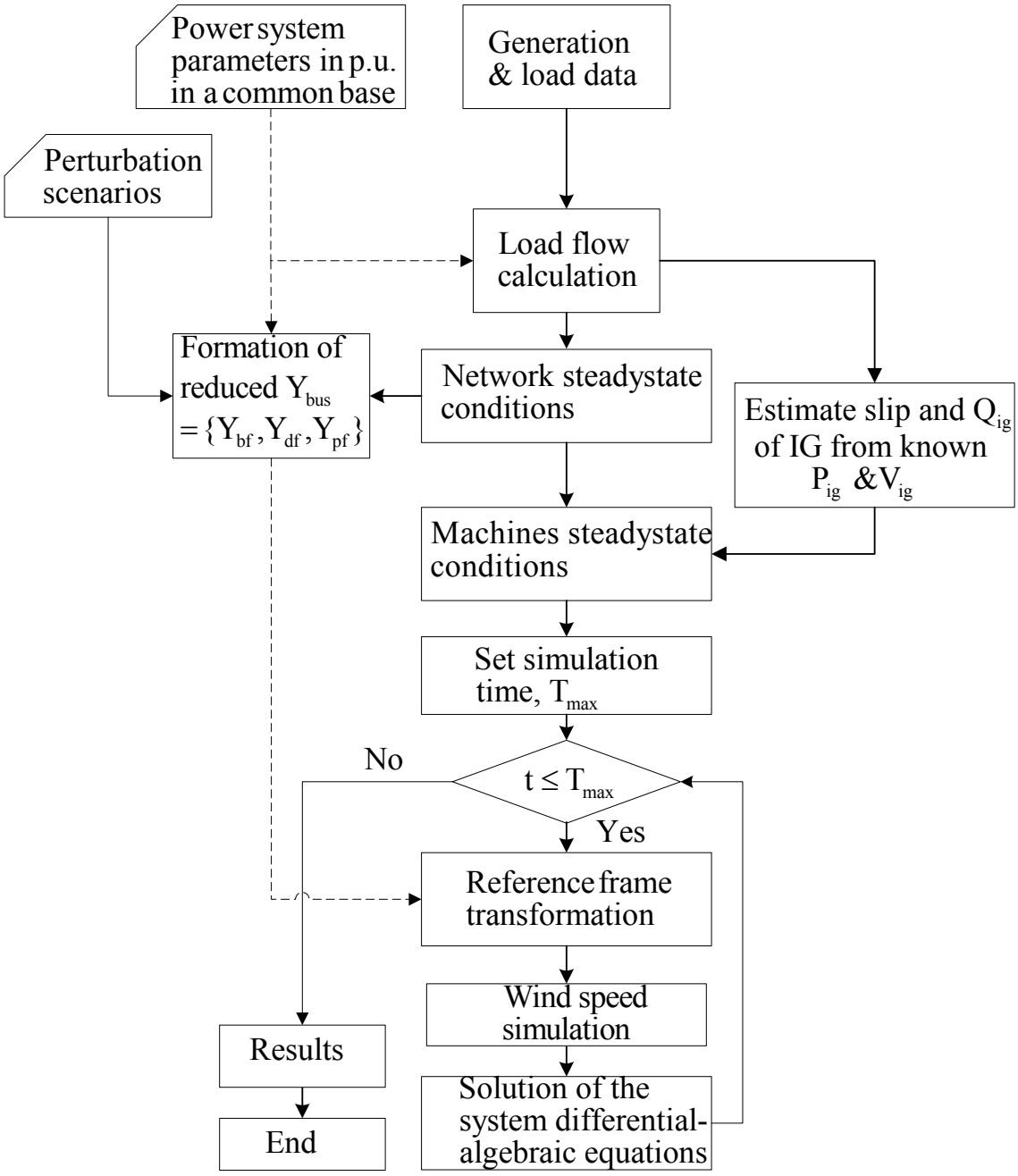

Figure 6.1: Transient analysis flow diagram for multimachine power system with wind power infeed.

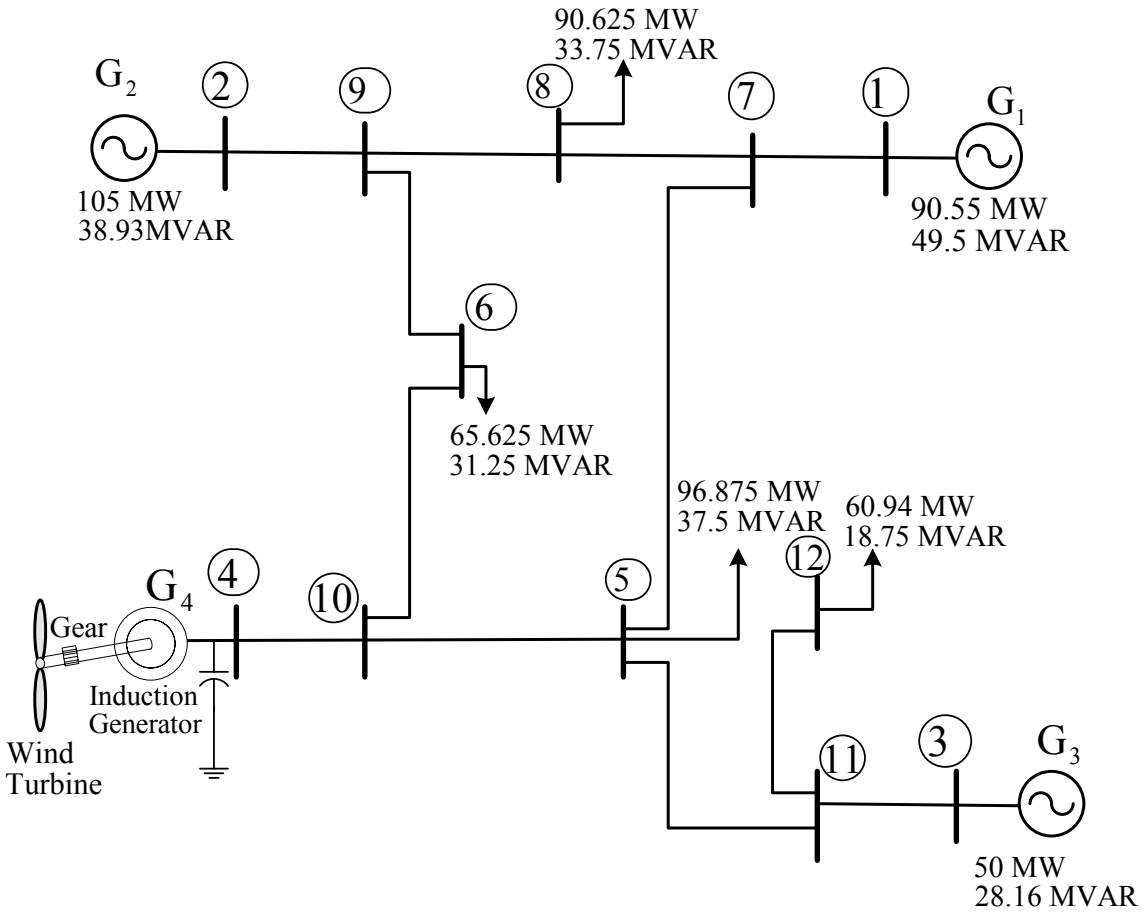

Figure 6.2: A 4-machine 12-bus system configuration

For the base-case it is assumed that 75 MW is supplied by the wind farm which has 50 generators with capacity of 2 MW each. This is approximately 23% wind-power share in the total generation. Equivalent model parameters of the wind-farm determined through the aggregation technique mentioned in Appendix F. It is assumed that the wind-farm is not provided with dynamic reactive power compensation, and wind-farm protection was not included.

6.2.1 Simulation Results

Transient behavior of the wind power integrated multimachine system has been investigated in different system configurations and disturbances. The impact of connection of induction generator through a weak as well as strong network connection has been examined and reported in the publication [107, 108]. It is observed that an induction generator does not pose additional transient stability problems if it is connected through a strong tie line. However, for a weak network connection, system instability may be initiated because of induction generator terminal voltage collapse under some disturbance conditions.

In this section, transient behavior of the wind generation system is investigated in different loading scenarios and fault clearing time. The responses are compared with 'all synchronous generator' cases.

A bolted 3-phase fault is simulated at bus 10, and it is cleared after 83 ms (a 5 cycle fault) by tripping the line 10 – 6. The responses are displayed through Figs 6.3 -6.5. For the base-case loading (P_{g4} = 0.75 pu) and all Sync Gen case, it is observed that the system is stable. The terminal voltage recovers smoothly and machines' speed deviations diminish with time as shown in Fig 6.3. But when wind generator comes in with the same loading, induction generator fails to survive this fault as can be seen from Figs 6.4 & 6.5. Induction generator terminal voltage collapses, which results in failure of the development of electromagnetic torque (Te) and corresponding power output (Pe) as can be seen in Fig 6.4. But the mechanical input torque T_m of the wind turbine does not change rapidly during the short interval. As a result, the induction generator accelerates

rapidly due to large difference between the mechanical and electrical torques as shown in Fig 6.5. The wind generator becomes unstable and requires to be disconnected from the power system. This temporary shutdown of induction generator may result in imbalance of generation and demand. In the absence of enough spinning reserve this may endanger the operation of other synchronous machines.

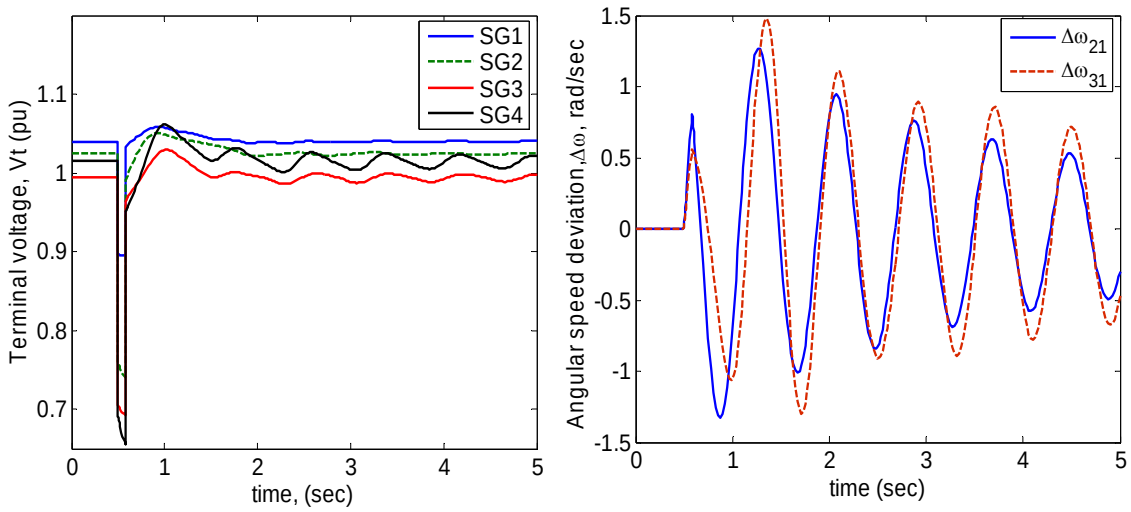

Figure 6.3: Generator terminal voltage variations, and deviations in rotor angular speed (Δω) when a three-phase fault at bus 10 is cleared after 83ms by opening the line 6-10. All Synchronous Generator case. Pe4=0.75 pu.

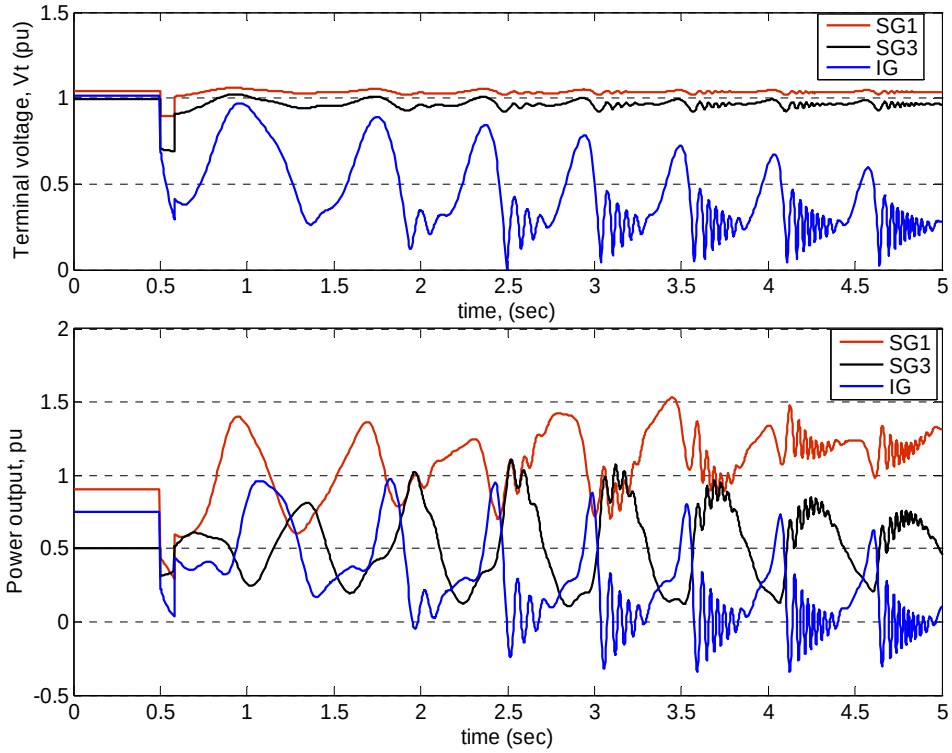

Figure 6.4: Variation of generator terminal voltage, and output power corresponding to fault mentioned in Fig. 6.3. Wind generation case. Pe4=0.75 pu.

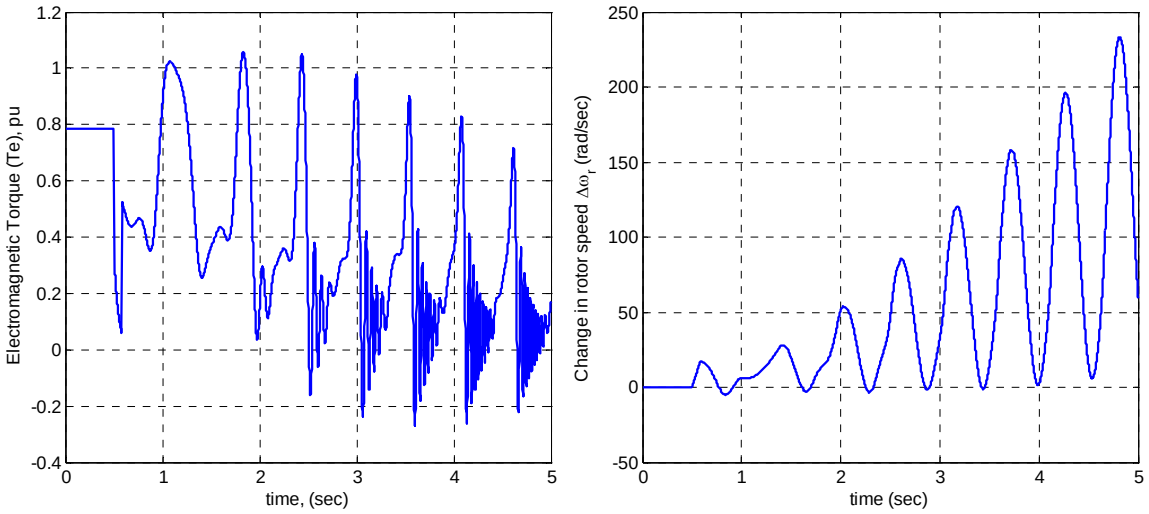

Figure 6.5: Induction generator electromagnetic torque and rotor speed variation corresponding to Fig. 6.4.

In the wind generation case, it is found that the network could tolerate the fault clearing time 83 ms only when the output of the induction generator is reduced to 70 MW as shown in Figs 6.6. The terminal voltage of IG is recovered marginally and the power swing of the machines also diminishes with time.

With regard to fault clearing time, it is observed that 0.70 pu loaded wind generator cannot survive even 6 cycles fault (100 ms) as can be seen in Figs 6.7. Whereas in the same network, 'All SG' case, 0.75 pu loaded G4 can withstand 150 ms (9 cycle fault) easily as can be seen in Figs 6.8.

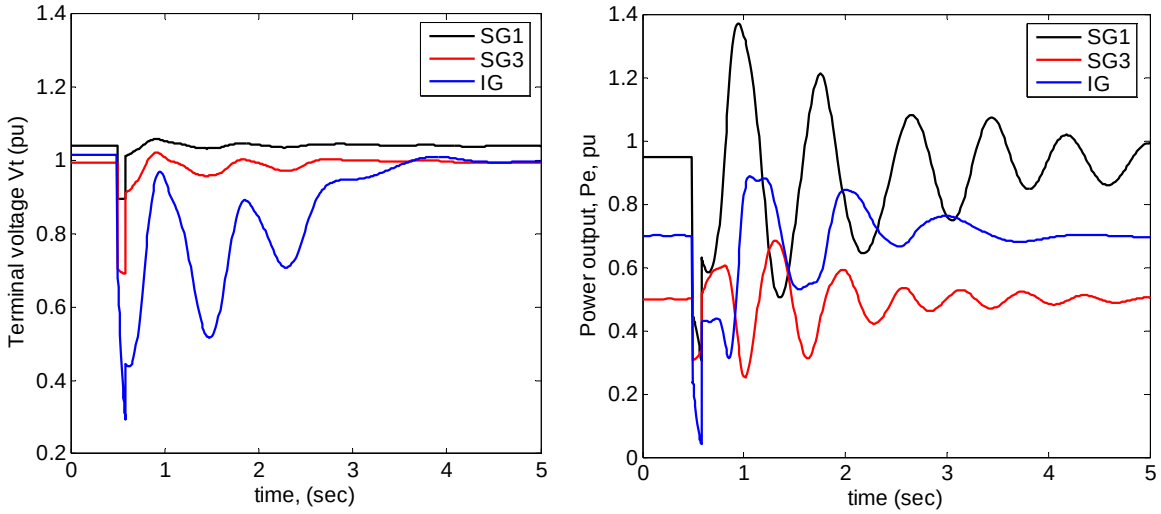

Figure 6.6: Variation of generator terminal voltage, and power output when the 3-phase fault on bus 10 is cleared after 83 ms by opening the line 6-10. Wind generation case. Pe4 = 0.70 pu.

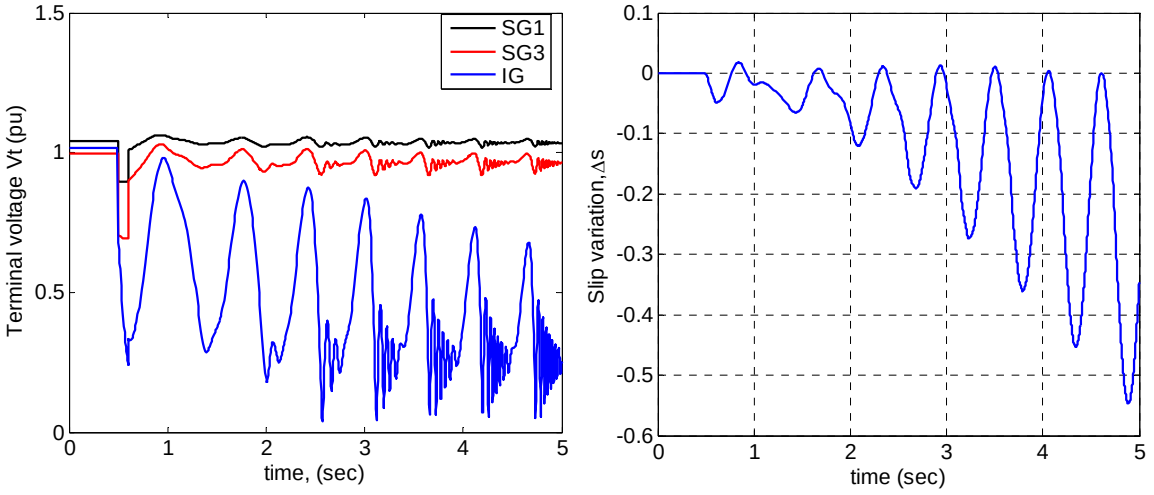

Figure 6.7: Variation of generator terminal voltage, and slip of IG when the 3-phase fault on bus 10 is cleared after 100 ms. Wind generation case. Pe4 = 0.70 pu.

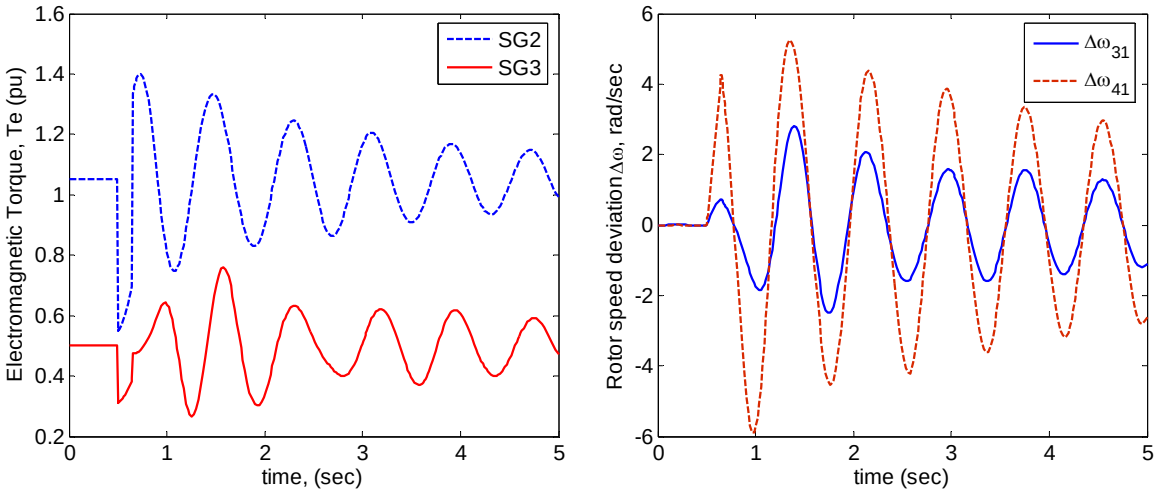

Figure 6.8: Generator electromagnetic torque and rotor speed deviation of SG when the fault at bus 10 is cleared after 150ms by opening the line 10-6. All SG case. Pe4=0.75 pu.

The loss of wind generation due to IG terminal voltage collapse is not only due to the fault at PCC (bus 10), but it may happen because of fault at other locations in the grid as shown in Figs 6.9-6.12. A 3-phase fault at bus 4 of duration 100 ms (self clearing type) caused voltage collapse which resulted in power swing in all remaining 3 SGs as shown in Figs 6.9 & 6.10. Similar voltage collapse also took place when a self clearing type 3-phase fault of 150ms duration appeared at bus 5 as well as 10. Although the severity of fault is similar to Fig 6.11, but power swing is much less as can be seen in Fig 6.12. This is attributed to the location of the fault which is now close to the asynchronous generator.

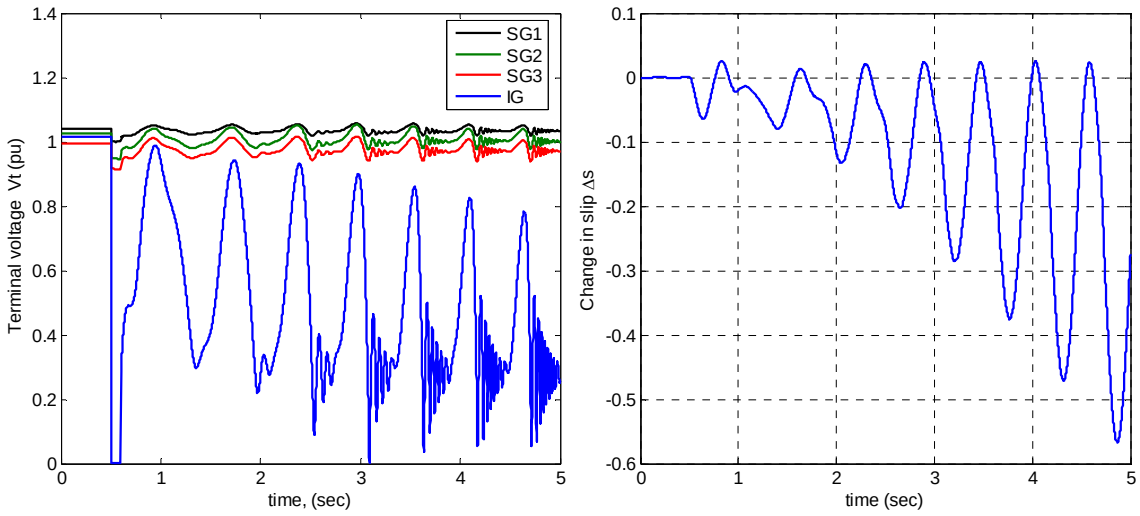

Figure 6.9: Generator terminal voltage responses and induction generator slip variations when fault at bus 4 is cleared after 100ms (self cleared). Wind generation case. Pe4=0.75 pu.

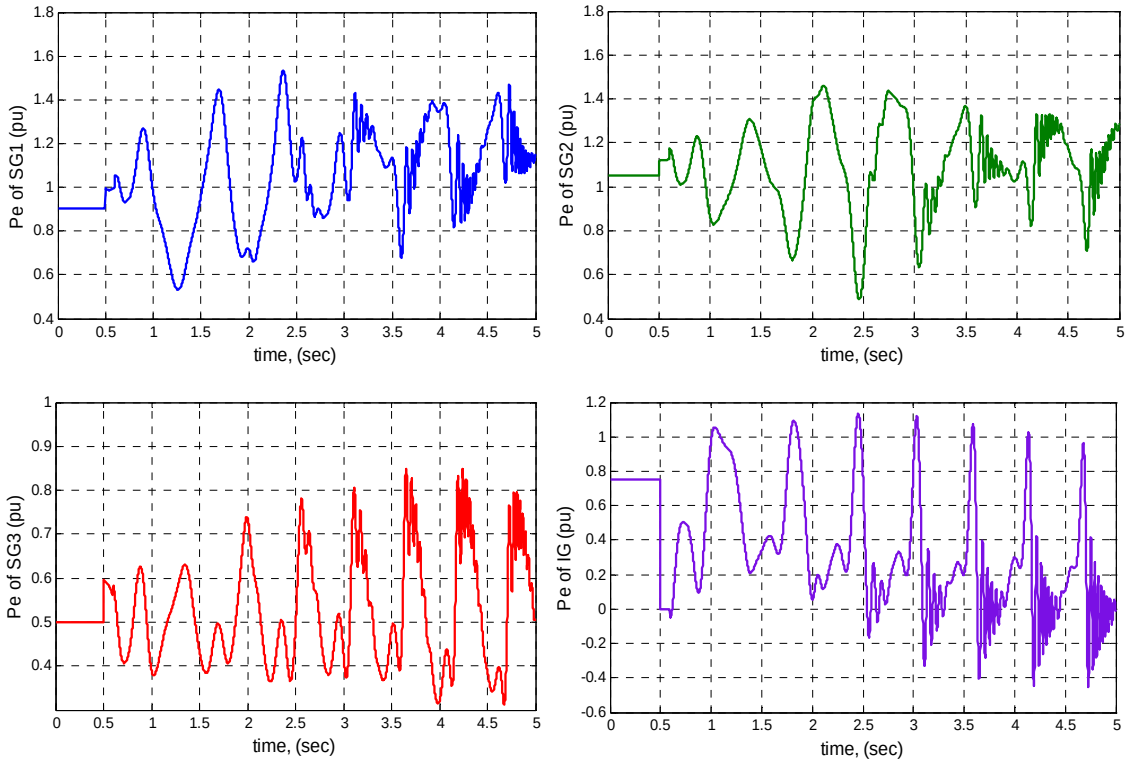

Figure 6.10: Generator output power variations when fault at bus 4 is cleared after 100ms (self cleared). Wind generation case. Pe4=0.75 pu.

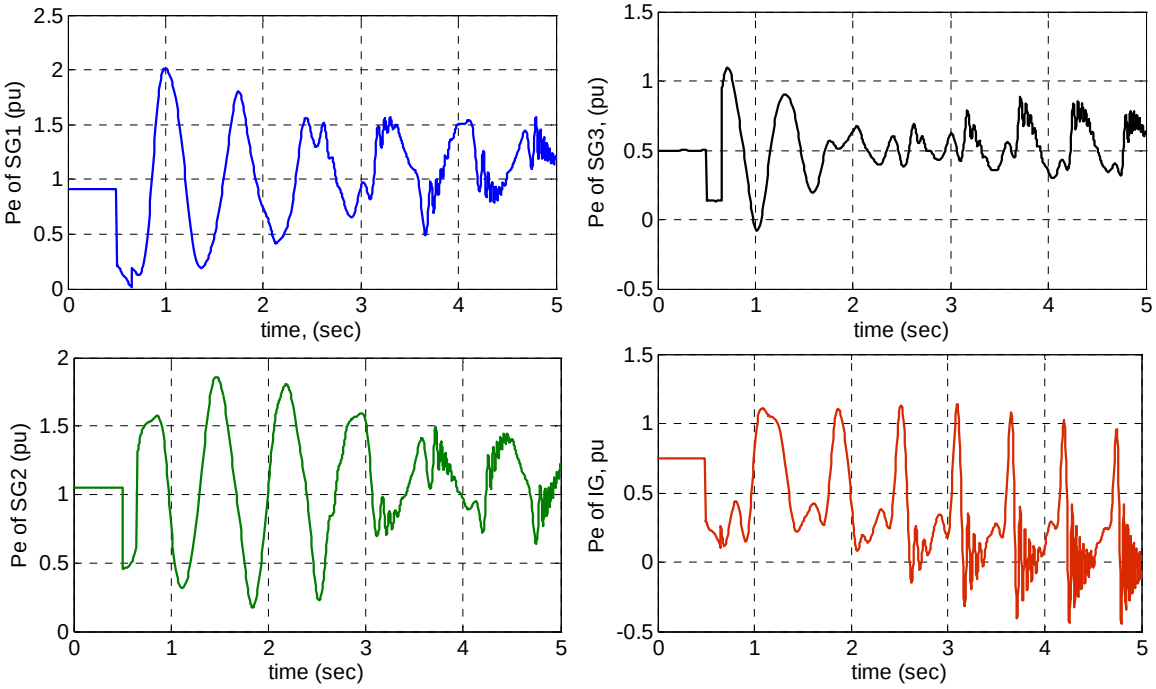

Figure 6.11: Generator output power variations when fault at bus 5 is cleared after 150ms (self cleared). Wind generation case. Pe4=0.75 pu.

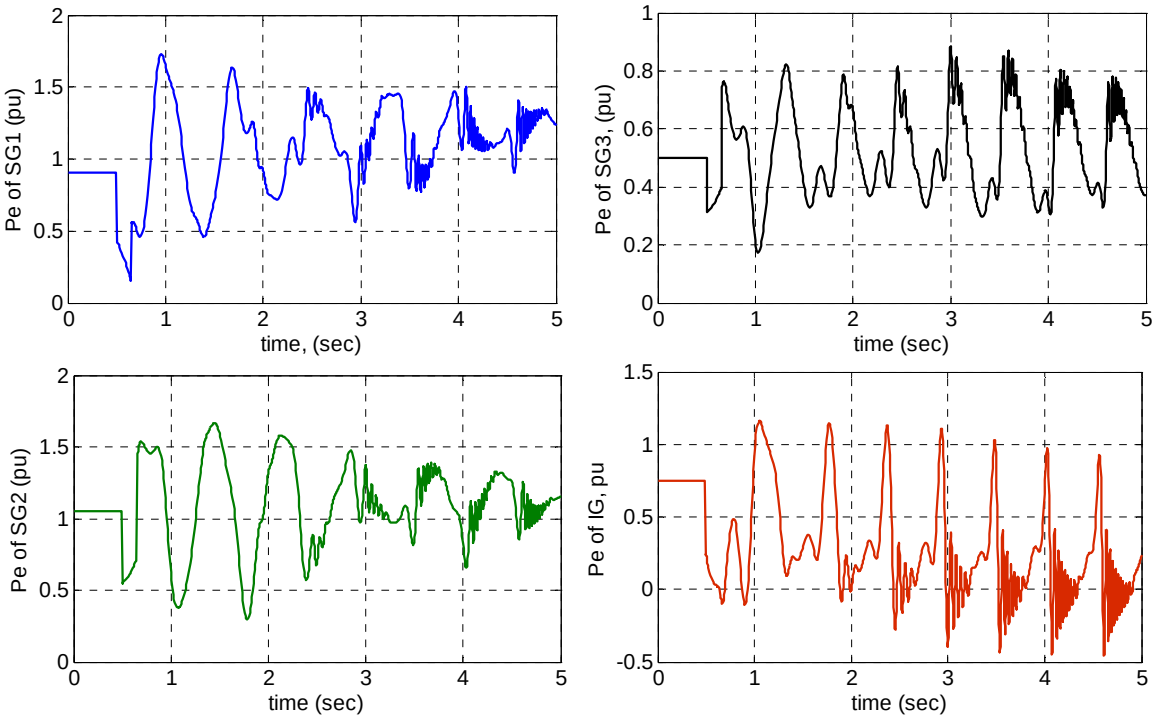

Figure 6.12: Generator output power variations when fault at bus 10 is cleared after 150ms (self cleared). Wind generation case. Pe4=0.75 pu.

6.3 SIMULATION OF 10 MACHINES NEW ENGLAND SYSTEM

10 machine 39 bus New England system is very well known to many power system researchers. In present work, this system used to study the dynamic behavior of a multimachine system containing several wind farms working at different operating conditions. Some of its characteristics are given in Table 6. 6.

TABLE 6.1 : Characteristics of the New England Test System

System characteristics	Value
# of buses	39
# of generators	10
# of loads	19
# of transmission lines	46
Total generation	6140.7MW 1264.3 Mvar
Total load	6097.1MW 1408.7 Mvar

6.3.1 Incorporation of wind generation in the New England System

Three synchronous generators (with generations mentioned in the bracket) G8 (775MW), G9 (540MW), G10 (260.4MW) are replaced by equivalent size of induction generators IG1, IG2, and IG3 respectively as shown in Fig 6.11. Equivalent model parameters of the wind-farm determined through the aggregation technique mentioned in Appendix F. The location of the wind generators are purposely chosen to have different impressions from the site selected. IG1 is connected at bus 8 which represents almost a radial connection of wind generators with the main grid. IG2 is connected at bus 9 which is very close to the swing generator, G1. This induction generator is supposed to receive maximum reactive power support from G1 at the time of crisis. IG3 is located at a moderate place connecting with bus 10.

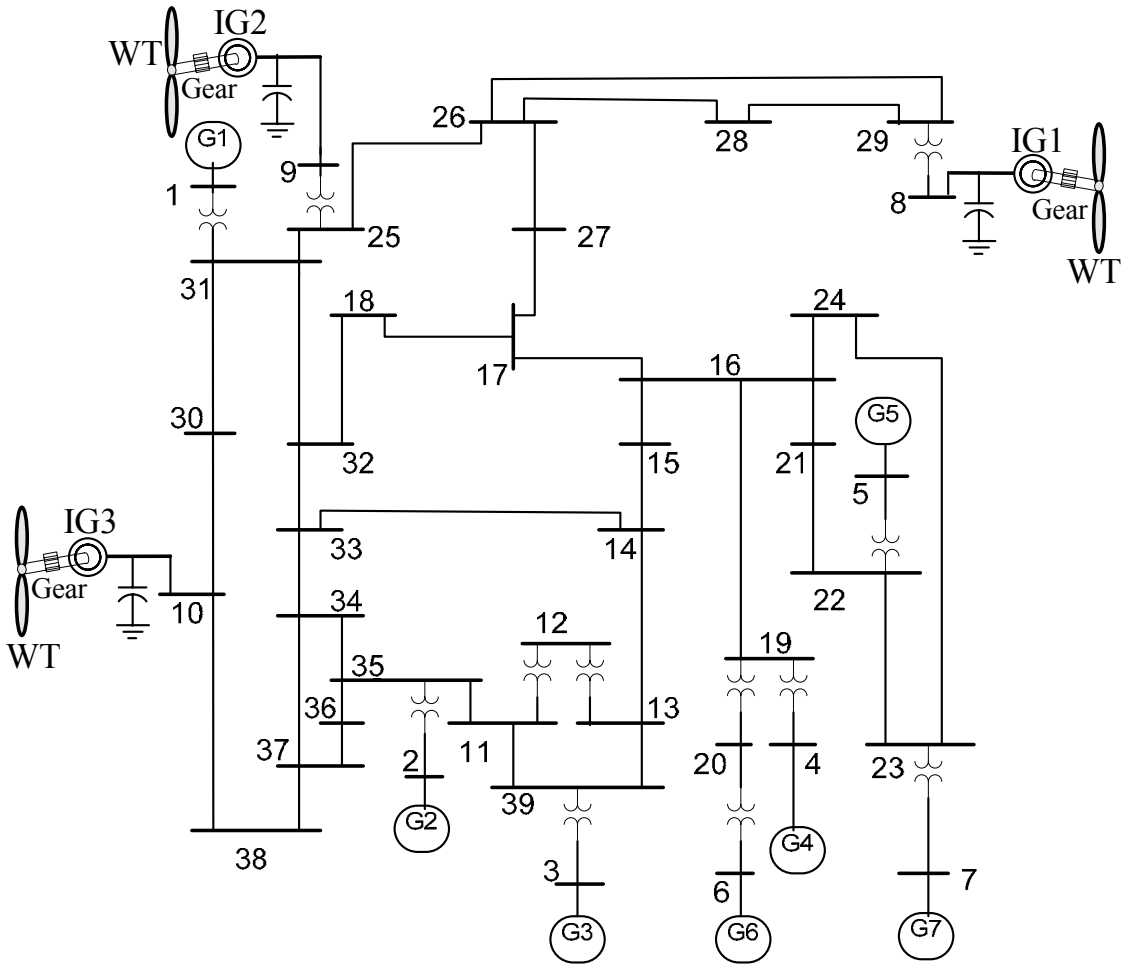

Figure 6.13: Wind generation infeed to the New England System

6.3.2 SIMULATION RESULTS

Transient behavior the multimachine system shown in Fig 6.13 is studied following the simulation technique mentioned in section 6.1. Here the particular attention is the transient behavior of IG1, IG2, and IG3 when their operating points are different. For this purpose, it is considered that each component IG at wind parks 1, 2, and 3 are operated

respectively at 77.5%, 65%, and 54% of their rated value. The corresponding operating slip values are: -1.37%, - 0.95% and -0.88% respectively.

A bolted 3-phase fault is simulated at bus 33, which is cleared after 150 msec by tripping the line 33-14. Fig 6.14, and Fig 6.15 show the terminal voltage, and angular speed responses respectively, when all the machines are synchronous generators. For clarity, plots of few machines are shown here. Others are of similar pattern. The smooth return of these variables to the pre-disturbance state show that the system is quite stable at this disturbance level.

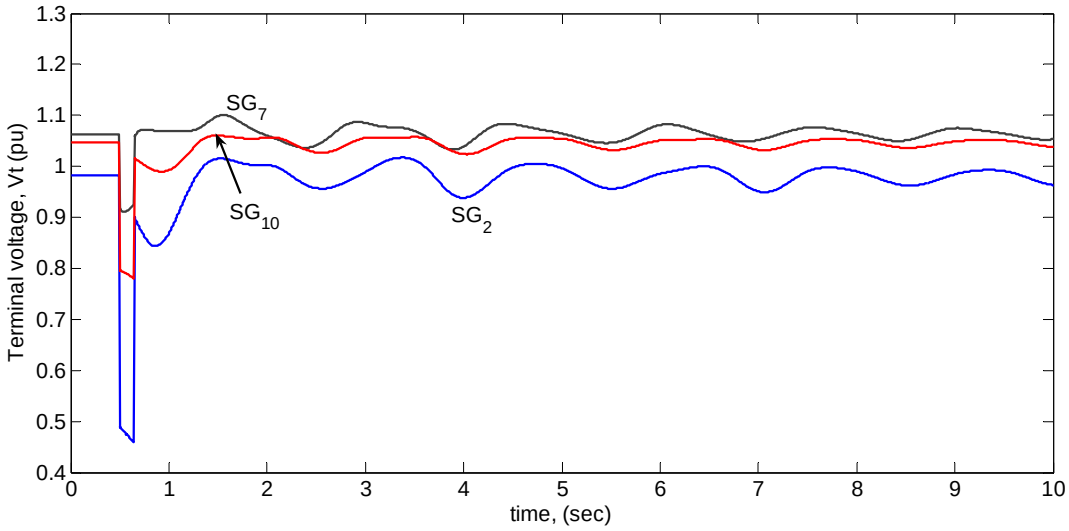

Figure 6.14: Terminal voltage response following a 3-phase fault at bus 33 for 150 msec. The fault is cleared by tripping the line 33-14. All synchronous case.

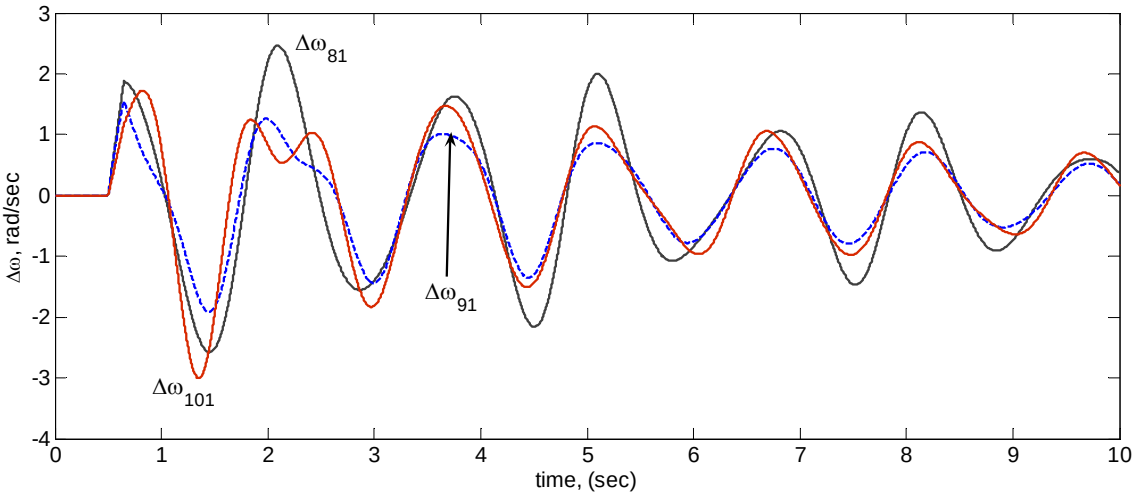

Figure 6.15: Angular speed response with the fault condition mentioned in Fig 6.14. All synchronous case.

For the same fault case, Fig 6.16 and Fig 6.17 show the terminal voltage response and electromagnetic torque response respectively with the wind generation system shown in Fig 6.13. For clarity electromagnetic torques (Te) of only IGs are shown in Fig 6.17. These show that three IGs are affected differently. IG1 is in the worst condition that fails to recover its terminal voltage. In effect, it lost development of electromagnetic torque (Te) as shown in Fig 6.17. Consequently, the rotor speed increases very rapidly as reflected by the slip variation shown in Fig 6.18. There are very slow decline of terminal voltage of IG2 and IG3. The corresponding changes in electromagnetic torque, and slip variations are also very minimal.

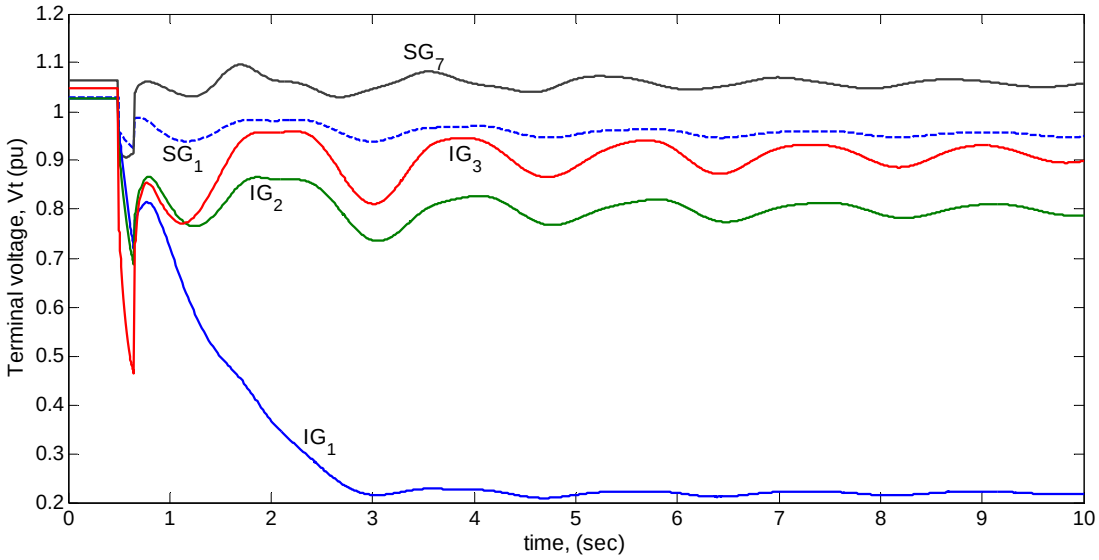

Figure 6.16: Terminal voltage response with the fault condition mentioned in Fig 6.14. Wind generation case.

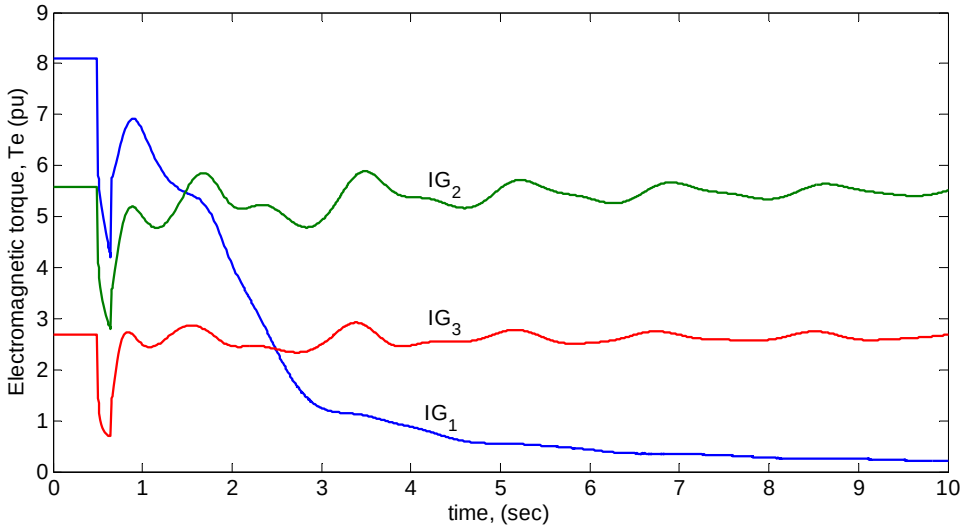

Figure 6.17: Electromagnetic torque response with the fault condition mentioned in Fig 6.14. Wind generation case.

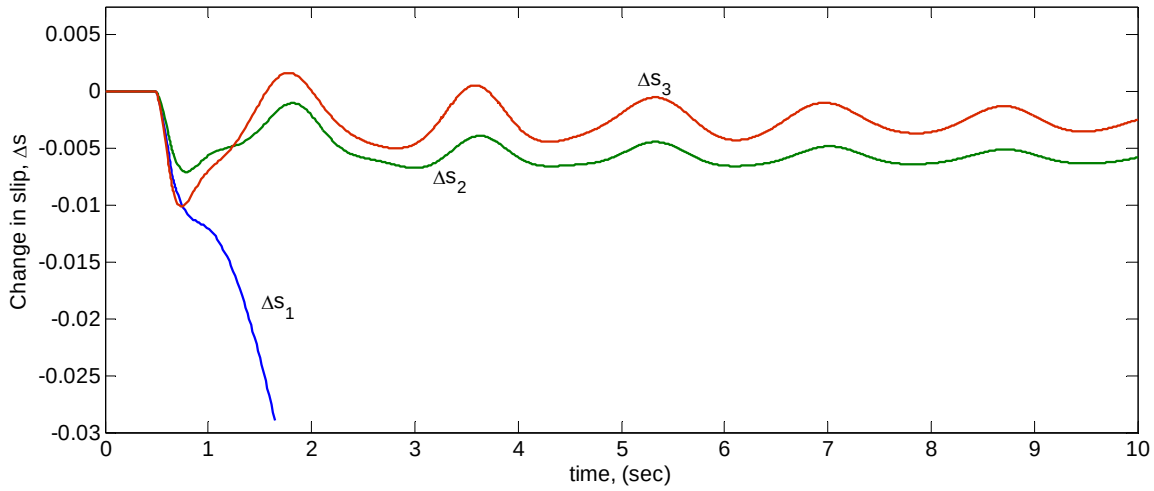

Figure 6.18: Induction generator slip variations with the fault condition mentioned in Fig 6.14. Wind generation case.

The terminal voltage collapse of IG1 could be attributed to the heavier loading and longer electrical distance from the support swing generator (G1). To examine this, the operating conditions of the IG1 are reduced slightly such that each single IG in wind park 1 is generating about 60% of its rated power. The corresponding operating slip is -1.05%. With same grid fault, the transient responses for the present case are depicted in Fig 6.19 – 6.21. They show induction generator terminal voltage response, variations in electromagnetic torque, and slip respectively. Fig 6.19 shows that although terminal voltages of all IGs returns to operating value, slower recovery is quite evident with IG1. This is attributed to the larger transmission line impedance due to longer distance from the swing generator G1. The corresponding slower recovery of slip (Δs) can be seen in Fig 6.21. The pattern of the deviation in other synchronous generators' rotor speed is

shown in Fig 6.22, which confirms the smooth return of the machines to the steady-state value.

The piece of information obtained from this study is that, if a wind farm is located far from the swing generator or main grid, local dynamic reactive power support is very important for the survival of the IG during grid fault of reasonable duration. This arrangement for reactive power support would allow operation of IG near rated value.

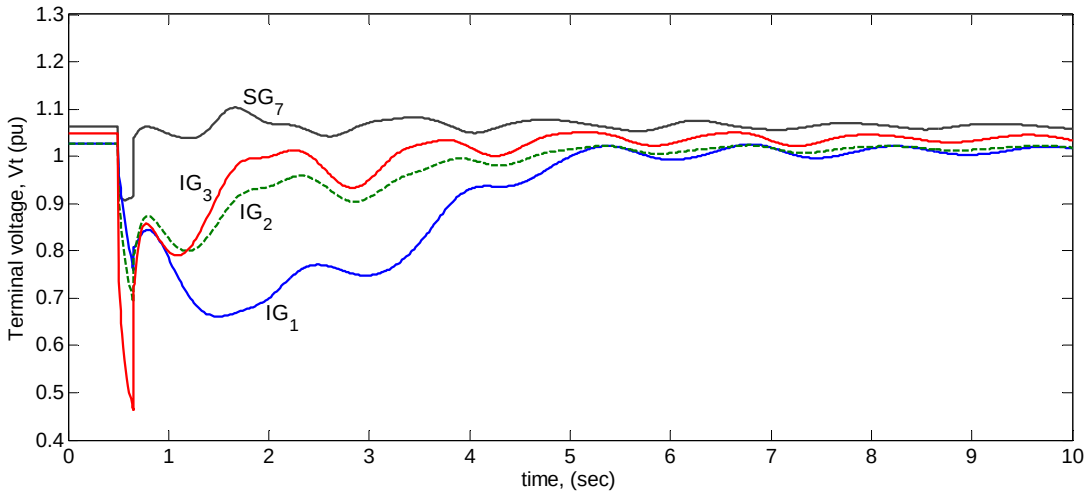

Figure 6.19: Terminal voltage response with the fault condition mentioned in Fig 6.14. Wind generation case.

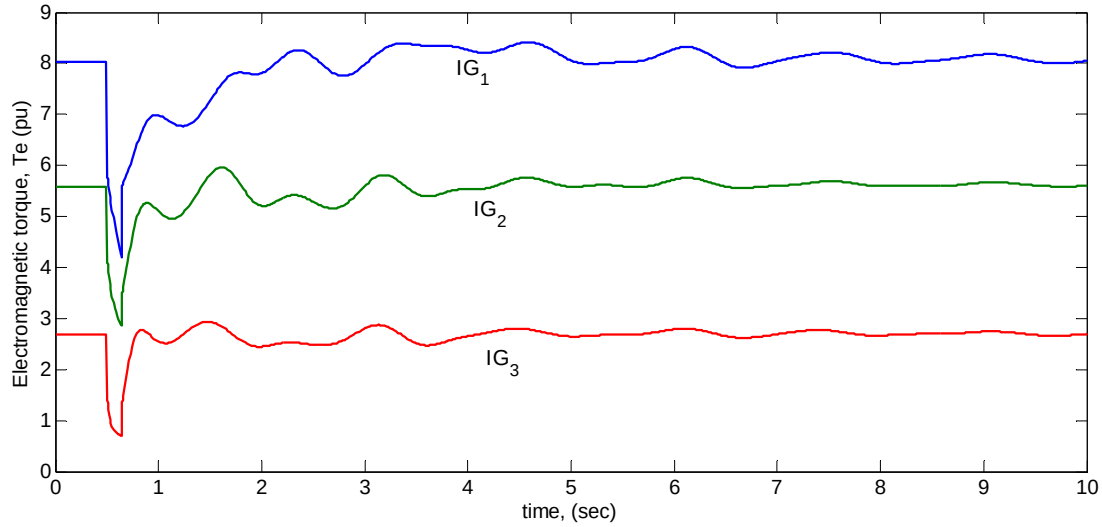

Figure 6.20: Induction generator electromagnetic torque response with the fault condition mentioned in Fig 6.14. Wind generation case.

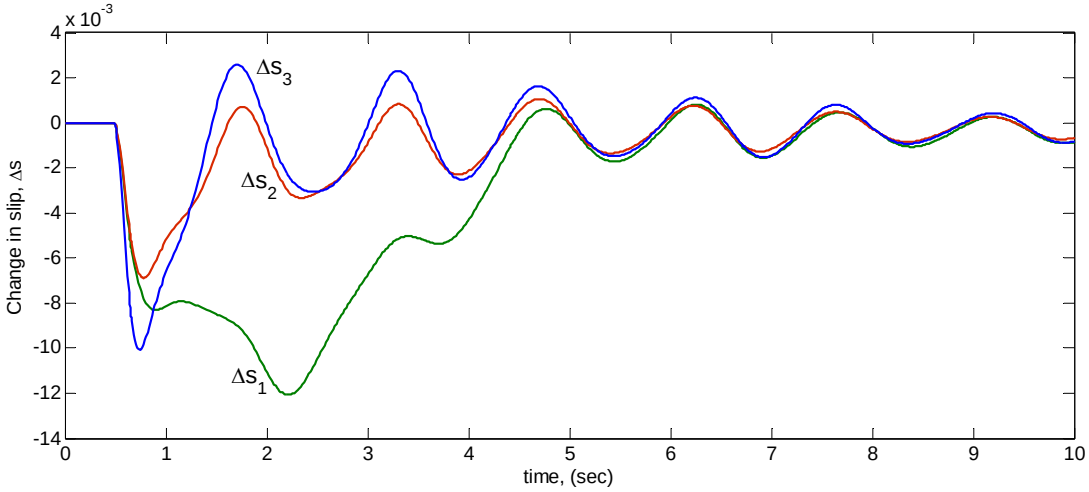

Figure 6.21: Changes in slip of IG1, IG2 and IG3 with the fault condition mentioned in Fig 6.14. Wind generation case.

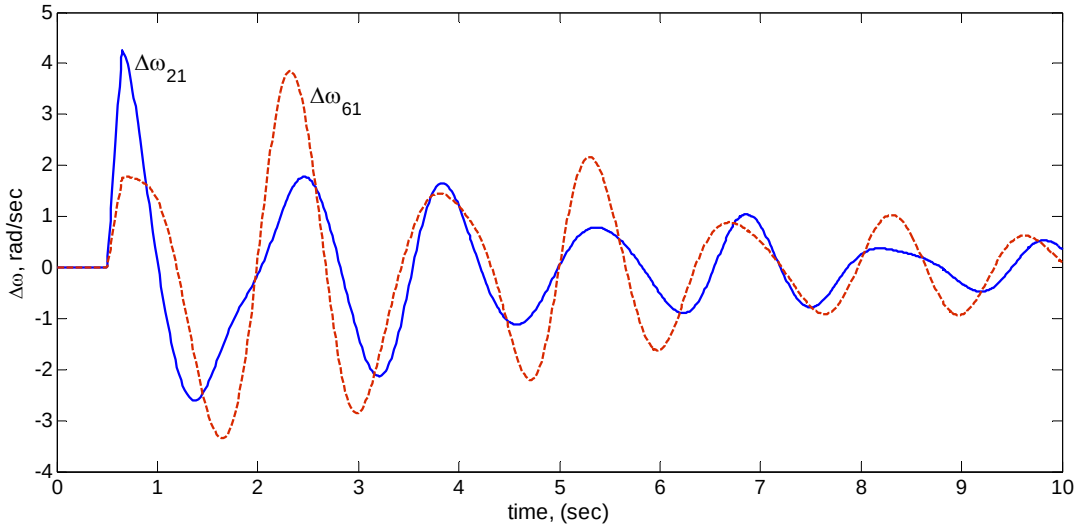

Figure 6.22: Synchronous generator rotor speed deviation (Δω) with the fault condition mentioned in Fig 6.14. Wind generation case.

6.4 FREQUENCY DOMAIN ANALYSIS WITH 4-MACHINE 12-BUS SYSTEM

To investigate the way in which the dynamic stability is influenced as the wind generation capacity is built up in stages to the full capacity situation, the wind generation of machine IG4 corresponding to Fig. 6.2, is gradually increased from lower value to higher value. The considered generations values are : 35MW, 55MW, 65MW, 75MW, 95MW, 105MW, 115MW, and 125MW. These correspond to approximately 10.6% to 38% of total system generation which is 329.17 MW. The full transmission capacity of line is assumed to be available in all the cases. For each loading, eigenvalues of the system are determined in the following way –

Following the technique mentioned in section 6.1, machine variables were initialized through loadflow solution and performing steady-state analysis. These steady-state values determine the machines' operating point. Eigenvalues are calculated around this operating point by using A_{matrix} of the linearized system. Modes of calculated eigenvalues are identified and contributions of individual state-variable to the modes are determined through participation factor method. Compilations of this information are presented graphically through Figs 6.23 – 6.26.

6.4.1 System Eigenvalues when Machine 4 is a Synchronous Generator

To observe the changes in the system eigenvalues when wind generation system is included, eigenvalues for 'all synchronous generator case' are also determined. Damping ratios of the oscillatory modes are calculated. Fig 6.23 shows the variation of individual mode damping-ratio with machine loading. From the participation factor analysis it is

identified that the upper 4 curves are associated with the excitation control of the generators. States contributing to this modes are E_{fd1} ($\lambda_{13,14}$), E_{fd2} ($\lambda_{11,12}$), E_{fd3} ($\lambda_{7,8}$), E_{fd4} ($\lambda_{9,10}$). The damping-ratios of these modes are very high, close to unity. Thus representing near non-oscillatory modes. Through participation factor analysis it is also identified that the lower 3 curves are associated with the electromechanical modes of the generators. States contributing to this modes are ω_2 δ_2 ($\lambda_{1,2}$), ω_3, δ_3 ($\lambda_{3,4}$), ω_4, δ_4 ($\lambda_{5,6}$). Damping ratios of these modes are less than 0.1. Out of these, electromechanical mode associated with Generator 4 has the lowest damping ratio.

Fig 6.24 shows the contour of eigenvalues with increased generator loading (G4). It is observed that all the eigenvalues lie in the left half of contour plot. This implies the AC system remains in dynamically stable condition throughout the span of loading variations on G4. Although Fig 6.24 shows damping ratios of the electromechanical modes decrease with generator loading, but the variations are fairly low.

6.4.2 System Eigenvalues when Machine 4 is a Wind Generator

Fig 6.25 shows the contour of eigenvalues as the share from wind generation increases. Damping ratios of the oscillatory modes are calculated. Fig 6.26 shows the variation of individual mode damping-ratio with machine loading. From the participation factor analysis it is identified that the upper 3 curves are associated with the excitation control of the synchronous generators. States contributing to these modes are E_{fd3} ($\lambda_{13,14}$), E_{fd2} ($\lambda_{11,12}$), $E_{fd1,}$ E_{q1} ($\lambda_{9,10}$). The damping-ratios of these modes are very high, close to unity. Thus representing near non-oscillatory modes. Participation factor analysis also identifies

that out of lower 4 curves, 2 are associated with the electromechanical modes of the generators 2 and 3. States contributing to this modes are: ω_2, δ_2 ($\lambda_{3,4}$), and ω_3, δ_3($\lambda_{5,6}$), respectively. Damping ratios of these modes are less than 0.1. The 3rd and 4th curves belong to wind generator system and represent damping-ratio of mode $\lambda_{7,8}$ and $\lambda_{1,2}$ respectively. States contributing predominantly to these modes are turbine mechanical ω_t, θ_s ($\lambda_{7,8}$) and rotor electrical E'_{q4} ($\lambda_{1,2}$) respectively.

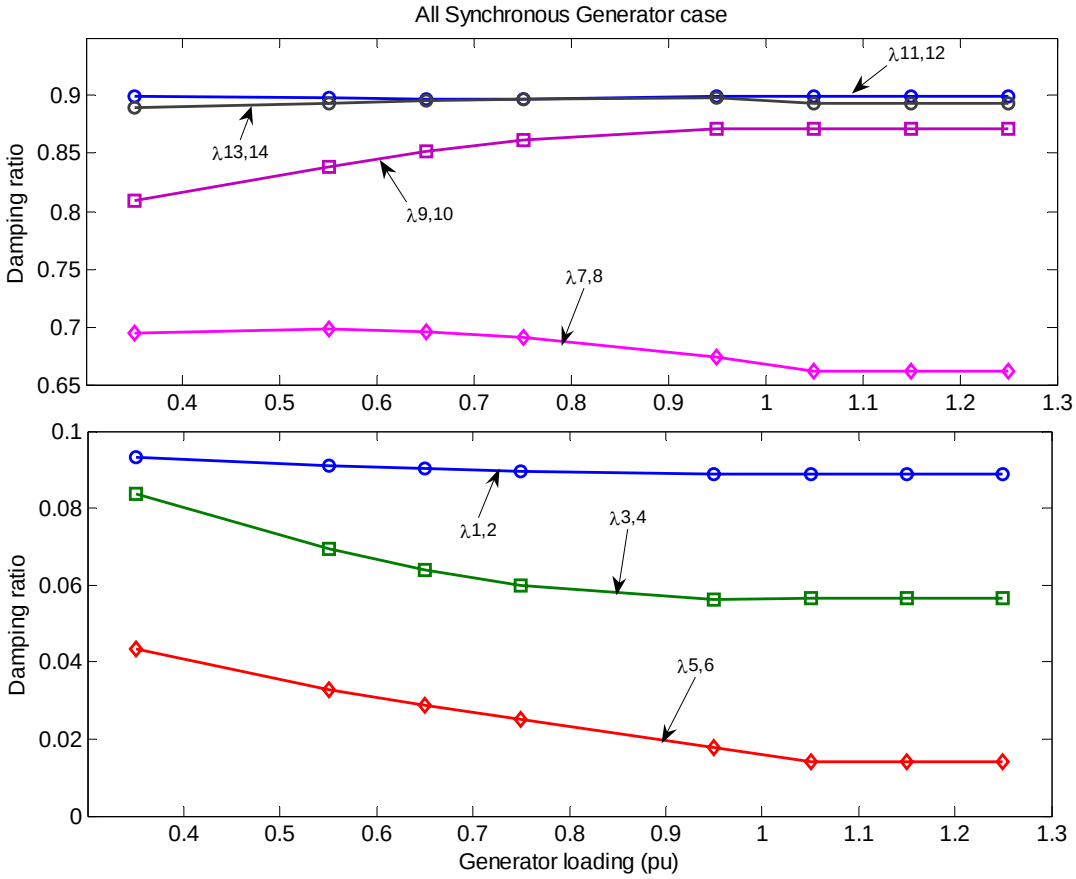

Figure 6.23: Variation of individual mode damping ratio with the loading of Gen 4 is increased. All Synchronous Genenerator case.

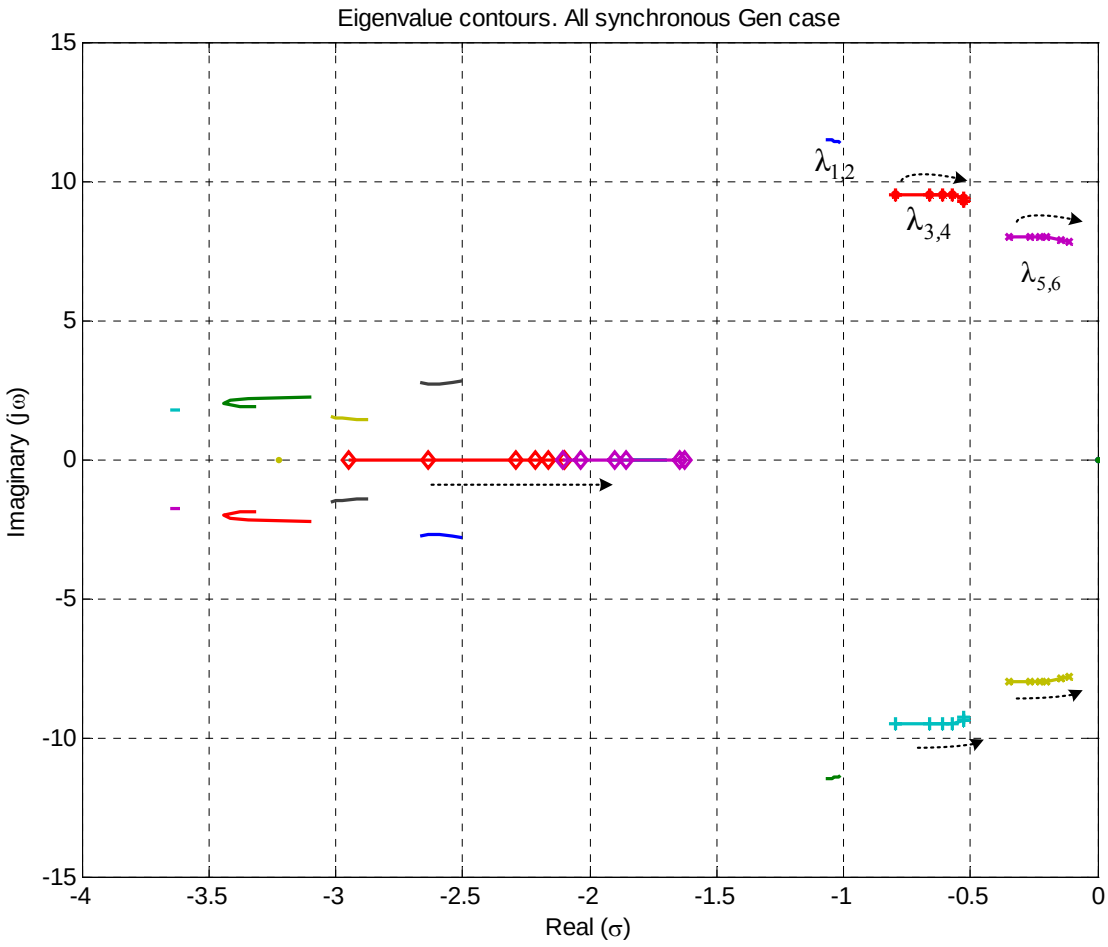

Figure 6.24: Contour of system eigenvalues as the loading on Gen 4 is increased. All synchronous generator case. The arrow indicates the trajectory with increased loading on G4.

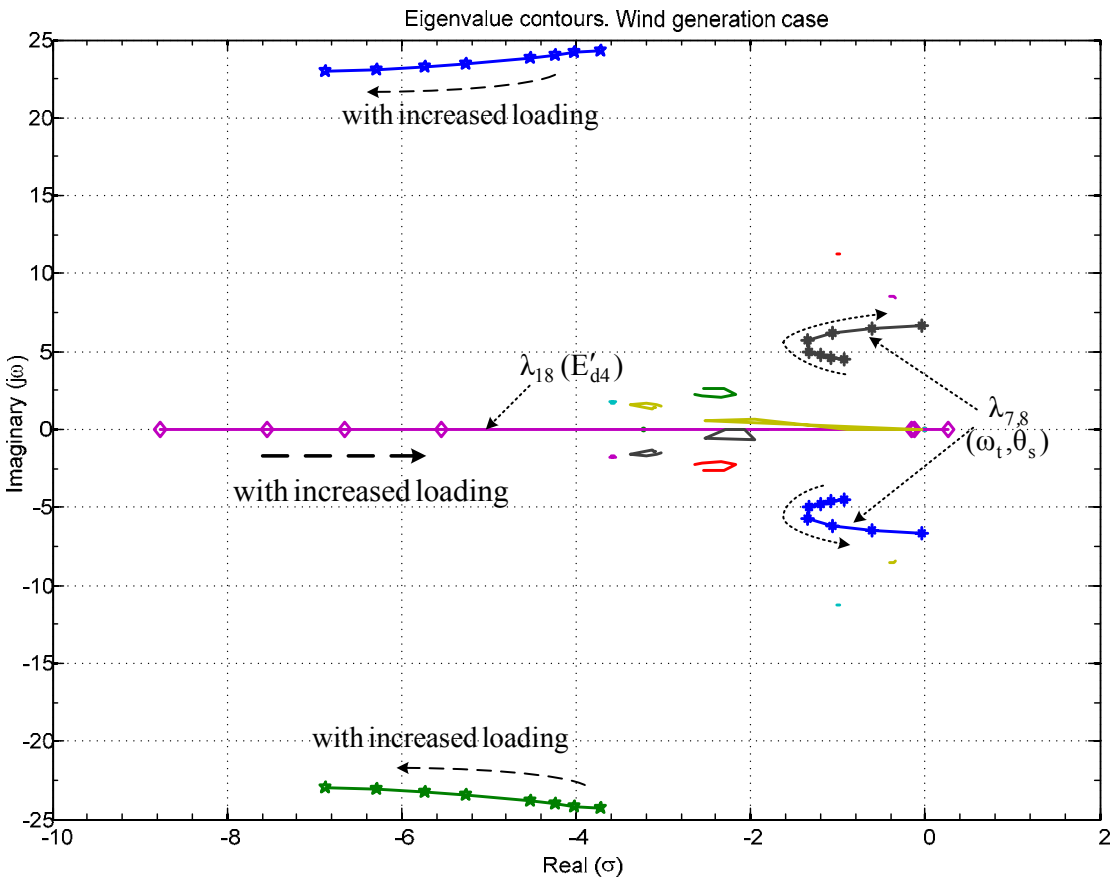

Figure 6.25: Contour of system eigenvalues as the wind generation increases. The arrow indicates the trajectory with increased loading on G4.

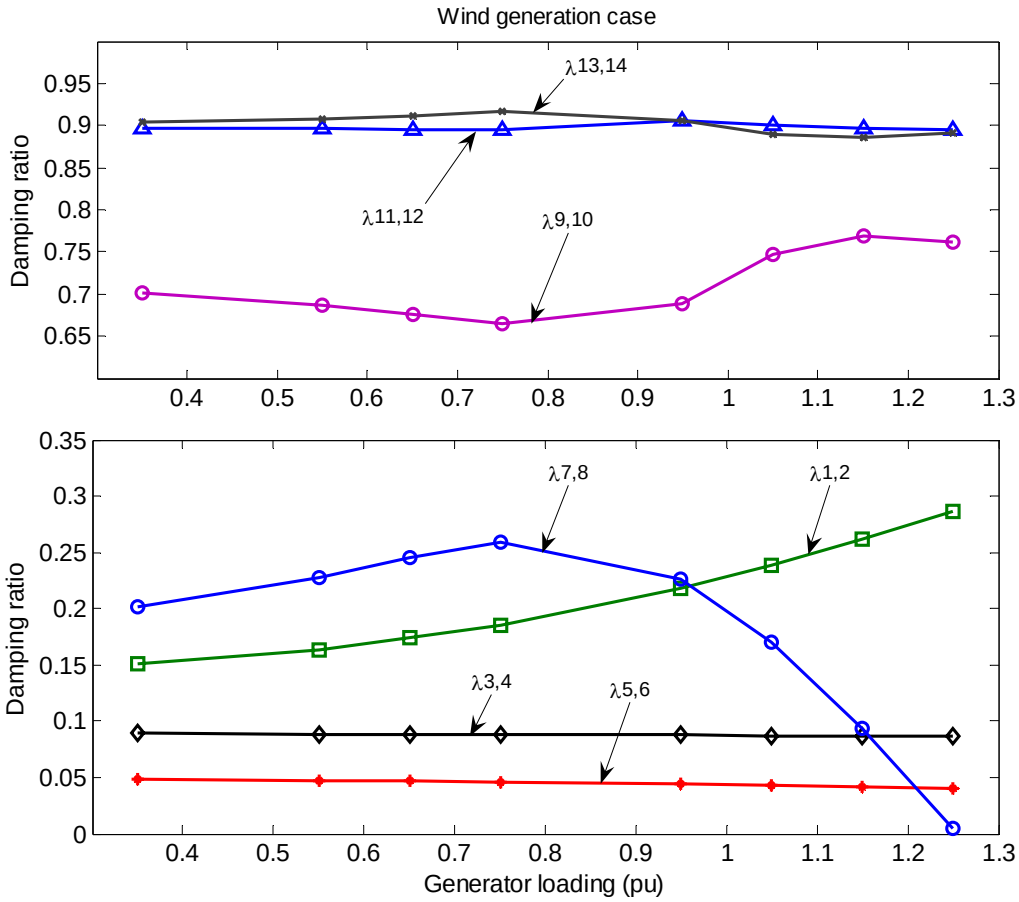

Figure 6.26: Variation of individual mode damping ratio with the increase of wind generation.

A number of changes can be observed when the synchronous Gen 4 is replaced by a wind generator. The dominant electromechanical mode ($\lambda_{5,6}$) of synchronous generator 4 is replaced by a mode ($\lambda_{1,2}$) having quite higher damping ratio and associated with rotor electrical state E'_{q4}. Moreover, the damping ratio of this mode ($\lambda_{1,2}$) increases with generator loading as depicted in Fig 6.25. All these are interpreted in the past works as the 'increase in network damping' [34, 109]. From the contour plot of eigenvalues, it is observed that the non-oscillating mode λ_{18}, initially has much higher negative value. But

as the wind generation increases, λ_{18} moves towards the imaginary axis, and eventually enters to the right-half-plane (RHP) at loading 1.25 pu. Thus makes the system dynamically unstable. States predominantly contributing to this mode is E'_{d4}. So this mode is responsible for initiating system instability. From Fig 6.25 it is observed that damping ratio of one of the dominant mode $\lambda_{7,8}$, initially was at quite higher value, and was increasing with generator loading until around 0.8 pu. Beyond that, it starts decreasing sharply. Therefore, this mode is critical for system instability. Participation factor identifies that this mode is related to turbine mechanical ω_t, θ_s. While damping-ratios of other two electromechanical mode for synchronous generator 2 & 3 make insignificant change with the increase in wind generation, a noticeable increase in damping ratio of exciter mode $\lambda_{9,10}$ (E_{fd1}, E_{q1}) of Gen1 is observed whereas that for turbine mechanical mode $\lambda_{7,8}$ started decreasing in the verge of system instability.

To examine whether addition of wind generator to the AC system improves network damping or not, machine 4 is perturbed with a torque pulse of 30% magnitude and 250 msec duration and speed response of machine 2 and machine 3 are recorded. The responses for both (i) all synchronous, and (ii) wind generation are compared. As shown in Fig 6.27, improvement in network damping is quite significant when wind generators are integrated to the AC system.

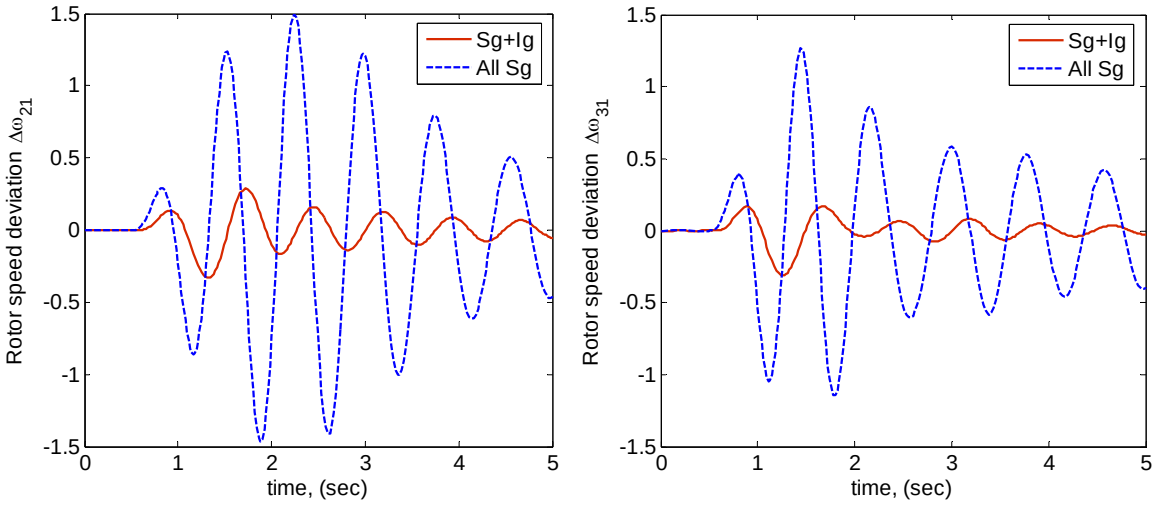

Figure 6.27: Synchronous generator speed response to 30% torque pulse for 250ms at applied at machine 4.

CHAPTER 7

MULTIMACHINE SYSTEM WITH ENERGY STORAGE DEVICES

This chapter studies the impact of energy storage devices like STATCOM/SCESS, on the performance of the multimachine system. The inclusion of the control devices in the multimachine model is followed by simulation results.

7.1 MULTIMACHINE SYSTEM MODEL WITH STATCOM/SCESS

For the multimachine system mentioned at Chapter 5, let us consider STATCOM/SCESS is installed at the generator bus of each induction generator as shown in Fig 7.1. For symmetry and ease of formulation, let us consider that the STATCOM/SCESS is installed with each machine. During simulation, injected STATCOM current (I_{st}) for non STATCOM machines are set equal to zero.

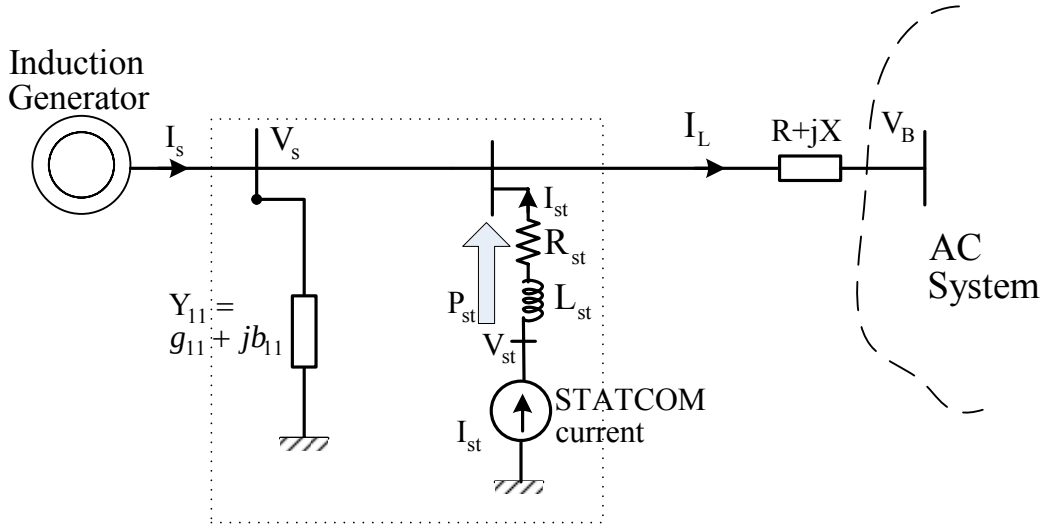

Figure 7.1: Simplified circuit diagram of induction generator installed with STATCOM/SCESS

In Chapter 5, with the introduction of transformation matrix T_1, the network quantities are transferred to machine reference frame. Thus, all the currents and voltages of STATCOM/SCESS are in the respective machine reference frame. This makes the treatment with STATCOM/SCESS controllers exactly same as the single machine infinite bus (SMIB) system described earlier. It is only required to embed properly STATCOM/SCESS currents (I_{st}) with the machine algebraic equations. The formulations are as follows –

Looking from the machine side, current injected to the ith network bus is given by

$$I_L = I_s - V_s Y_{11} + I_{st} \tag{7.1}$$

Where, I_{st} is the current injected by the STATCOM. In d-q terms (7.1) can be written as

$$\begin{bmatrix} i_{ds} \\ i_{qs} \end{bmatrix} = \begin{bmatrix} I_{Ld} - i_{std} \\ I_{Lq} - i_{stq} \end{bmatrix} + \begin{bmatrix} g_{11} & -b_{11} \\ b_{11} & g_{11} \end{bmatrix} \begin{bmatrix} v_{ds} \\ v_{qs} \end{bmatrix} \tag{7.2}$$

Substitute (7.2) into stator voltage equation (5.9) and solve for v_{ds} and v_{qs}

$$\begin{bmatrix} v_{ds} \\ v_{qs} \end{bmatrix} = [C_1] \begin{bmatrix} e'_d \\ e'_q \end{bmatrix} - [C_1 A_1] \begin{bmatrix} I_{Ld} - i_{std} \\ I_{Lq} - i_{stq} \end{bmatrix} \tag{7.3}$$

C_1 and A_1 are as defined in Chapter 5.

Terminal voltage for the i^{th} machine is given by

$$V_B = V_s - z_{12} I_L \tag{7.4}$$

Breaking current and voltages into d-q coordinates (7.4) can be written as –

$$\begin{bmatrix} V_{Bd} \\ V_{Bq} \end{bmatrix} = [C_1] \begin{bmatrix} e'_d \\ e'_q \end{bmatrix} - [D_1 + C_1 A_1] \begin{bmatrix} I_{Ld} \\ I_{Lq} \end{bmatrix} + [C_1 A_1] \begin{bmatrix} I_{std} \\ I_{stq} \end{bmatrix} \tag{7.5}$$

Equation (7.5) is for individual machine and its d-q components can be written as

$$\begin{aligned} V_{Bd} &= k_{11} e'_d + k_{12} e'_q - k_{21} I_{Ld} - k_{22} I_{Lq} + k_{31} I_{std} + k_{32} I_{stq} \\ V_{Bq} &= k_{13} e'_d + k_{14} e'_q - k_{23} I_{Ld} - k_{24} I_{Lq} + k_{33} I_{std} + k_{34} I_{stq} \end{aligned} \tag{7.6}$$

here, k_{11}, k_{12}, k_{13}, k_{14}, k_{21}, k_{22}, k_{23}, k_{24}, k_{31}, k_{32}, k_{33}, and k_{34} are scalars whose value depends on system impedances and admittances. For n number of machine buses, the vector of bus voltages can be written as:

$$\begin{bmatrix} V_{BNd} \\ V_{BNq} \end{bmatrix} = \begin{bmatrix} K_{11} & K_{12} \\ K_{13} & K_{14} \end{bmatrix} \begin{bmatrix} E'_d \\ E'_q \end{bmatrix} - \begin{bmatrix} K_{21} & K_{22} \\ K_{23} & K_{24} \end{bmatrix} \begin{bmatrix} I_{LNd} \\ I_{LNq} \end{bmatrix} + \begin{bmatrix} K_{31} & K_{32} \\ K_{33} & K_{34} \end{bmatrix} \begin{bmatrix} I_{stNd} \\ I_{stNq} \end{bmatrix} \tag{7.7}$$

Where,

$$I_{stNd} = [I_{std1}, I_{std2}, \ldots\ldots I_{stdn}]^T; \quad I_{stNq} = [I_{stq1}, I_{stq2}, \ldots\ldots I_{stqn}]^T;$$

K_{31}, K_{32}, K_{33}, and K_{34} are diagonal matrices whose elements are respectively k_{31}, k_{32}, k_{33}, and k_{34} of each machine as mentioned in (7.6).

At steady-state, STATCOMs are considered floating, i.e. $I_{stNd} = 0$; $I_{stNq} = 0$;

Finally, substituting V_{BNd} & V_{BNq} from (7.7) in (5.33) and solving for I_{LNd} & I_{LNq} we obtain,

$$\begin{bmatrix} I_{LNd} \\ I_{LNq} \end{bmatrix} = [D_2 A_2 B_2] \begin{bmatrix} E'_d \\ E'_q \end{bmatrix} + [D_2 A_2 F_2] \begin{bmatrix} I_{stNd} \\ I_{stNq} \end{bmatrix} \tag{7.8}$$

Where,

$$F_2 = \begin{bmatrix} K_{31} & K_{32} \\ K_{33} & K_{34} \end{bmatrix}$$

All other quantities are as defined in Chapter 5.

By substituting (7.8) in (7.3) an expression for V_{ds} and V_{qs}, in terms of system states can be obtained as:

$$\begin{bmatrix} V_{ds} \\ V_{qs} \end{bmatrix} = f_1\left(\begin{bmatrix} E'_d \\ E'_q \end{bmatrix}, \begin{bmatrix} I_{std} \\ I_{stq} \end{bmatrix}\right) \tag{7.9}$$

Similarly, by substituting (7.8) & (7.9) in (7.2) an expression for I_{ds} & I_{qs} in terms of states can be obtained as

$$\begin{bmatrix} I_{ds} \\ I_{qs} \end{bmatrix} = f_2\left(\begin{bmatrix} E'_d \\ E'_q \end{bmatrix}, \begin{bmatrix} I_{std} \\ I_{stq} \end{bmatrix}\right) \tag{7.10}$$

The algebraic equations (7.9) & (7.10) along with differential equations (5.4 – 5.8), (5.12 – 5.13), (5.16 – 5.18), and (4.6), (4.7), (4.10), (4.11) can be combined together to obtain state model of multimachine wind power system with STATCOM/SCESS as:

$$\dot{x} = f(x,u) \tag{7.11}$$

where,

$$x = [E'_q \;\; E'_d \;\; \omega_r \;\; \delta \;\; E'_{fd} \;\; \omega_t \;\; \theta_s \;\; i_{std} \;\; i_{stq} \;\; V_{dc} \;\; E_{sc} \;\; i_{sc}]', \; u = [m \;\; \psi \;\; D_r]'.$$

7.2 SIMULATION RESULTS

The multimachine system shown in Figure 7.2 was simulated for studying the dynamic performance of STATCOM/SCESS. The generation and load data for the base case are given in Appendix B. It is assumed that approximately 23% of the total generation is supplied by the wind farm which has 50 generators with capacity of 2 MW each. In the load flow analysis, the induction generator (IG) is represented as a PV bus. Steady-state calculation is performed to determine initial slip and reactive power consumed by the IG. At the IG terminal appropriate reactive power is provided by a fixed capacitor. Then, with the obtained loadflow solution, the generators are initialized by solving its set of differential algebraic equations with all time derivatives set equal to zero. All types of damping were disregarded to obtain worst-case scenario.

Table 7.1: Operating points of multimachine wind system with STATCOM/SCESS

SG1	SG2	SG3	IG
$V_t = 1.04\angle 0°$pu Pg = 0.9055 pu Qg = 0.495 pu α= 4.44°	$V_t = 1.025\angle 1.42°$pu Pg = 1.05 pu Qg = 0.389 pu α= 34.62°	$V_t = 1.04\angle 0°$pu Pg = 0.5 pu Qg = 0.2816 pu α= 19.132°	$V_t =$ $1.015\angle 14.47°$pu Pg = 0.75 pu Slip, so = - 1.357%

α is the machine angle with respect to swing bus. MVA_{base} = 100.

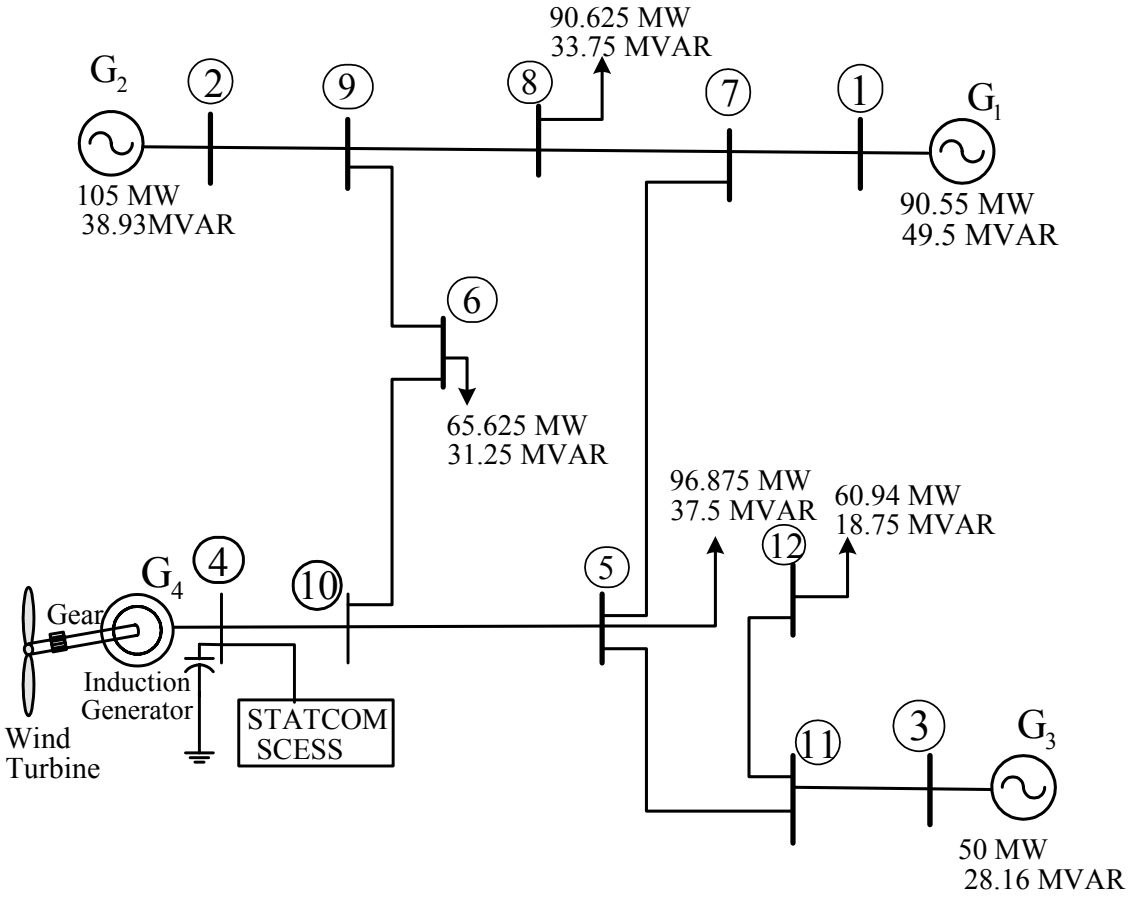

Figure 7.2**:** Multimachine system configuration with STATCOM/SCESS

Two cases with the wind generation system are simulated and compared – (i) without and (ii) with STATCOM/SCESS. As it was observed from the SMIB study that the performance of STATCOM/SCESS with decoupled P-Q control was better compared to STATCOM Q control only, so only P-Q control is considered here. The multimachine system is transiently perturbed by applying a bolted 3-phase fault at bus 10 for 150 msec. The fault is cleared by opening the line 10-6.

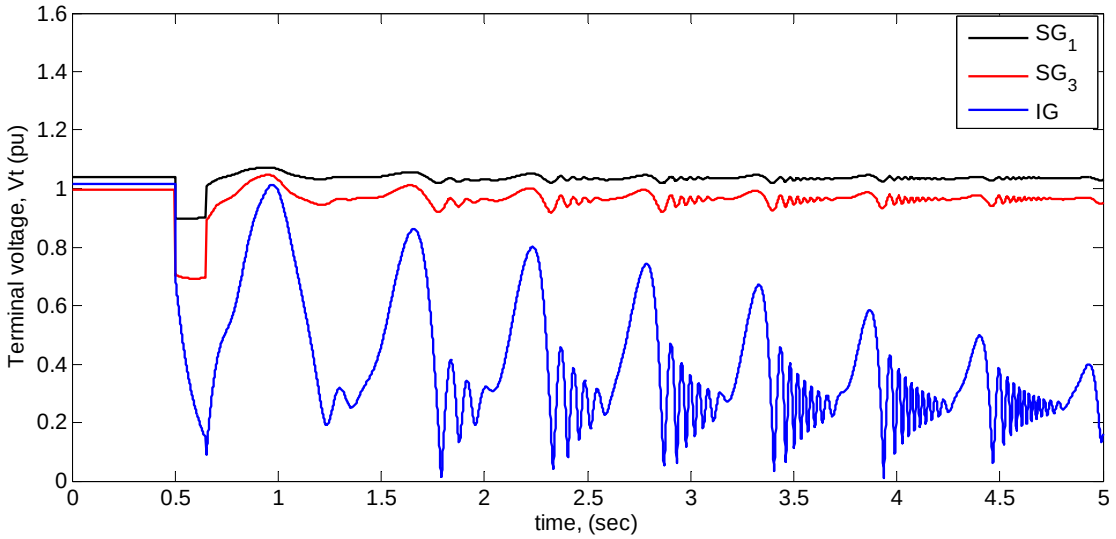

Figure 7.3: Terminal voltage response with no control on IG. Voltage profile for SG2 is in between SG1 & SG3.

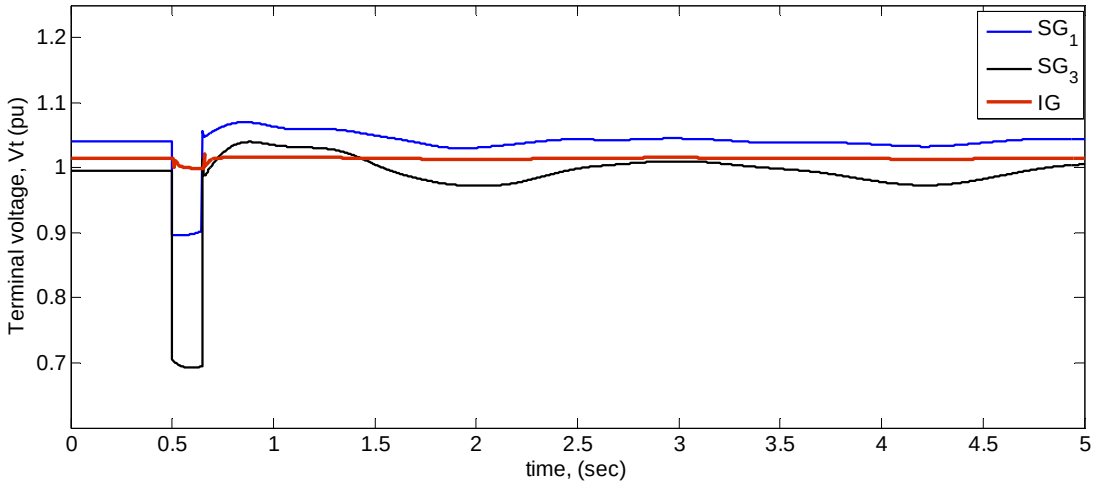

Figure 7.4: Terminal voltage response when IG is supported by STATCOM/SCESS.

Fig 7.3 shows the terminal voltage response without any control on the induction generator (IG). As mentioned earlier, during fault induction generator accelerates, and

terminal voltage and flux collapse. When the fault is cleared, it requires extra reactive power (Q) support for quick recovery of its flux and terminal voltage. For no control case, in the absence of such Q support, induction generator fails to recover its terminal voltage as can be seen in Fig 7.3. For the synchronous generators, with equipped automatic voltage regulator (AVR) action, terminal voltage is quickly recovered after the fault is cleared.

In the case of IG aided by STATCOM/SCESS, the P-Q controller senses the deviation in local bus voltage and injects required reactive power to quickly restore the local bus voltage. This prevents IG terminal voltage collapse as shown in Fig 7.4. Fig 7.5 shows the injected reactive power by the STATCOM/SCESS controller.

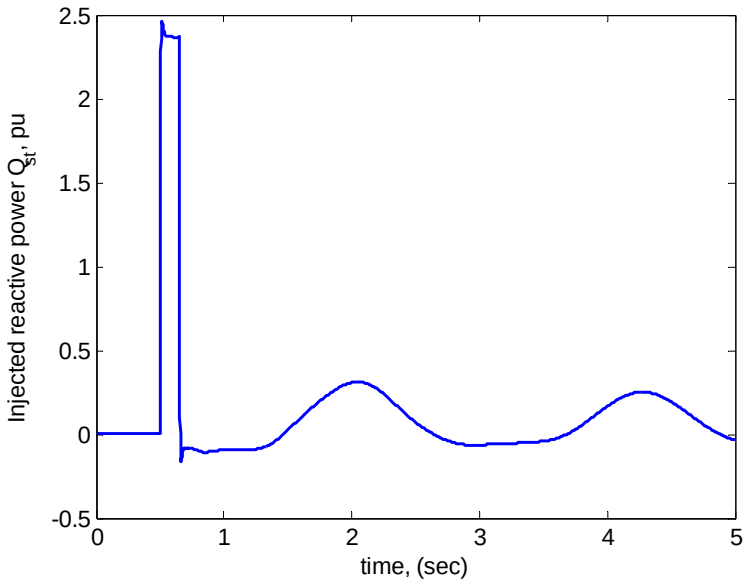

Figure 7.5: Injected reactive power by the STATCOM/SCESS controller

Fig 7.6 shows the variation in induction generator rotor speed ($\Delta\omega_r$) (a) without any control, and (b) with STATCOM/SCESS respectively. With no control, the oscillations in rotor speed grows dangerously requiring temporary separation from the main AC system, where as with STATCOM/SCESS rotor speed remains under control which returns to operating values after brief oscillations.

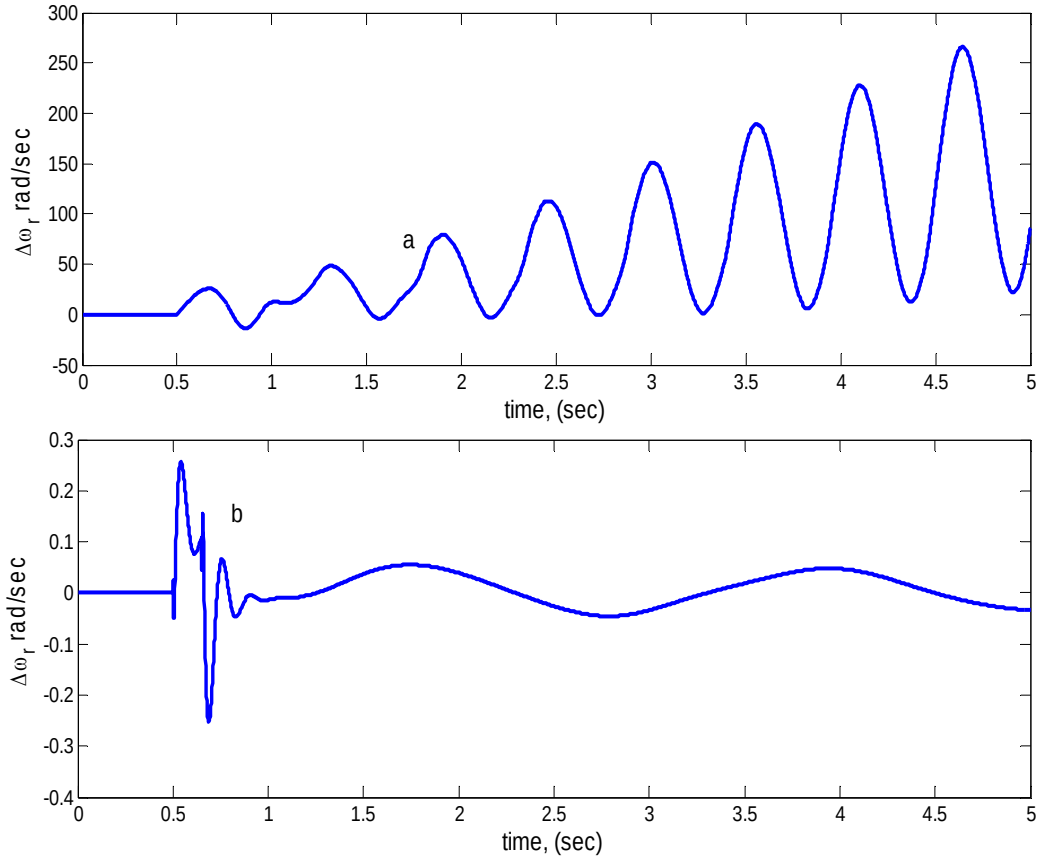

Figure 7.6: Variation in IG rotor speed, $\Delta\omega_r$ (a) no control, and (b) with STATCOM/SCESS.

Fig 7.7 and 7.8 show the transients in generators' output power without any control and with STATCOM/SCESS respectively. With no control, as the IG voltage and flux collapse, it also fails to generate power as shown in Fig 7.7. Whereas with

STATCOM/SCESS IG power out remains almost constant and all the synchronous generators output power return to the operating values after some oscillations.

Due to these power swings in the uncontrolled case, rotor speed swing also increases as can be seen in Fig 7.9. However, aiding induction generator with STATCOM/SCESS this oscillations in rotor become very small and die down quickly.

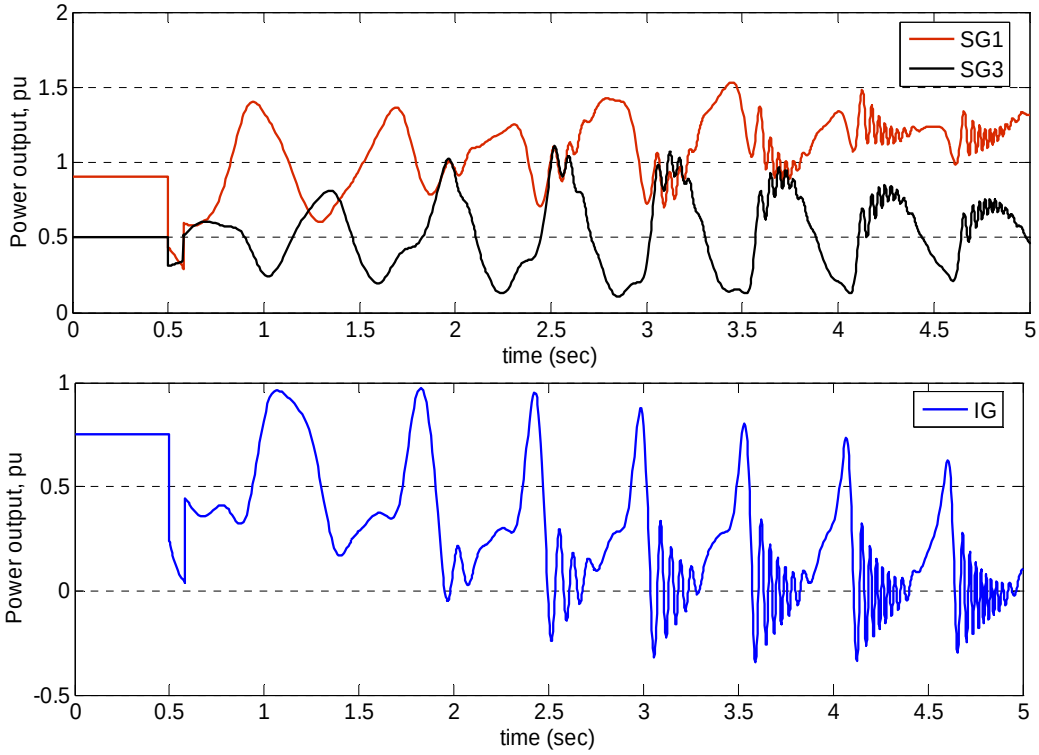

Figure 7.7: Generator power output with no control on IG

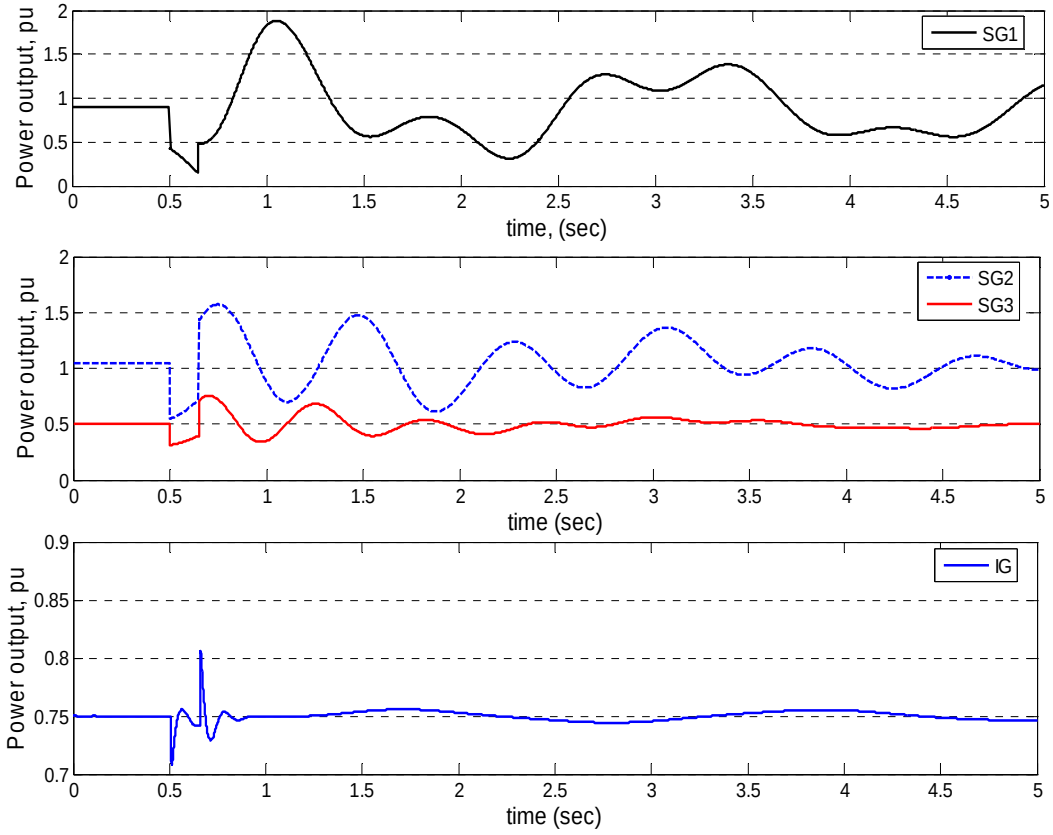

Figure 7.8: Generator power output with STATCOM/SCESS

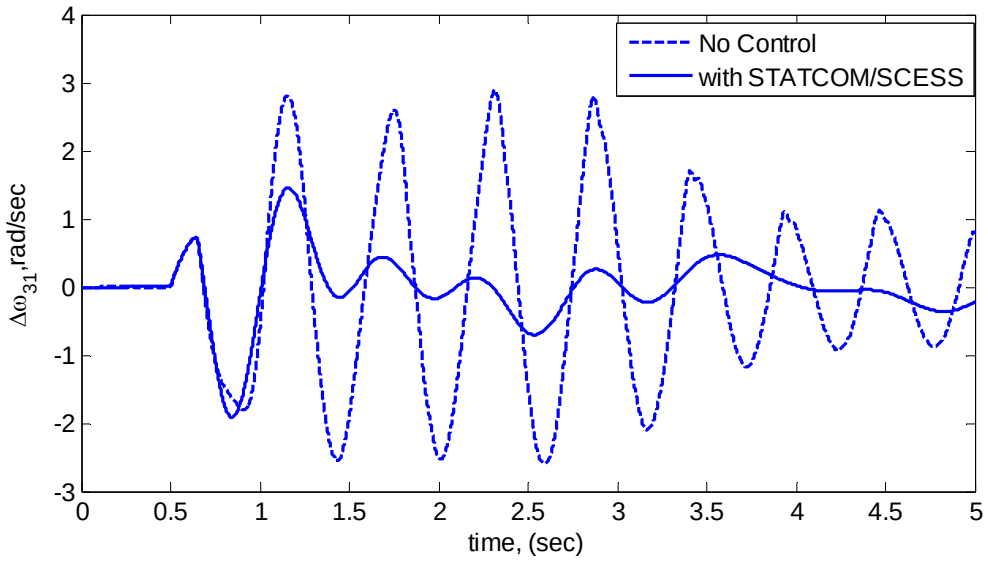

Figure 7.9: Comparison of synchronous generator angular speed variations with & without STATCOM/SCESS

Dynamic performance of wind generation system with simple STATCOM having Q control only was tested and compared with that of both P & Q control. Fig 7.10 shows the output power variation of the IG when the system was perturbed with the same fault as mentioned in Fig 7.8. From Fig 7.10 it is very clear that with P & Q control transients are much less that of with Q control only. This is attributed to the controller's ability for compensating of real power in addition to reactive power.

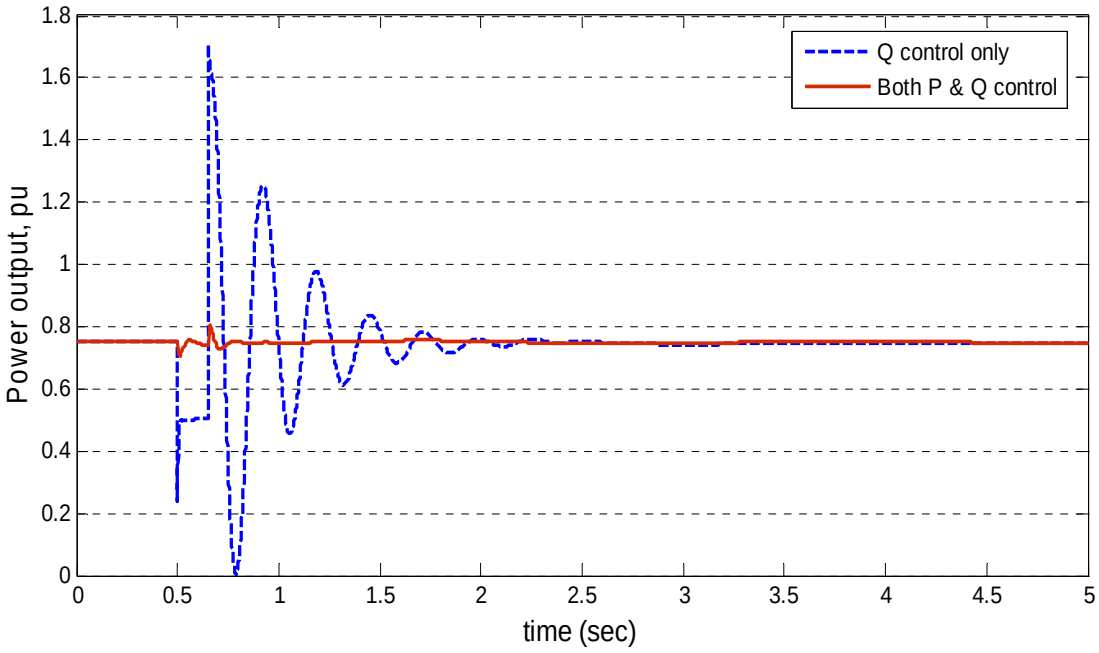

Figure 7.10: Comparison of performance between Q control, and both P & Q control of STATCOM/SCESS

7.3 FAULT RIDE-THROUGH REQUIREMENT

As Grid Code requirements for wind farm connection are becoming increasingly demanding, supporting controller design should be tested for its capability to meet-up

these requirements. Since squirrel-cage induction generator (SCIG) based wind generators on their own have difficulty meeting these requirements, any controller providing FRT support would add a great value in the SCIG based wind generator operation. To this end, the proposed STATCOM/SCESS controller performance is tested to meet FRT requirement as mentioned in US Grid Code for wind generators.

A bolted 3-phase fault is simulated at the grid connection point (bus 10) and the fault is cleared after 625 ms by tripping the line 6-10. Fig 7.11 shows the terminal voltage response when the induction generator is equipped with STATCOM/SCESS. It senses the deviation in terminal voltage and promptly injects required Q (reactive power) to restore the terminal voltage. There is almost negligible terminal voltage variation of IG, this exhibits excellent performance for meeting FRT requirement.

Thus it is observed that squirrel-cage induction generator (SCIG) based wind generators when supported by STATCOM/SCESS can achieve significant withstand capability against grid fault. It experiences almost negligible rotor speed variation, maintains constant terminal voltage, and resumes delivery of smoothed (almost transient free) power to the grid immediately after the fault is cleared.

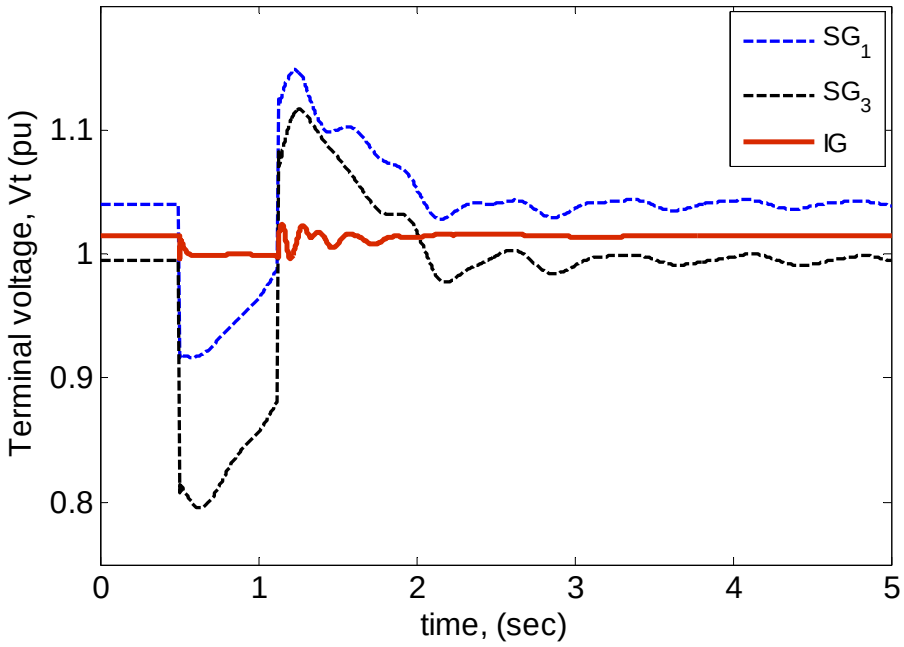

Figure 7.11: Terminal voltage response when the fault at grid bus 10 is cleared after 625 ms by opening the line 6-10.

CHAPTER 8

CONCLUSIONS

8.1 SUMMARY AND CONCLUSIONS

The impact of wind power infeed on dynamic performance of a power system is investigated through detailed modeling of wind generator system when it is connected (i) to an infinite grid, and (ii) to a finite grid system comprised of several synchronous machines. Induction generator based variable-speed wind generation system is considered here. The entire system model considers the dynamics of the turbine-generator rotating shaft system, generator electrical system, controllers, and the utility grid.

For the dynamic model of multimachine wind-ac system, a general transformation matrix is defined for the transformation of machine and network quantities to a common reference frame. In this work, network quantities are transformed to machine reference frame in order to facilitate controller design attached to generator terminal. Since the controller becomes local to the machine, its input/output variables do not require further reference frame transformation.

For each type of grid connection mentioned, both time domain and frequency domain analyses were performed to study transient and dynamic characteristics of the system. The considered systems are – A 4 machine 12 bus system, 10 machine 39 bus New England system as well as single machine infinite bus system.

Eigenvalue analysis for both single machine as well as multimachine system revealed that the mode of instability of induction generator based wind generation system is different from that of conventional synchronous generator based AC system. For wind system, the modes responsible for system instability are: (i) rotor electrical, associated with e'_d, and (ii) mechanical, associated with ω_t and θ_s. Rotor electrical mode is generally non-oscillatory in contrast to lightly damped electromechanical mode of synchronous generator. The degree of coupling between rotor mechanical and electrical dynamics as reflected by the participation factors depends on the operating point.

Through a number of simulation studies it is observed that wind turbine driven induction generators are vulnerable to transient disturbances like wind gust and fault on the system. The fixed capacitor located at the generator terminal cannot normally cater for the reactive power demand during the disturbance period. Without support reactive power compensation scheme, unacceptable level of frequency and voltage transients may develop. These may lead to system separation even for smaller or mid-level disturbances.

In this study, two reactive power compensation schemes have been proposed for dynamic performance improvement of the wind generation systems. These are –

(a) through variable susceptance control where the excitation capacitance is automatically adjusted depending on the stator terminal voltage variation, and (b) through STATCOM reactive power control, which maintains induction generator terminal voltage dynamically. Further improvement in transient profile has been brought in by incorporating additional PID control with scheme (a) and real power control in scheme (b) by supporting STATCOM with bulk energy storage devices. Two types of energy storage system (ESS) have been considered – BESS and SCESS. A decoupled P – Q control strategy has been implemented on STATCOM/ESS.

It has been observed that both schemes (a) & (b) have good potential for providing excellent transient profile. The STATCOM, however, has been shown to provide superior performance. This is attributed to the STATCOM's fast response capability and ability of independent reactive control. The best performance is obtained with STATCOM/ESS. It is observed that wind generators when supported by STATCOM/ESS can achieve significant withstand capability in the presence of grid fault. It experiences almost negligible rotor speed variation, maintains constant terminal voltage, and resumes delivery of smoothed (almost transient free) power to the grid immediately after the fault is cleared.

With regard to grid integration, it is observed that tie-line impedance has significant influence on IG terminal voltage fluctuation following a disturbance in the system. Wind generator connected to the grid with larger tie-line impedance may be prone to frequent

terminal voltage collapse due to grid fault. In this case, local reactive compensation has been shown to be crucial.

8.2 FURTHER STUDIES

1. Other wind energy technologies like doubly-fed induction generator (DFIG), permanent magnet synchronous generator (PMSG) can be considered.
2. Auxiliary controls on synchronous generators and also turbine actions have not been considered. They could be included in further study.
3. In the present study, loads are modeled as constant impedance. Extension can be made to consider frequency dependent loads or dynamic loads.
4. Wind-generator system and the controllers developed in this study can be extended to simulate with RTDS (Real Time Digital Simulation) for electromagnetic transients.
5. Other types of controller like fuzzy-logic, adaptive control etc. can be attempted for dynamic reactive compensation.
6. Intelligent computation techniques can be adopted to tune controller parameters.
7. Dynamic performance of wind generator system can be investigated employing other short term energy storage devices like superconducting magnetic energy storage (SMES), flywheel, etc.
8. Pitch control can be applied in conjunction with generator side controls and overall system performance can be investigated. Additionally, reduction in required reactive as well as real power compensations can be examined.

Appendix A

Voltage behind Transient Reactance model of Induction Generator: Full order model

Induction generator model is derived from the voltage-current-flux relations originally developed for induction motor [49]. In this thesis generator convention is used *i.e.* current flowing out of the machine is considered positive. With this convention, the dynamics of stator and rotor flux linkage components is synchronously rotating d-q reference frame are given by -

$$-R_s i_{ds} - \frac{\omega_e}{\omega_b}\Psi_{qs} + \frac{1}{\omega_b}\dot{\Psi}_{ds} = v_{ds} \qquad (A1)$$

$$-R_s i_{qs} + \frac{\omega_e}{\omega_b}\Psi_{ds} + \frac{1}{\omega_b}\dot{\Psi}_{qs} = v_{qs} \qquad (A2)$$

$$-R_r i_{dr} - s\Psi_{qr} + \frac{1}{\omega_b}\dot{\Psi}_{dr} = v_{dr} \qquad (A3)$$

$$-R_r i_{qr} + s\Psi_{dr} + \frac{1}{\omega_b}\dot{\Psi}_{qr} = v_{qr} \qquad (A4)$$

The flux linkages and currents are related through:

$$\left.\begin{aligned}\Psi_{ds} &= -x_{ss} i_{ds} - x_m i_{dr}\\ \Psi_{qs} &= -x_{ss} i_{qs} - x_m i_{qr}\end{aligned}\right\} \qquad (A5)$$

$$\left.\begin{aligned}\Psi_{dr} &= -x_{rr} i_{dr} - x_m i_{ds} \\ \Psi_{qr} &= -x_{rr} i_{qr} - x_m i_{qs}\end{aligned}\right\} \tag{A6}$$

The definition of transient reactance (x'), voltage behind transient reactance (e'_d, e'_q), and rotor time constant (T'_o) give –

$x' = x_s + \left(\frac{1}{x_m} + \frac{1}{x_r}\right)^{-1}$; x′ is also called short circuit reactance, and the above can be simplified as-

$$x' = x_{ss} - \frac{x_m^2}{x_{rr}} \tag{A7}$$

Where,

$x_{ss} = x_s + x_m$ and $x_{rr} = x_r + x_m$ which are also called open circuit reactance

$\text{Rotor time constant} \quad T_0' = \frac{x_{rr}}{\omega_0 R_r}$

And

$$e_d' = -\frac{x_m}{x_{rr}}\Psi_{qr}; \qquad e_q' = \frac{x_m}{x_{rr}}\Psi_{dr} \tag{A8}$$

Using (A6) & (A8) the rotor current can be represented in terms of e'_d, e'_q as

$$i_{dr} = -\frac{e_q'}{x_m} - \frac{x_m}{x_{rr}} i_{ds} \quad \text{and} \quad i_{qr} = \frac{e_d'}{x_m} - \frac{x_m}{x_{rr}} i_{qs} \tag{A9}$$

Similarly, using (A5) , (A7) & (A8) the stator flux linkage can be represented in terms of e'_d, e'_q as

$$\Psi_{ds} = -x' i_{ds} + e'_q \quad \text{and} \quad \Psi_{qs} = -x' i_{qs} - e'_d \tag{A10}$$

Substitute Ψ_{dr}, Ψ_{qr}, i_{dr}, i_{qr} from (A8) & (A9) in (A3) & (A4) to get

$$\dot{e}'_q \frac{x_{rr}}{x_m} = \omega_b R_r \left(-\frac{e'_q}{x_m} - \frac{x_m}{x_{rr}} i_{ds}\right) + s\omega_b \left(-e'_d \frac{x_{rr}}{x_m}\right) + \omega_b v_{dr}$$

$$-\dot{e}'_d \frac{x_{rr}}{x_m} = \omega_b R_r \left(\frac{e'_d}{x_m} - \frac{x_m}{x_{rr}} i_{qs}\right) - s\omega_b e'_q \frac{x_{rr}}{x_m} + \omega_b v_{qr}$$

The above can be simplified to

$$\dot{e}'_q = -\frac{1}{T'_0}\left[e'_q + \left(x_{ss} - x'\right) i_{ds}\right] - s\omega_b e'_d + \frac{x_m}{x_{rr}} \omega_b v_{dr} \tag{A11}$$

$$\dot{e}'_d = -\frac{1}{T'_0}\left[e'_d - \left(x_{ss} - x'\right) i_{qs}\right] + s\omega_b e'_d - \frac{x_m}{x_{rr}} \omega_b v_{qr} \tag{A12}$$

Using (A10) substitute Ψ_{ds} & Ψ_{qs} in (A1) & (A2) to get

$$-x' \dot{i}_{ds} + \dot{e}'_q = \omega_b R_s i_{ds} + \omega_e \left(-x' i_{qs} - e'_d\right) + \omega_b v_{ds}$$

$$-x' \dot{i}_{qs} - \dot{e}'_d = \omega_b R_s i_{qs} - \omega_e \left(-x' i_{ds} + e'_q\right) + \omega_b v_{qs}$$

Using (A11) & (A12), $\dot{e}'_d$ and $\dot{e}'_q$ can be eliminated from the above equations, and simplified to

$$\dot{i}_{ds} = -\frac{1}{x'}\left[\frac{1}{T_0'}\left(x_{ss} - x'\right) + \omega_b R_s\right] i_{ds} + \omega_b i_{qs} + \frac{(1-s)\omega_b}{x'} e_d' - \frac{e_q'}{x' T_0'} - \frac{\omega_b}{x'} v_{ds} + \frac{\omega_b x_m}{x_{rr} x'} v_{dr} \tag{A13}$$

$$\dot{i}_{qs} = -\omega_b i_{ds} - \frac{1}{x'}\left[\frac{1}{T_0'}\left(x_{ss} - x'\right) + \omega_b R_s\right] i_{qs} + \frac{e_d'}{x' T_0'} + (1-s)\frac{\omega_b}{x'} e_q' - \frac{\omega_b}{x'} v_{qs} + \frac{\omega_b x_m}{x_{rr} x'} v_{qr} \tag{A14}$$

Equation (A11) – (A14) can be written in more compact form as-

$$\begin{aligned}
\dot{i}_{ds} &= A_{11} i_{ds} + A_{12} i_{qs} + A_{13} e_d' + A_{14} e_q' + B_{11} v_{ds} + B_{13} v_{dr} \\
\dot{i}_{qs} &= A_{21} i_{ds} + A_{22} i_{qs} + A_{23} e_d' + A_{24} e_q' + B_{22} v_{qs} + B_{24} v_{qr} \\
\dot{e}_d' &= A_{31} i_{ds} + A_{32} i_{qs} + A_{33} e_d' + A_{34} e_q' + B_{34} v_{qr} \\
\dot{e}_q' &= A_{41} i_{ds} + A_{42} i_{qs} + A_{43} e_d' + A_{44} e_q' + B_{42} v_{dr}
\end{aligned} \tag{A15}$$

Where,

$$A_{11} = -\frac{1}{x'}\left[\frac{1}{T_o'}(x_{ss} - x') + \omega_b R_s\right] = A_{22}; \qquad A_{12} = \omega_b; \qquad A_{21} = -A_{12}$$

$$A_{13} = (1-s)\frac{\omega_b}{x'}; \qquad A_{24} = A_{13}; \qquad A_{14} = -\frac{1}{T_o' x'}; \qquad A_{23} = \frac{1}{T_o' x'} = -A_{14}$$

$$A_{31} = 0; \qquad A_{32} = \frac{(x_{ss} - x')}{T_o'}; \qquad A_{33} = -\frac{1}{T_o'}; \qquad A_{34} = s\omega_b$$

$$A_{41} = -\frac{(x_{ss} - x')}{T_o'} = -A_{32}; \quad A_{42} = 0; \quad A_{43} = -s\omega_b = -A_{34}; \quad A_{44} = -\frac{1}{T_o'} = A_{33}$$

$$b_{11} = -\frac{\omega_b}{x'} = b_{22}; \qquad b_{13} = \frac{x_m \omega_b}{x_{rr} x'} = b_{24}; \qquad b_{34} = -\frac{x_m \omega_b}{x_{rr}}; \qquad b_{42} = -b_{34}$$

Appendix B

Wind generator system parameters

TABLE B1: Data for Generator, transmission line, STATCOM, battery, supercapacitor, and turbine

Induction Generator		Turbine
Stator resistance, R_s = 0.048 pu		Blade radius, R = 37.5m
Rotor resistance, R_r = 0.018 pu		Air density, $\rho = 1.225$ kg/m^3
Stator reactance, x_s = 0.075 pu		Gear-ratio = 1:75
Rotor reactance, x_r = 0.12 pu		Pitch angle, β=0.
Mutual reactance, x_m = 3.8 pu		Mean wind speed V_w=10m/sec
Damping ratio, D = 0.00		Inertia constant of turbine, H_t = 2.5 pu
Inertia constant of generator, H_g = 0.5 pu		
f = 60 Hz		Transmission line (total)
V_{dr}=0.0012 pu; V_{qr}=0.0015 pu		Resistance, R=0.1 pu
		Reactance, X=0.55 pu

STATCOM Circuit

R_{st}=0.01 pu; L_{st} = 0.15 pu; C_{dc} = 1 pu;

Supercapacitor & dc-dc converter

L_{sc}=0.18 pu; R_{sc}=0.1 pu; C_{sc}=350 pu (2.1 Farad)

Multimachine system data

TABLE B2: A 4-machine 12-bus system generation, load, and line data

Generation and load data: nominal case

	Generation		Load	
Bus #	Pg, MW	Qg, MVAR	PL, MW	QL, MVAR
1	90.55	49.5		
2	105	38.93		
3	50	28.16		
4	75	0.0		
5			96.875	37.5
6			65.625	31.25
8			90.625	33.75
12			60.938	18.75

Line data on 100 MVA Base

From bus	To bus	R (pu)	X (pu)	B/2 (pu)
1	7	0	0.05	0
2	9	0	0.05	0
4	10	0.08	0.4	0
3	11	0	0.05	0
11	12	0.018	0.1167	0.0175
11	5	0.009	0.10	0.035
5	10	0.009	0.1167	0.035
10	6	0.009	0.135	0.035
6	9	0.009	0.1075	0.035
9	8	0.009	0.11	0.049
8	7	0	0.1333	0.035
7	5	0.009	0.1333	0.035

TABLE B3: 4-Machine 12-bus system machine nominal operating points

SG1	SG2	SG3	IG
$V_t = 1.04\angle 0°$pu Pg = 0.9055 pu Qg = 0.495 pu α= 4.44°	$V_t = 1.025\angle 1.42°$pu Pg = 1.05 pu Qg = 0.389 pu α= 34.62°	$V_t = 1.04\angle 0°$pu Pg = 0.5 pu Qg = 0.2816 pu α= 19.132°	$V_t = 1.015\angle 14.47°$pu Pg = 0.75 pu Slip, so = - 1.357%

α is the machine angle with respect to swing bus. MVA_{base} = 100.

Synchronous Generators Data

X_d =[0.1460 0.8953 1.3125 1.3125]'; X_q =[0.0969 0.8645 1.2578 1.2578]';

X_d' =[0.0608 0.1198 0.1813 0.1813]'; X_q' =[0.0969 0.1969 0.2500 0.2500]';

H =[23.64 6.4 3.01 3.01]'; T_{do}' =[8.96 6.0 5.89 5.89]';

T_{qo}' =[0.31 0.535 0.60 0.60]'; K_a =[20 20 20 20]';

T_a =[0.2 0.2 0.2 0.2]'; R_s =[0 0 0 0]';

K_E =[1 1 1 1]'; T_E =[0.314 0.314 0.314 0.314]';

K_F =[0.063 0.063 0.063 0.063]'; T_F =[0.35 0.35 0.35 0.35]';

Appendix C

Modeling of STATCOM with Battery

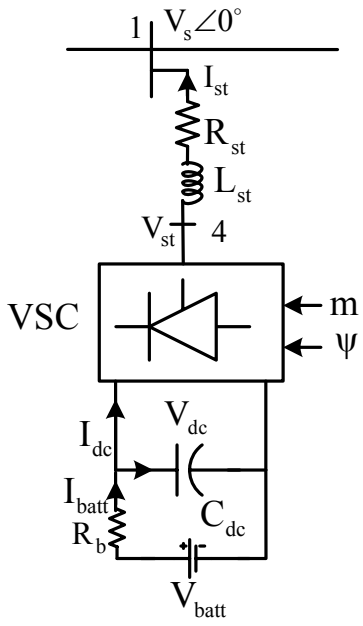

Figure C1: STATCOM with battery

Figure C1 shows the section of STATCOM with a battery, which is connected to the system bus 1 by a transformer. R_{st} and L_{st} represent the resistance and inductance of the transformer including STATCOM converter-losses, respectively. The battery is represented by an ideal DC voltage source V_{batt}, and a resistor R_b. STATCOM is modeled as a controllable voltage source V_{st}=m$V_{dc}\angle\psi$, where m and ψ are the modulation index

and phase angle defined by VSC PWM. The dynamic current voltage relationship of the STATCOM is obtained from -

$$L_{st}\frac{di_{st}}{dt}+R_{st}i_{st}=mV_{dc}\angle\psi-V_s \tag{C1}$$

Equation (C1) can be broken-up in synchronously rotating d-q reference frame and in pu it can be written as-

$$\frac{di_{std}}{dt}=\omega_b\left(-\frac{R_{st}}{L_{st}}i_{std}+\frac{\omega}{\omega_b}i_{stq}+\frac{mV_{dc}}{L_{st}}\cos\psi-\frac{V_m}{L_{st}}\right) \tag{C2}$$

$$\frac{di_{stq}}{dt}=\omega_b\left(-\frac{\omega}{\omega_b}i_{std}-\frac{R_{st}}{L_{st}}i_{stq}+\frac{mV_{dc}}{L_{st}}\sin\psi-\frac{V_m}{L_{st}}\right) \tag{C3}$$

When an inverter of a STATCOM operates in sinusoidal pulse with modulation mode (SPWM) mode, its output voltage must satisfy the following equations

$$e_{xd}=V_{dc}m\cos\psi \tag{C4}$$

$$e_{xq}=V_{dc}m\sin\psi$$

The instantaneous active power on the ac side of is calculated by

$$P_{ac}=e_{xd}i_{std}+e_{xq}i_{stq} \tag{C5}$$

and the power on the dc side of the inverter can be expressed by:

$$P_{dc}=V_{dc}I_{dc} \tag{C6}$$

Considering that the instantaneous active power exchanged between the ac and dc side of the inverter should be same , equation (C7) must hold:

$$P_{ac} = P_{dc} \tag{C7}$$

Using KCL on the dc side we can have

$$C_{dc}\frac{dV_{dc}}{dt} = I_{batt} - I_{dc} \tag{C8}$$

Combining (C4), (C5), (C6), (C7) & (C8) the dynamic equation for the dc side with battery is obtained as:

$$\begin{aligned}\frac{dV_{dc}}{dt} &= -\frac{m}{C_{dc}}\left(i_{std}\cos\psi + i_{stq}\sin\psi\right) + \frac{I_{batt}}{C_{dc}} \\ &= -\frac{m}{C_{dc}}\left(i_{std}\cos\psi + i_{stq}\sin\psi\right) + \frac{V_{batt} - V_{dc}}{R_b C_{dc}}\end{aligned} \tag{C9}$$

Equation (C2), (C3) & (C9) represents dynamic model of STATCOM with battery energy storage system (STATCOM/BESS)

Modeling of STATCOM with Supercapacitor

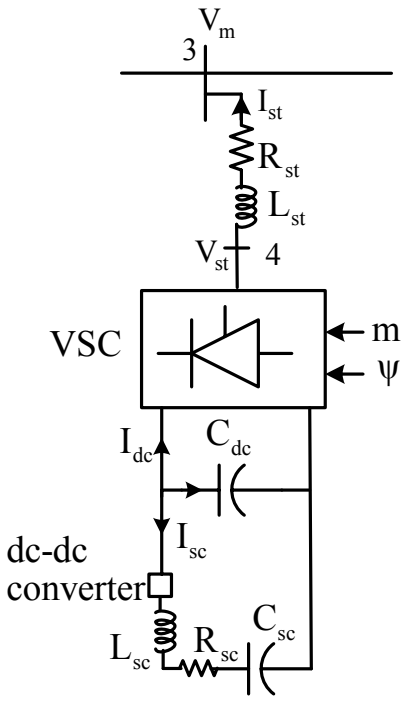

Figure C2: STATCOM with Supercapacitor

Figure C2 shows the section of STATCOM with a supercapacitor unit, which is connected to the system bus 2 by a transformer Tr. Applying KCL on the dc side we can have

$$C_{dc}\frac{dV_{dc}}{dt} = -I_{dc} - I_{sc} \tag{C10}$$

Using power balance between ac and dc side of the STATCOM (i.e. $P_{dc}=P_{ac}$) and following similar steps as STATCOM/BESS, the dynamic equation for the dc side with supercacitor can be obtained as:

$$\frac{dV_{dc}}{dt} = -\frac{m}{C_{dc}}\left(i_{std}\cos\psi + i_{stq}\sin\psi\right) - \frac{I_{sc}}{C_{dc}} \tag{C11}$$

Considering dc-dc converter duty ratio (Dr), (C11) becomes

$$\frac{dV_{dc}}{dt} = -\frac{m}{C_{dc}}\left(i_{std}\cos\psi + i_{stq}\sin\psi\right) - \frac{D_r I_{sc}}{C_{dc}} \tag{C12}$$

Appendix D

LVRT Requirements of various Grid Codes

Grid codes issued during the last years invariably demand that wind farm must withstand voltage dips to a certain percentage of the nominal voltage (down to 0% in some cases) and for a specified duration. Such requirements are known as Fault Ride Through (FRT) or Low Voltage Ride Through (LVRT) and are described by a voltage vs. time characteristics curve as shown in Fig D1. For clarity, LVRT requirements of some countries are shown here [100- 102]. The FRT requirements also include fast active and reactive power restoration to the prefault values after the system voltage returns to normal operation levels.

As depicted in Fig D1, LVRT rule issued by Federal Energy Regulatory Commission (FERC), USA [100], says that if the voltage remains at a level greater than 15% of the nominal voltage for a period that does not exceed 0.625 seconds, the plant must stay online. Further, if the voltage returns to 90% of the nominal voltage within 3 seconds of the beginning of the voltage drop (with the voltage at any given time never falling below minimum voltage indicated by the solid line in Fig D1), the plant must stay online. Two key features of this regulation are:

1. A wind generating plant must have low voltage ride-through capacity down to 15% of the rated line voltage for 0.625 seconds.
2. A wind generating plant must be able to operate continuously at 90% of the rated line voltage, measured at the high voltage side of the wind plant substation transformer(s).

According to grid code of Great Britain [103], the generator has to remain connected to the power system for atleast 140 ms when the voltage on the high voltage side of the transmission system is zero.

Similarly, Spanish grid code [104], says that the wind generator has to remain connected to the power system at least until 500 ms after the occurrence of a fault during which the PCC voltage is 20% of the nominal value.

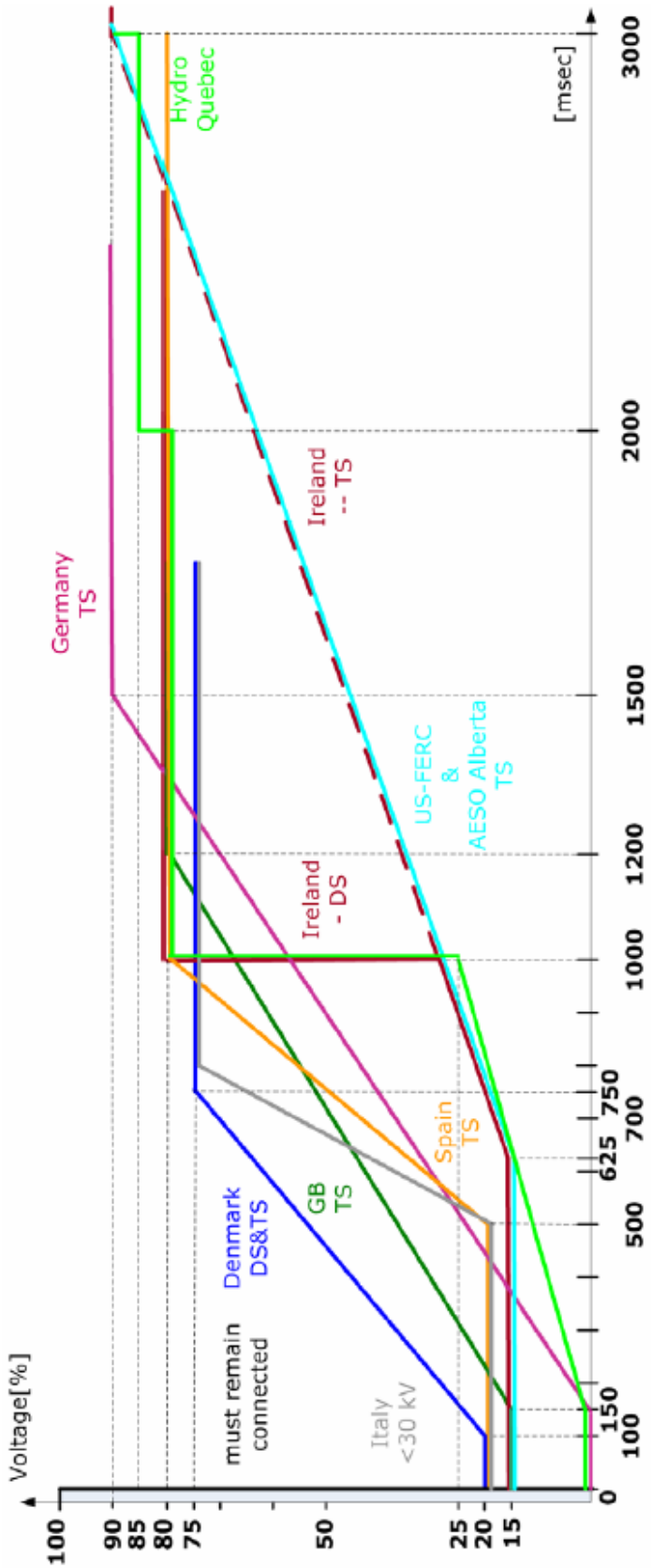

Fig D1: Summary regarding fault ride through capability of wind turbines/farms in national grid codes

Appendix E

Linearization Coefficients of Multimachine System

The linearized model of the multimachine system is given by

$$\dot{X} = A_{sys} X + BU \tag{D1}$$

$$where,\ X = [\Delta E'_q\ \ \Delta E'_d\ \ \Delta\omega\ \ \Delta\delta\ \ \Delta E_{fd}\ \ \Delta\omega_t\ \ \Delta\theta_t]^T\ and\ U = [\Delta T_m\ \ \Delta V_{ref}]^T$$

$$A_{sys} = \begin{bmatrix} As_{11} & As_{12} & 0 & As_{14} & As_{15} \\ As_{21} & As_{22} & 0 & As_{24} & 0 \\ As_{31} & As_{32} & As_{33} & As_{34} & 0 \\ 0 & 0 & As_{43} & 0 & 0 \\ As_{51} & As_{52} & 0 & As_{54} & As_{55} \end{bmatrix} \tag{D2}$$

The expression for the matrix elements are:

$$A_{s11} = A_{e12} + A_{e13} N_{12}; \qquad A_{s12} = A_{e14} + A_{e13} N_{11}$$

$$A_{s13} = A_{e15}; \qquad A_{s14} = A_{e13} N_{13}; \qquad A_{s15} = A_{e11}$$

$$A_{s21} = A_{e23} + A_{e22} N_{22}; \quad A_{s22} = A_{e21} + A_{e22} N_{21}; \quad A_{s23} = A_{e24};$$

$$A_{s24} = A_{e22} N_{23}; \qquad A_{s25} = 0$$

$$A_{s31} = A_{e32} + A_{e33}N_{12} + A_{e34}N_{22}; \qquad A_{s32} = A_{e31} + A_{e33}N_{11} + A_{e34}N_{21}$$

$$As_{33} = -diag(\frac{D}{M}); \qquad A_{s34} = A_{e33}N_{13} + A_{e34}N_{23}$$

$$A_{s43} = diag(\omega_b)$$

$$A_{s51} = A_{e51}N_{32} + A_{e52}N_{42}; \quad A_{s52} = A_{e51}N_{31} + A_{e52}N_{41};$$

$$A_{s54} = A_{e51}N_{33} + A_{e52}N_{43}; \quad As_{55} = -diag(\frac{1}{T_A})$$

Where,

$$A_{e11} = diag\left(\frac{1}{T'_{do}}\right); \quad A_{e12} = -diag\left(\frac{1}{T'_{do}}\right); \quad A_{e13} = -diag\left(\frac{x_d - x'_d}{T'_{do}}\right)$$

$$A_{e14}(ng,ng) = -s_o\omega_o; \quad A_{e15}(ng,ng) = \omega_o E_{d10}(ng)$$

$$A_{e21} = -diag\left(\frac{1}{T'_{qo}}\right); \quad A_{e22} = diag\left(\frac{x_q - x'_q}{T'_{qo}}\right)$$

$$A_{e23} = zeros(ng); \quad with \quad A_{e23}(ng,ng) = s_o\omega_o$$

$$A_{e24} = zeros(ng); \quad with \quad A_{e24}(ng,ng) = -\omega_o E_{q10}(ng)$$

$$Ae_{31} = -diag(\frac{I_{d0}}{M}); \quad Ae_{32} = -diag(\frac{I_{q0}}{M});$$

$$Ae_{33} = -diag(\frac{E'_{d0} + (x'_q - x'_d)I_{q0}}{M}); \quad Ae_{34} = -diag(\frac{E'_{q0} + (x'_q - x'_d)I_{d0}}{M})$$

$$Ae_{51} = -diag(\frac{K_A}{T_A}\frac{v_{d0}}{v_{t0}}); \quad Ae_{52} = -diag(\frac{K_A}{T_A}\frac{v_{q0}}{v_{t0}})$$

$$N_{31} = I - R_s N_{11} + X_{q1} N_{21}; \qquad N_{32} = -R_s N_{12} + X_{q1} N_{22}$$

$$N_{33} = -R_s N_{13} + X_{q1} N_{23}$$

$$N_{41} = -R_s N_{21} - X_{d1} N_{11} \qquad N_{42} = I - R_s N_{22} - X_{d1} N_{12}$$

$$N_{43} = -R_s N_{23} - X_{d1} N_{13}$$

$$\begin{bmatrix} N_{11} & N_{12} & N_{13} \\ N_{21} & N_{22} & N_{23} \end{bmatrix} = [inv(Nx1)](Nx2)$$

Where,

$$Nx1 = \begin{bmatrix} (I + G_1 R_s - B_1 X_{d1}) & -(G_1 X_{q1} + B_1 R_s) \\ (G_1 X_{d1} + B_1 R_s) & (I + G_1 R_s - B_1 X_{q1}) \end{bmatrix} \; and \; Nx2 = \begin{bmatrix} G_1 & -B_1 & G_2 \\ B_1 & G_1 & B_2 \end{bmatrix}$$

$$R_s = diag(r_s); \qquad X_{d1} = diag(x'_d); \qquad X_{q1} = diag(x'_q)$$

$$M_1 = \begin{bmatrix} m_1 & m_3 \\ m_4 & m_6 \end{bmatrix}; \qquad M_2 = \begin{bmatrix} m_2 \\ m_5 \end{bmatrix}$$

$$G_1 = real(M_1); \quad B_1 = imag(M_1); \quad G_2 = real(M_2); \quad B_2 = imag(M_2)$$

Appendix F

Aggregated Model Representation

Application of the aggregation techniques to a fixed-speed machine can be realized as an algebraic (i.e. scalar) addition of the swing equation for N turbines of the wind farm [57]. This is given in *pu* (on machine rating) in (E.1).

$$2H^{agg}\frac{d\omega}{dt} = P_m^{agg} - P_e^{agg} \tag{E.1}$$

Where,

$$H^{agg} = \sum_{i=1}^{N} H_i;\ P_m^{agg} = \sum_{i=1}^{N} P_{mi};\ and\ P_e^{agg} = \sum_{i=1}^{N} P_{ei}$$

$$P_{mi} = \frac{1}{2}\rho_{air} v^3 C_p(\lambda) \qquad and\ \lambda = \frac{R\omega}{v}$$

Fig E.1 shows the schematic representation of an aggregated wind turbine. The aggregated mechanical torque corresponding to aggregated mechanical power P_m^{agg} drives the aggregated inertia constants H^{agg} of the turbines and the generator. In the aggregated model, Z_{IG}^{agg} is the aggregated impedance of the wind turbine generator, Z_{Tr}^{agg} is the aggregated impedance of the generator transformer and X_C^{agg} is the reactance of the power factor correction capacitors. The aggregated impedances are given in (E.2)

assuming the turbines have the same electrical parameters. If the electrical parameters are different, then the aggregated impedance for the wind turbine generator can be obtained in a similar way to that used for aggregating induction motors. It is also important that the aggregated model provides the same fault-current contribution at the grid connection point *A*. For this condition to be valid, the impedance seen at point *A* looking into the wind-farm should be same before and after the aggregation [57].

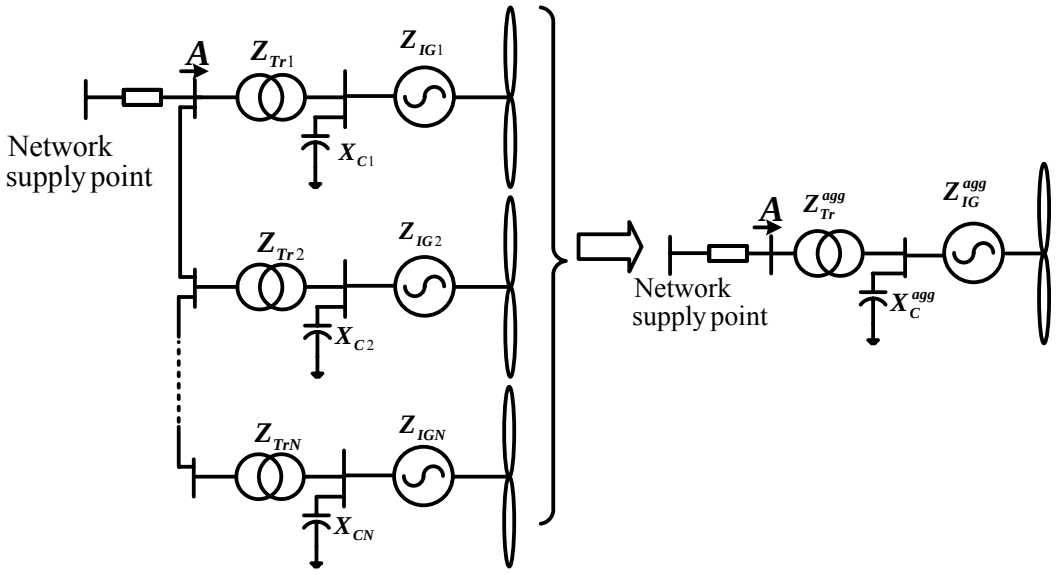

Figure E.1: Aggregated model of N fixed speed wind turbines

$$Z_{Tr}^{agg} = \frac{Z_{Tr}}{N};\quad Z_{IG}^{agg} = \frac{Z_{IG}}{N};\ \text{and}\ X_C^{agg} = \frac{X_C}{N} \tag{E.2}$$

Where, $Z_{IG} = f(x_s, x_r, x_m, R_s, R_r)$

Determination of the number of WTs and calculation of pu values

The generated power output of a fixed-speed wind turbine is directly related to the wind speed. Depending on local wind conditions, wind turbines may not operate at rated values. If each IG of *y* MW rated capacity is operating at *x*% of its rated value then to obtain a total of P_{tot} MW from a wind farm, required number of identical IGs is given by

$$N = \frac{P_{tot}}{(x/100)y}$$

IG parameters of each machine are usually given in *pu* values based on its own machine rating. The *pu* values of equivalent IG in terms of system base are given by

$$[x_s^{agg}, x_r^{agg}, x_m^{agg}, R_s^{agg}, R_r^{agg}] = [x_s, x_r, x_m, R_s, R_r] \times \frac{1}{N} \times \left(\frac{MVA_{Base}^{system}}{MVA_{Base}^{machine}} \right) \times \left(\frac{KV_{Base}^{machine}}{KV_{Base}^{system}} \right)^2$$

$$[H_t^{agg}, H_m^{agg}, K_s^{agg}] = [H_t, H_m, K_s] \times N \times \left(\frac{MVA_{Base}^{machine}}{MVA_{Base}^{system}} \right)$$

Where,

$x_s, x_r, x_m, R_s, R_r, H_t, H_m, K_s$ are the values in terms of machine base.

REFERENCES

[1]. L. Munteanu, A. L. Bratcu, N. A. Cutululis. *Optimal Control of Wind Energy Systems – Towards a global approach. Advances in Industrial Control.* London : Springer – Verlag, Limited, 2008.

[2]. Z. Chen, F. Blaabjerg, "Wind energy – the world's fastest growing energy source", *IEEE Power Electron. Soc. Newsletter*, 18(3), 2006, pp.15-19.

[3]. AWEA Annual Wind Report – 2009, Available at http://www.awea.org/pubs, on March 20, 2010.

[4]. The European Wind Energy Association. Wind Power in Europe. *EWEA Publications.* Online, Available at http://www.ewea.org/. October 5, 2007.

[5]. L.H. Hansen, L. Helle, and G. F. Blaabjer, "Conceptual survey of generators and power electronics for wind turbines", *Technical Report* Riso-R-1205 (EN), Riso National Laboratory, Roskilde, Denmark.

[6]. F.V. Hulle, "Large scale integration of wind energy in the European power supply analysis, issue and recommendations", *EWEA Technical Report*, December 2005.

[7]. N. M., Kirby, L. Xu, M. Luckett, and W. Siepmann, "HVDC transmission for large offshore windfarms". *IEEE Power Engineering Journal*, s.l. : June 2002.

[8]. T., Ackermann "Transmission systems for offshore windfarms". *IEEE Power Engg Review*, s.l. : Dec 2002.

[9]. Lu, Weixing and B. T. Ooi, "Multiterminal LVDC system for optimal acquision of power in windfarm using induction generators". *IEEE Trans. Power Electronics*, July 2002, 4, s.l. : Vol. 17.

[10]. C. L. Masters, "Voltage rise – The big issue when connecting embedded generation to long 11kV overhead lines", *Power Engineering Journal*, 2002, 5-12.

[11]. F. D. Kanellos, and Hatziargyriou, N D. "The effect of variable-speed wind turbines on the operation of weak distribution networks", *IEEE Trans on Energy Conversion*, Vol. 17, issue 4, 2002.

[12]. Rodriguez-Amenedo, Arnalte, J L S and Burgos, J C. "Automatic generation control of a windfarm with variable speed wind turbines". *IEEE Trans on Energy Conversion*, Vol. 17. Issue 2, June 2002.

[13]. S. K. Salman, and A.L.J. Teo, "Windmill modeling consideration and factors influencing the stability of a grid-connected wind power based embedded generator", *IEEE Trans on Power Systems*, 2003, Vol 18, pp. 793-802.

[14]. F. Mei, and B. Pal, "Modal analysis of grid-connected Doubly Fed Induction Generator", *IEEE Trans on Energy Conversion*, Vol. 22 No. 3 2007, pp. 728-736.

[15]. C. Jauch, P. Sørensen, I. Norheim, C. Rasmussen, "Simulation of the impact of wind power on the transient fault behavior of the Nordic power system", *Electric Power Systems Research*, Vol. 77, 2007,pp. 135-144.

[16]. D. J. Vowles, C. Samarasinghe, M. J. Gibbard, G. Ancell, "Effect of wind generation on small-signal stability – A New Zealand example". *IEEE Power and Energy General meeting – Conversion and delivery of Electrical Energy in the 21st century*. July 20-24, 2008. pp. 1-8.

[17]. R. D. Fernandez, Mantz, R. J., and Battaiotto, P.E. "Impact of wind farms on a power system. An eigenvalue analysis approach". *Renewable Energy*. 2006, doi:10.1016/j.renene. 2006.07.009.

[18]. K. Elkington, V. Knazkins, M. Ghandhari, "On the stability of power systems containing doubly fed induction generator-based generation", *Electric Power Systems Research* (2008), 1477-1484.

[19]. C. Jauch, T. Cronin, P. Sørensen, B. Bak-Jensen, "A Fuzzy Logic Pitch Angle Controller for Power System Stabilisation", *Wind Energy*, Vol. 10, 2007, pp. 19-30.

[20]. T. Senjyu, T. Senjyu, R. Sakamoto, N.Urasaki, H.Higa, K.Uezato and T.Funabashi "Output power control of wind turbine generator by pitch angle control using minimum variance control", *Journal of Electrical Eng Japan*, Vol. 154, issue 2, 2006, pp. 10–18.

[21]. C. Jauch, S. M. Islam, P. Sørensen, and B. Bak-Jensen, "Design of a Wind Turbine Pitch Angle Controller for Power System Stabilisation", *Renewable Energy*, Vol. 32, 2007, pp. 2334–2349.

[22]. E.S. Abdin and W, Xu. "Control design and dynamic performance analysis of a wind turbine-induction generator unit", *IEEE Transactions on Energy Conversion*, Vol. 15, Issue 1, 2000, pp. 91-96.

[23]. T. Ahmed, K. Nishida, K. Soushin, and M. Nakaoka, “Static VAR compensator-based voltage control implementation of single-phase self-excited induction generator”, *IEE Proc.-Gener. Transm. Distrib*., Vol. 152, Issue 2, 2005, pp. 145-156.

[24]. J. L. Munda, and H. Miyagi, “Stability Analysis and Control of a Wind Turbine Driven Induction Generator”, *Electric Power Components and Systems*, 30, 2002, 1223-1233.

[25]. Woei-Luen Chen; Yuan-Yih Hsu, "Controller design for an induction generator driven by a variable-speed wind turbine," *IEEE Transactions on Energy Conversion*, vol.21, no.3, pp.625-635, Sept. 2006.

[26]. C. Schauder and H., Mehta. “Vector analysis and control of advanced static VAR compensators”, *IEE Proceedings-C*, Vol. 140, Issue 4, 1993, pp. 299-306.

[27]. S. Morris, P.K.Dash, K.P.Basu, “A fuzzy variable structure controller for STATCOM”, *Electric power system research* 65, 2003, pp 23-34.

[28]. L.O. Malik , Y.X.Ni, C.M.Shen, “STATCOM with fuzzy controllers for interconnected power systems”, *Electric power system research*, 55, 2000 pp 87-95.

[29]. M. F. Kandlawala, “Investigation of dynamic behavior of power system installed with STATCOM”, *M.Sc Thesis*, King Fahd University of Petroleum and Minerals, December 2001.

[30]. H.F.Wang, “Phillips-Hefron model of power systems installed with STATCOM and applications”, *IEE proceedings on generation, transmission and distribution*, vol. 146, no.5, September 1999, pp 521-527.

[31]. A. Arulampalam, B., Ekanayake J. and N., Jenkins. “Application study of a STATCOM with energy storage”, *IEE Proc Gener. Transm. Distrib*., Vol. 150, issue 3, 2003, pp. 378-384.

[32]. S. M. Muyeen, R. Takahashi, M. H. Ali, T. Murata, J. Tamura, “Transient stability augmentation of power system including wind farms by using ECS”, *IEEE Trans on Power Systems*, 2008, Vol. 23, issue 3, pp. 1179-1187.

[33]. X.G. Wu, Arulampalam, A. Zhan, C., and Jenkins, N. “Application of a Static Reactive Power Compensator (STATCOM) and a Dynamic Braking Resistor (DBR) for the stability enhancement of a large wind farm”, *Wind Engineering Journal*, Vol. 27, issue 2, 2003, pp. 93-106.

[34]. J.G. Slootweg. “Wind power – modeling and impact on power system dynamics”, *Ph. D. Thesis*. Delft Technical University, Netherland. 2003.

[35]. V. Akhmatov, “Analysis of dynamic behaviour of electric power systems with large amount of wind power”. *Ph. D. Thesis*. Technical University of Denmark. 2003. ISBN 87-91184-18-5.

[36]. A.D. Hansen, L.H. Hansen, “Wind turbine concept market penetration over 10 years (1995-2004)”, *Wind Energy*, 10(1), 2007, pp. 81-97.

[37]. E. Spooner, P. Gordon, J. R. Bumby, and C. D. French, “Lightweight ironless-stator PM generators for direct-drive wind turbines,” *Inst. Electr. Eng. Proc. Elect. Power Appl.*, vol. 152, no. 1, pp. 17–26, Jan. 2005.

[38]. M. R. Dubois, “Optimized permanent magnet generator topologies for direct-drive wind turbines” *Ph.D. dissertation*, Delft Univ. Technol., Delft, The Netherlands, 2004.

[39]. M. P. Papadopoulos, S. A. Papathanassiou, Boulaxis, N. G. and Tentzerakis, S. T. “Voltage quality change by grid-connected wind turbines”, *European Wind Energy Conference*. Nice, France : . s.n., 1999. pp. 783–785.

[40]. T. Petru, and Thiringer, T. “Active flicker reduction from a sea-based 2.5 MW wind park connected to a weak grid”, *Proc. Nordic Workshop on Power and Industrial Electronics*. Aalborg, Denmark : s.n., 2002.

[41]. A. Larsson, P. Sørensen, F. Santjer. “Grid Impact of Variable-Speed Wind Turbines”, *European Wind Energy Conference* (EWEC '99). Nice, France, 1-5 Mars : s.n., 1999. pp. 786-789.

[42]. Freris, L. L. *Wind energy conversion systems*. s.l. : Prentice Hall, 1990.

[43]. J.G. Slootweg, J.G. Slootweg, S.W.H. Hann, H. Polinder, and W.L. Kling, “General model for representing variable speed Wind Turbines in Power System Dynamics Simulations”, *IEEE Trans on Power Systems*, Vol. 18, issue 1, 2003, pp. 144-151.

[44]. Sørensen, P., Hansen, A.D. and Rosas, P.A.C. “Wind Models for Simulation of Power Fluctuations From Wind Farms”, *Journal of Wind Engineering & Industrial Aerodynamics*, 2002, pp. 1381-1402.

[45]. P. Sørensen, A. Hansen, L. Janosi, J. Bech, and B. Bak-Jensen, “Simulation of Interaction between Wind Farm and Power System”, *Risø National Laboratory*, Roskilde, Denmark : 2001.

[46]. V. Akhmatov. *Induction Generators for Wind Power*. s.l. : Multi-Science Publishing Company, Ltd, 2005.

[47]. J.G. Slootweg, H., Polinder and W.L., Kling. “Dynamic Modeling of a Wind Turbine with Direct Drive Synchronous Generator and back to back voltage source; converter and its controls”, *European Wind Energy Conf and Exhibition*. Copenhagen, Denmark : s.n., 2001. pp. 53-56.

[48]. A. D. Hansen, F. Iov, P. Sørensen, N. Cutuluis, C. Jauch, F. Blaabjerg, “Dynamic wind turbine models in power system simulation tool DIgSILENT”, *Technical Report*. 2nd Edition. Risø National Laboratory, Technical University of Denmark. Roskilde, Denmark : s.n., 2007. Riso-R-1400.

[49] P. C. Krause, O. Wasynczuk and A.D., Sudhoff. *Analysis of Electric Machinery and drive systems.* s.l. : IEEE Press, Wiley Interscience, 2002.

[50]. T. Thiringer and J., Luomi. “Comparison of Reduced-Order Dynamic Models of Induction Machines”, *IEEE Transactions on Power Systems*, Vol. 16, issue 1, 2001, pp. 119-126.

[51]. P. Ledesma and J., Usaola. “Effect of Neglecting Stator Transients in Doubly Fed Induction Generator Models*”, IEEE Transactions on Energy Conversion*, Vol. 19, issue 2, 2004, pp. 459-461.

[52]. L. Holdsworth, X. G. Wu, J. B. Ekanayake, and N. Jenkins, “Comparison of Fixed Speed and Doubly Fed Induction Wind Turbines during Power System Disturbances”, *IEE Proceedings - Generation, Transmission and Distribution*, Vol. 150, issue 3, May 2003, pp. 343-352.

[53]. M.V.A. Nunes, J. A. Pecas Lopes, Hans Helmut Zürn, Ubiratan H. Bezerra, Rogerio G. Almeida, “Influence of the Variable-Speed Wind Generators in Transient Stability Margin of the Conventional Generators Integrated in Electrical Grids”, *IEEE Transactions on Energy Conversion*, Vol. 19, issue 4, Dec 2004, pp. 692-701.

[54]. J. B. Ekanayake, L. Holdsworth, and N. Jenkins. “Comparison of 5th Order and 3rd Order Machine Models for Doubly Fed Induction Generator (DFIG) Wind Turbines”, *Electric Power Systems Research*, Vol. 67, issue 3, Dec 2003,pp. 207-215.

[55]. P. Ledesma, and J. Usaola. “Doubly Fed Induction Generator Model for Transient Stability Analysis”, *IEEE Transactions on Energy Conversion*, Vol. 20, issue 2, June 2005, pp. 388-397.

[56]. V. Akhmatov. “An aggregated model of a large wind farm with variable-speed wind turbines equipped with doubly-fed induction generators”, *Wind Engineering*, Vol. 28, Issue 4, 2004, pp. 479-488.

[57]. Shafiu, O. Anaya-Lara, G. Bathurst, N. Jenkins, "Aggregated wind turbine models for power system dynamic studies", *Wind Engineering*, Vol. 30, issue 3, 2006, pp. 171-186.

[58]. J. G. Slootweg, and W.L. Kling. "Aggregated modeling of wind parks in power system dynamic simulations" *IEEE Bologna Power Tech Conference*. Bologna, Italy. June 23-26, 2003.

[59]. P. Kundur, *Power System Stability and Control*, EPRI Power System Engineering Series, 1994.

[60]. P.M. Anderson and Fouad, A. A. *Power System Control and Stability*. IEEE Power System Engineering Series, New York : 2003.

[61]. System dynamic performance subcommittee of the Power system engineering committee of the Power Engineering Society . Eigenanalysis and Frequency Domain Methods for Power Systems: Dynamic Performance. Piscataway : IEEE, 1989. IEEE 90TH0292-3-PWR.

[62]. P. W. Sauer, and M. A. Pai, *Power system dynamics and stability*, Prentice Hall, NJ, 1998.

[63]. G. S. Stavrakakis, G. N. Kariniotakis, "A general simulation algorithm for the accurate assessment of isolated diesel-wind turbines systems integration—Part I: A general multimachine power system model", *IEEE Trans. on Energy Conversion*, EC-10 (3), (1995), pp.577-583.

[64]. G. N. Kariniotakis, and G. S. Stavrakakis, "A general simulation algorithm for the accurate assessment of isolated diesel-wind turbines systems interactions. Part II: Implementation of the algorithm and case-studies wind induction generators", *IEEE Trans on Energy Conversion*, vol. 10, No. 3, Sept. 1995, pp. 584-590.

[65]. R. D. Fernandez, P.E. Battaiotto, R.J. Mantz, "Wind farm non-linear control for damping electromechanical oscillations of power systems", *Renewable Energy*, 33, 2008, pp. 2258-2265.

[66]. O. Anaya-Lara, F. M. Hughes, N. Jenkins, G. Strbac, "Influence of windfarms on power system dynamic and transient stability", *Wind Engineering*, Vol. 30, issue 2, 2006, pp. 107-127.

[67]. V. Akhmatov. "System Stability of Large Wind Power Networks: A Danish Study Case", *International Journal of Electrical Power & Energy Systems*, Vol. 28, issue 1, January 2006, pp. 48-57.

[68]. J. M. Rodríguez, J.L. Fernández, D.Beato, R.Iturbe, J.Usaola, Member,P.Ledesma, and J.R. Wilhelmi, "Incidence on power system dynamics of high penetration of

fixed speed and doubly fed wind energy systems: Study of the Spanish Case", *IEEE Trans on Power Systems*, Vol. 17, issue 4, Nov 2002, pp. 1089-1095.

[69]. W. Freitas, Da Silva, L.C.P. and Morelato, A. "Small-Disturbance Voltage Stability of Distribution Systems with Induction Generators", *IEEE Transactions on Power Systems*, Vol. 20, issue 3, Aug 2005, pp. 1653 - 1654.

[70]. W. Freitas, Vieira, J.C.M.; da Suva, L.C.P.; Affonso, C.M.; Morelato, A. "Long-term voltage stability of distribution systems with induction generators", *IEEE Power Engineering Society General Meeting*. Vol. 3, 2005. pp. 2910 - 2913 .

[71]. J.O.G. Tande. "Applying Power Quality Characteristics of Wind Turbines for Assessing Impact on Voltage Quality", *Wind Energy*, Vol. 5. s.l. : 2002.

[72]. P. Rosas, "Dynamic influences of wind power on the power system", *Ph. D. Thesis*. Section of Electrical Power Engineering, Denmark Technical University. Ørsted : s.n., 2003.

[73]. A. Petersson, T.Thiringer, L. Harnefors, T.Petru, "Modeling and Experimental Verification of Grid Interaction of a DFIG Wind Turbine", *IEEE Transactions on Energy Conversion*, Vol. 20, issue 4, Dec 2005, pp. 878-886.

[74]. H. S. Bronzeado, EAN, Feitosa; PAC, Rosas; MS, Miranda; MEM, de Barros; J, Rohatgi, "Investigation of the Behaviour of Wind Turbines Under Low Turbulence Wind Conditions and Their Interaction With the Distribution Grid", *Wind Engineering*, Vol. 24, issue 2, 2000, pp. 101-109.

[75]. V. Akhmatov, H. Knudsen and A.H. Nielsen. "Advanced Simulation of Windmills in the Electric Power Supply", *International Journal of Electrical Power & Energy Systems*, Vol. 22, issue 6, 2000, pp. 421-434.

[76]. Z. Chen, Hu, Y. and Blaabjerg, F. "Stability improvement of induction generator-based wind turbine systems", *IET Renew. Power Gener.*, Vol. 1, issue 1, 2007, pp. 81–93.

[77]. P., Bousseau. "Solutions for the grid integration of wind farms – A survey", *European Wind Energy Conf.* Nov 12-16, 2004.

[78]. S. M. Muyeen, Muyeen S.M., Takahashi R., Ali M. H., Murata T., and Tamura J., "Stabilization of wind turbine generator system by STATCOM", *IEEJ Trans. Power Energy*, Vol. 126, issue 10, B, 2006,pp. 1073-1082.

[79]. Z. Saad-Saoud, Lisboa M.L., Ekanayake J.B., Jenkins N., and Strbac G. "Application of STACOMs to wind farms", *Proc. Inst. Elect. Eng. Gen. Transm. Distb.*, Vol. 145, issue 5, 1998, pp. 511-517.

[80]. A. Causebrook, Atkinson D.J, Jack A.G. “Fault ride-through of large wind farms using Dynamic Breaking Resistors”, *IEEE Trans on Power Systems.*, Vol. 22, issue 3, 2007, pp. 966-975.

[81]. Z. Yang, C. Shen, L. Zhang, M. L. Crow, L. Dong, S. Pekarek, and S. Atcitty “Integration of a STATCOM and battery energy storage”, *IEEE Trans. Power Syst*, Vol. 16, issue 2, 2001, pp. 254-260.

[82]. C. Abbey and Joos, Geza. “Super capacitor energy storage for wind energy applications”, *IEEE Trans on Industry Applications*, Vol. 43, issue 3, May 2007, pp. 769-776.

[83]. Zorpette, Glenn. “Super Charged”, *IEEE Spectrum*, Jan 2005, pp. 32-35.

[84]. L. Zubieta and R. Bonert. “Characterization of double-layer capacitors for Power Electronice Applications”, *IEEE Trans on Industry Applications*, Vol. 36, issue 1, 2000, pp. 199-204.

[85]. G, Ezzat and Bakhoum. “New Mega-Farad Ultracapacitors”, *IEEE Transactions on Ultrasonics, Ferroelectrics, and Frequency control*, Vol. 56, issue 1, Jan 2009, pp. 14-21.

[86]. J. Wang, Zhang, Jiancheng and Zhong, Yun. “Study on a Super Capacitor Energy Storage system for improving the operating stability of Distributed Generation system”, *3rd Int Conf on Electric Utility Deregulation and Restructuring and Power Technology*, 2008.

[87]. A. Arulampalam, A. Arulampalam, M. Barnes, N. Jenkins and J.B. Ekanayake, “Power quality and stability improvement of a wind farm using STATCOM supported with hybrid battery energy storage”, *IEE Proc. Gener. Transm. Distrib.*, Vol. 153, 6, Nov 2006, pp. 701-710.

[88]. A. M., Voorden, A.M. Voorden, L. M. R.Elizondo, G.C. Paap,J.Verboomen, L.Sluis, “The Application of Super Capacitors to relieve Battery-storage systems in Autonomous Renewable Energy Systems”, *IEEE Power Tech Lausanne,*1-5 July 2007. pp. 479-484.

[89]. A. Abedini and A., Nasiri. “Application of super capacitors for PMSG wind turbine power soothing”, *34th Annual Conf of IEEE Industrial Electronics, IECON 2008*. Nov 10-13, 2008. Orlando, FL : pp. 3347-3351.

[90]. Li, Wei and Geza Joos, “A power electronic interface for a battery supercapacitor hybrid energy storage system for wind applications”, *IEEE PESC Conf. Rhodes*: June 15-19, 2008. pp. 1762-1768.

[91]. S. Breban, S.Breban, M.Nasser, A.Vergnol, B.Robyns, M.M. Radulescu, “Hybrid wind/microhydro power system associated with a supercapacitor energy storage device – Experimental results”, *Int Conf on Electrical Machines*. 2008. pp. 1-6.

[92]. S. Heier. *Grid Integration of Wind Energy Conversion Systems*. 2nd Edition. John Wiley & Sons, Ltd, 2007.

[93]. R., Datta and Ranganathan, V.T. “Variable-speed wind power generation using doubly fed wound rotor induction machine – comparison with alternative schemes”, *IEEE Trans. Energy Conversion*, Vol. 17, Issue 3, 2002, pp. 414-21.

[94]. Rogers, Graham. *Power System Oscillations*. [ed.] Series Editor: M.A. Pai. Canada s.l. : Kluvwer’s Power Electronic and Power Systems Series., 2000.

[95]. A.H.M.A. Rahim and M. Ahsanul Alam. “Dynamic Performance Enhancement of a Grid Connected Wind Generation System”. *International Journal of Simulation and Modeling*, Vol. 29, Issue 4, 2009.

[96]. IEEE Special Stability Controls Working Group Report. Static VAR compensator models for power flow and dynamic performance simulation. *IEEE Trans. Power Syst.*: 9 (1): . 1994. pp. 229-240.

[97]. N. G. Hingorani and L. Gyugy, *Understanding FACTS: Concepts and Technology of Flexible AC Transmission Systems*, Piscataway, NJ, IEEE Press, 2000, Ch 5.

[98]. K.R. Padiyar, *FACTS Controllers in Power Transmission and Distribution*, New Age International (P) Ltd Publishers, New Delhi, 2007, Ch 6.

[99]. M. B. Camara, H, Gualous, F. Gustin, and A. Berthon, “Design and new control of DC/DC Converters to share Energy between Supercapacitors and Batteries in hybrid vehicles”, *IEEE Transactions on Vehicular Technology*, Vol. 57, Issue 5, Sept 2008, pp. 2721-2735.

[100]. FERC. *Interconnection for wind energy, Final Rule*. [Online] FERC, USA, June 2005. http://www.ferc.gov.

[101]. M. Tsili, S. Papathanassiou, “A review of grid code technical requirements for wind farms”, *IET Renewable Power Generation*, vol. 3, issue 3, 2009, pp. 308-332.

[102]. F. Iov, A. Hansen, P. Söerensen, N. Cutululis, “Mapping of Grid Faults and Grid Codes”. *Risoe National Laboratory*, Denmark : 2007.

[103]. The Grid Code. UK : National Grid Electricity Transmission plc, Revision 24. Issue 3. Nov 19, 2007.

[104]. A. Morales, X. Robe, J. L. Rodriguez-Amenedo, S. Arnalte, Z. R. Zubiaur, Z. Torbado, “Advanced Grid Requirements for the Integration of Wind Farms into the Spanish Transmission System”. *European Wind Energy Conference and Exhibition*, EWEC 2007. 7-10, 2007.

[105]. P. B. Malatestas, M. P. Papadopoulos, G. Stavrakakis, “Modeling and identification of Diesel-wind turbines systems”, *IEEE Trans on Power Systems*, vol. 8. No. 3, August 1993, pp. 1091-1095.

[106]. E. Feijoo and J, Cidras. “Modeling of wind farms in the load flow analysis”, *IEEE Trans on Power Systems*, Vol. 15, Issue 1, 2000, pp. 110-115.

[107]. M. Ahsanul Alam, and A.H.M.A.Rahim. “Dynamic Performance Improvement of Wind Generation System connected to a Multimachine Power System”, *International Energy Journal (IEJ)*, Vol. 10, Issue 2, 2009, pp. 101-112. ISSN 1513-718X.

[108]. M. Ahsanul Alam, and A.H.M.A. Rahim, “Dynamic Impact of Wind Generation System on Multi-machine Power System”, *3rd Int. Conf. on Modeling, Simulation & Applied Optimization (ICMSAO’09)*, Jan 2009.

[109]. E., Hagstrom, I., Norheim and K., Uhlen. “Large-scale wind power integration in Norway and impact on damping in the Nordic grid”, Wind Energy Journal, Vol. 8, No. 3, pp. 375–384. 2005.

Bibliography

The following articles related to single machine model have been published as part of KFUPM/SABIC project SAB 2006-01. The support provided by the respective organization is acknowledged.

1. A.H.M.A.Rahim and M. Ahsanul Alam, "Variable susceptance excitation control for dynamic performance improvement of a stand-alone wind turbine induction generator system", *Int. Journal of Renewable Energy Technology*, Vol. 1, No. 1. pp. 1-16, April, 2009.

2. A.H.M.A.Rahim, M. Ahsanul Alam, and M.F. Kandlawala, "Dynamic Performance Improvement of an Isolated Wind Turbine Induction Generator", *Journal of Computers & Electrical Engineering, Volume 35, Issue 4, July 2009, Pages 594-607.*

3. A.H.M.A.Rahim and M. Ahsanul Alam, "Dynamic Performance Enhancement of a Grid Connected Wind Generation System", *International Journal of Simulation and Modeling, Volume 29 No. 4, 2009*, pp. 410-416.

4. A.H.M.A. Rahim, M. Ahsanul Alam and M.F. Kandlawala, "Dynamic Performance Improvement of an Isolated Wind Turbine Induction Generator", *4th IEEE-GCC Conference, Bahrain*, 11-14 Nov, 2007.

5. M. F. Kandlawala, A. H. M. A. Rahim and M. Ahsanul Alam, "Dynamic Performance of a Wind Generation System with Thyristor Controlled Capacitor Compensation", *7th Saudi Engineering Conference, Riyadh,* 26-28 Nov, 2007.

6. T. T. Nguyen; M. F. Kandlawala ; A. H. Rahim,; M. A. Alam,; "Dynamic performance of a grid connected wind generation system with fuzzy logic controlled variable capacitance compensation", Australasian Universities Power Engineering Conference, 2008. AUPEC '08. 14-17 Dec. 2008 Page(s):1 – 6.

7. A.H.M.A. Rahim and M. Ahsanul Alam, "Robust Susceptance Controller for an Isolated Variable Speed Wind Generator System", 3rd Int. Conf. on Modeling, Simulation & Applied Optimization (ICMSAO'09), Jan. 2009.

The following material extracted from the present work has been published in the following:

1. M. Ahsanul Alam and A.H.M.A.Rahim, "Dynamic Performance Improvement of Wind Generation System connected to a Multimachine Power System", *International Energy Journal (IEJ), Volume 10, Issue 2, June 2009*, ISSN 1513-718X, pp. 101-112.

2. M. Ahsanul Alam and A.H.M.A. Rahim, "Dynamic Impact of Wind Generation System on Multi-machine Power System", 3rd Int. Conf. on Modeling, Simulation & Applied Optimization (ICMSAO'09), Jan. 2009.

3. M. Ahsanul Alam**,** A.H.M.A. Rahim, and M. A. Abido, "Supercapacitor based Energy Storage System for effective fault ride through of wind generation system", *IEEE Symposium on Industrial Electronics, Bari, Italy*, June 2010. (Accepted)

4. A.H.M.A. Rahim, M. Ahsanul Alam, Ibrahim El Amin, M.A. Abido, Z. Al-Hamouz, Belhadj C.A., and M. Kassas, "Voltage stability control of a wind generation system", IEEE Int. Energy Conf ENERGYCON 2010, Manama, Bahrain, December 18-22, 2010 (submitted).

The following manuscripts from the present work, are under submission:

1. M. Ahsanul Alam, A.H.M.A. Rahim, and M.A. Abido, "Enhancement of power grid with wind generators supported by supercapacitor based energy storage system",

2. M. Ahsanul Alam, A.H.M.A. Rahim, and M.A. Abido, "On the instability of induction generator based wind generation system and counter measures",

Vitae

- Md. Ahsanul Alam
- Born in Dinajpur, Bangladesh on 31st December, 1968.
- Permanent address: P.O. – Daudpur 5281, District – Dinajpur, Bangladesh
- Email: m_ahsanul@yahoo.co.in; ahsan@duet.ac.bd
- Received Bachelor of Science degree in Electrical & Electronic Engineering from Bangladesh University of Engineering & Technology, Dhaka, in 1992. Master of Science degree in Electrical Engineering from University of Technology Malaysia, Kuala Lumpur, in 1996.
- Worked with the R & D division of Nippon Telephone & Telegraphy (NTT), Tokyo, Japan, in 1996.
- Worked with the consulting division of Global Lightning Technologies Pvt Ltd (GLT), Kuala Lumpur, Malaysia, from 1996 to 1998.
- Worked as a faculty at Dhaka University of Engineering & Technology, Gazipur, Bangladesh, from 1998 to 2004.
- Joined King Fahd University of Petroleum & Minerals in February 2005.